AN ABSTRACT OF THE THESIS OF

Georgina Price for the degree of Master of Science in Geology presented on January 31, 1986.

Title: GEOLOGY AND MINERALISATION, TAYLOR-WINDFALL GOLD PROSPECT, BRITISH COLUMBIA, CANADA. Redacted for Privacy

Abstract approved: _____

The Taylor-Windfall gold prospect, located in south western British Columbia, is hosted by Cretaceous tuffaceous andesites, underlain by granodiorite phases of the Coast Range Plutonic Complex. Mining exploration companies were attracted to the area because of low transportation costs, and a favourable geologic environment defined by high angle deep-seated faults, andesite host rocks, proximal plutonic rocks, widespread hydrothermal alteration, and past gold production.

Although a surface exposure of about 2 km^2 is highly siliceous, similar to the sinter of an epithermal hot spring-related precious metal deposit, the alteration assemblages (propylitic, high temperature corundum-andalusite, phyllic and argillic) present on surface, in subsurface exposures and diamond drill core, more closely approximate assemblages of a deeper porphyry system. Major oxide data indicate that MgO, CaO, and Na_2O were depleted, and Al_2O_3 and SiO_2 were added during hydrothermal alteration coincident with metalisation.

Porphyry deposits are known to contain recoverable quantities of gold, however, a low potential for open pit and underground gold ore was demonstrated by the results of the 1984 exploration program.

Reserves calculated from two tourmaline-tennantite-sphalerite-galena-chalcopyrite-tetradymite veins are about 1000 metric tons of about 0.4 ounces of gold per ton.

Geology and Mineralisation, Taylor-Windfall Gold Prospect, British Columbia, Canada

by

Georgina Price

A THESIS

submitted to

Oregon State University

in partial fulfillment of
the requirements for the
degree of

Master of Science

Completed January 26, 1986

Commencement June 1986

APPROVED:

Redacted for Privacy

Professor of Geology in charge of major

Redacted for Privacy

Head of Department of Geology

Redacted for Privacy

Dean of Graduate School

Date thesis is presented January 26, 1986.

ACKNOWLEDGEMENTS

This study was funded by Westmin Resources Ltd., Esso Minerals of Canada, and the Federal Government of Canada. I would like to thank Westmin and Esso personnel, particularly Ron Lane and Ron Britten, for their aid and encouragement. Sincere thanks is also extended to Ron Senechal for his help with XRD analyses and John Knight for help with SEM-EDS analyses. I am grateful to my collegues for their time and support of this project, and their friendship. My major professor, Dr. Cyrus Field is thanked for his patience, advice and critical reading of the manuscript.

Finally I take this opportunity to acknowledge all my mentors in the exploration industry (Peter Tegart, Joan Carne, Jeffrey Abbott, John Gammon, and Jenna Hardy). Thank you for making work exciting, and for teaching me the odd thing or two that one does not learn in school.

TABLE OF CONTENTS

LIST OF FIGURES

LIST OF PLATES

LIST OF TABLES

GEOLOGY AND MINERALISATION, TAYLOR-WINDFALL GOLD PROSPECT, BRITISH COLUMBIA, CANADA

INTRODUCTION

The purposes of this investigation are twofold: first, to describe the Taylor-Windfall prospect in sufficient geologic detail to postulate its origin, and second, to construct a qualitative model that may be used in the search for and the evaluation of other similar mineral deposits. According to Beane (1982),

> "The critical problem is to define and understand those parameters which are diagnostic of hydrothermal conditions necessary for development of economic grades of metalization."

Methods of investigation

The author mapped two levels of underground workings and the immediate surface area, and assisted Ron Lane in logging 800 metres of diamond drill core. Over 100 samples, representative of the variety of altered host rocks and vein material were collected from all three locations for petrological and chemical studies. Thin section and polished section examinations in combination with x-ray diffraction analyses constituted the majority of the laboratory work. Over 500 bulk rock and drill core samples were collected and analysed for trace elements. Limited whole rock geochemistry, scanning electron microscope-energy dispersive system analyses, and fossil studies were conducted. All field work was done in the summer of 1984, and laboratory work was undertaken and completed in the following fall and spring of 1985.

Location and physiography

The Taylor-Windfall prospect (an inactive mine) is located 210 km north of Vancouver, British Columbia, at the south end of Taseko Lakes, as shown in Figure 1 (NTS 92 O/3, Clinton Mining District; Latitude: 51° 07' N; Longitude: 123° 21' W).

Road access is via Highway 20 from Williams Lake to Hanceville, and on to the property via a four wheel-drive summer road. Travel from Hanceville takes between four and eight hours depending on the condition of the road and creeks that must be crossed. It is advisable to have a winch, chain, shovel and saw. Float planes may land at the south end of Taseko Lake, which is 12 km by road northwest of the property. There is no dock, but the beach is adequate for loading. A 300 m airstrip, in need of upgrading, is located adjacent to the road 4 km west of Taylor-Windfall. Less than 500 m from the mine, are gravel bars on the Taseko River which have sufficient clearance to land a helecopter.

Pleistocene glaciers have carved out broad U-shaped valleys, which were further deepened by receding alpine glaciers (Dolmage, 1924). Altitudes range from 1600 to 2600 m, and relief is moderate. Glacial morphology may obscure or accentuate geologic structure.

Tree line is about 1800 m. Vegetation is sparse, and consists of lodgepole pine (pinus contorta Dougl.), western hemlock [(Tsuga heterophylla (Raf.) Sarg.)], alpine fir [(Abies lasiocarpa (Hook.) Nutt.)], and minor undergrowth. Outcrop exposure is less than 15 percent.

Taylor-Windfall is located in the centre of a sheep guiding area (owner: Sherwood Henry), that is frequented by hunters and hikers. Neither the forestry nor the fishing industry is active

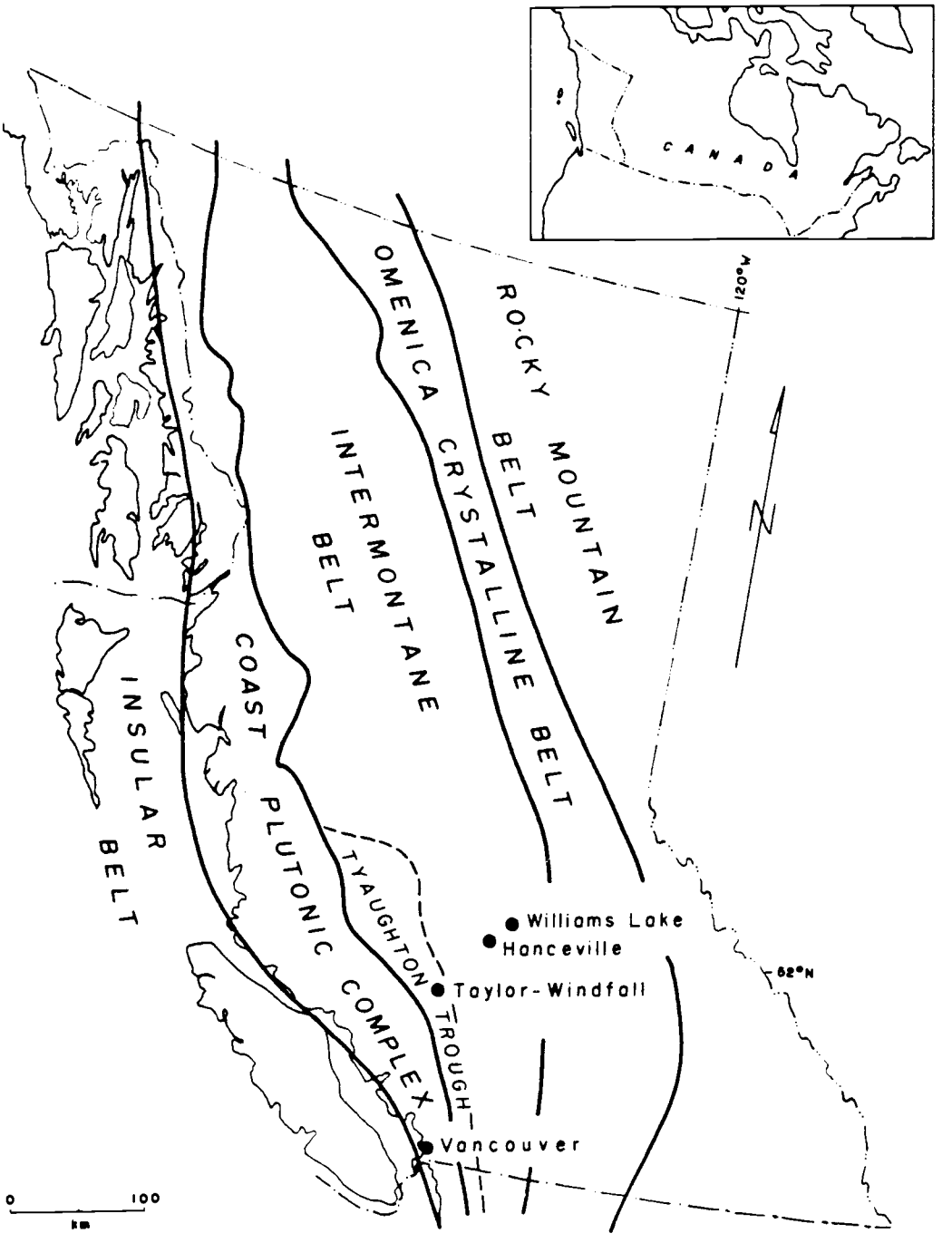

Figure 1. Location map that includes the structural and physiographic belts of the Canadian Cordillera. Modified after Monger and Price (1979) and Wheeler et al.(1972).

in the area.

Precipitation is not extreme, as the Coast Range, west of Taylor-Windfall, blocks out marine weather systems. Road access is limited to June through October, when there is no snow in the higher passes. The high elevation results in year round cool temperatures. Mid-summer freezes are not uncommon.

Previous work - regional

The Taseko area was examined briefly by G. M. Dawson of the Geological Survey of Canada in 1886. Other federal government reconnaissance surveys were conducted by Galloway (1917), Mackenzie (1921), Dolmage (1924; 1929), Cairnes (1943), Jeletzky and Tipper (1968), and Tipper (1978).

MacKenzie (1921) described in detail silicified and pyritized tuff beds, and examined the latter for their economic potential as iron ore deposits. Dolmage (1924, 1929) mapped the area and visited mineral prospects.

Tipper (1963, 1969, 1978), and other employees of the Geological Survey of Canada under his supervision, mapped the Taseko Lakes map sheet at a scale of 1:125,000 during the field seasons of 1961-1965, 1974, and 1976. Results of this work were published in an Open File, (shown on the compilation map of Figure 2) thus the project is assumed to be incomplete. Descriptions and interpretations of the geology are in the report entitled **"Upper Jurassic and Cretaceous rocks of the Taseko Lakes Map-area and their bearing on the geological history of southwestern B.C."**, by Jeletzky and Tipper (1968).

McMillan (1976) of the B.C. Ministry of Mines, Energy and Petroleum Resources (B.C.D.M.) mapped an area of 80 by 70 km (which

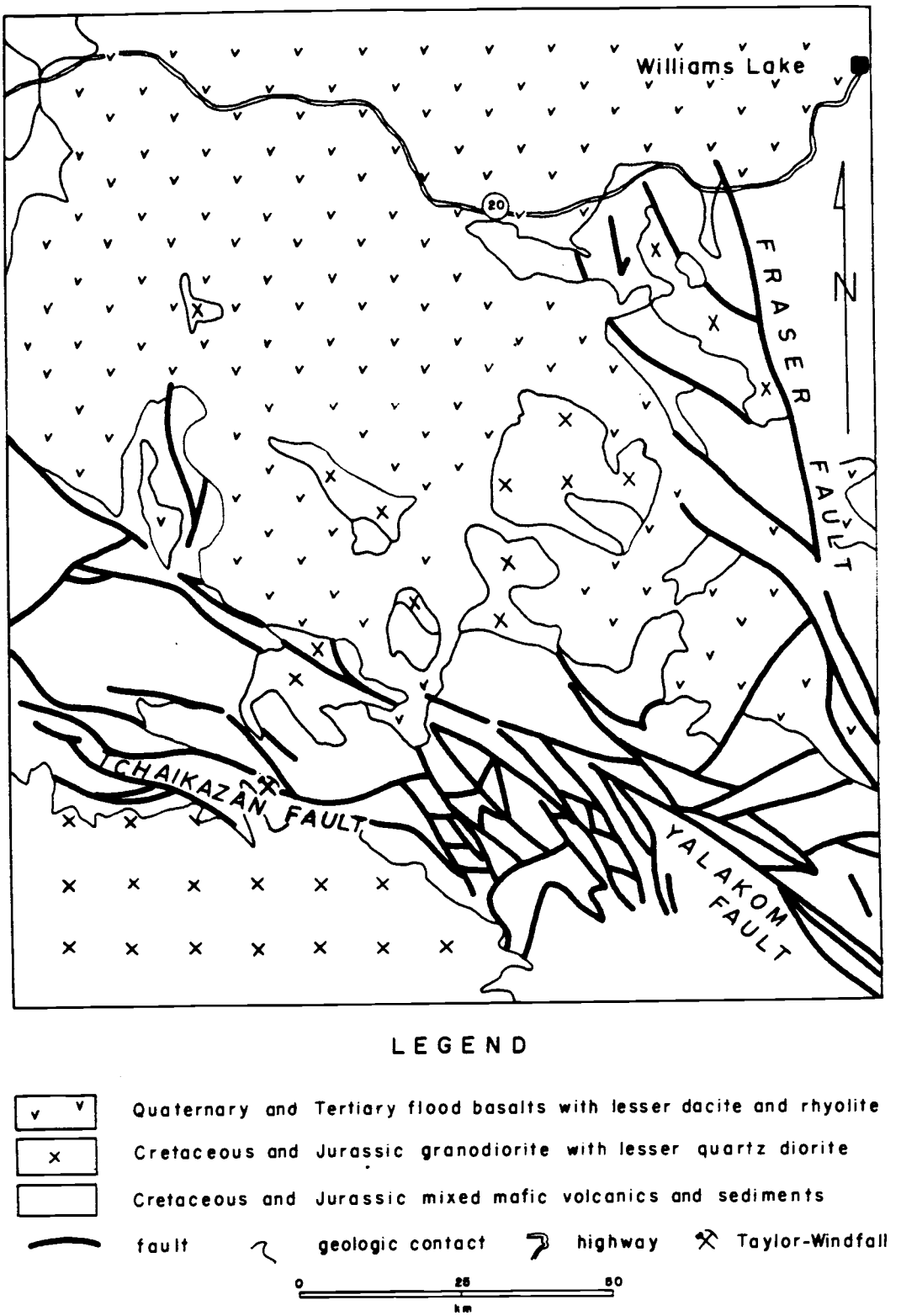

Figure 2. Geology and tectonics of the Taseko Lakes area. Modified after Roddick et al. (1979).

includes the Taylor-Windfall property) at a scale of approximately 1:125,000. The main purpose of McMillan's work was to examine the sulphide mineralisation at the Empress, Spokane, Buzzer, Rowbottom, and, Mowhawk showings, as located in Figure 3. He also analysed 19 samples of intrusive and extrusive rocks for major oxides, and dated three samples using the K-Ar technique. McMillan did not attempt to correlate his units with those mapped by Tipper. Although limited descriptions of sulphide showings in the region are given by the B.C.D.M. in numerous annual reports, which date from 1920 to present, it is beyond the scope and purposes of this study to describe or to discuss these many prospects individually.

Previous work - property

In 1920, a Mr. Taylor discovered free gold hosted in eluvium (near the 1707 m level). An unknown quantity of gold was panned directly from the soil, and milled from a chlorite-tourmaline mixture found on a dip slope and in fractures. Over the next ten years a number of short adits were driven, trenches dug, and an extensive camp and Ross Mill were constructed. In the 1930's, following the discovery of the 'Shaft Shear Zone' (by diamond drilling and subsequent underground work), a 3- to 4-ton per day Straub amalgamation table mill was built. By the late 1930's, there were three levels of underground workings (greater than 800 m in total length). More detailed historical descriptions are given in the following B.C.D.M. annual reports: 1921 (p. G194); 1922 (p. N138); 1923 (p. A168); 1924 (p. B145); 1931 (p. A110); 1934 (p. F24); and 1935 (p. F17-F21). Exploration and development of the property was curtailed from the late 1930's until the mid-1950's. The underground

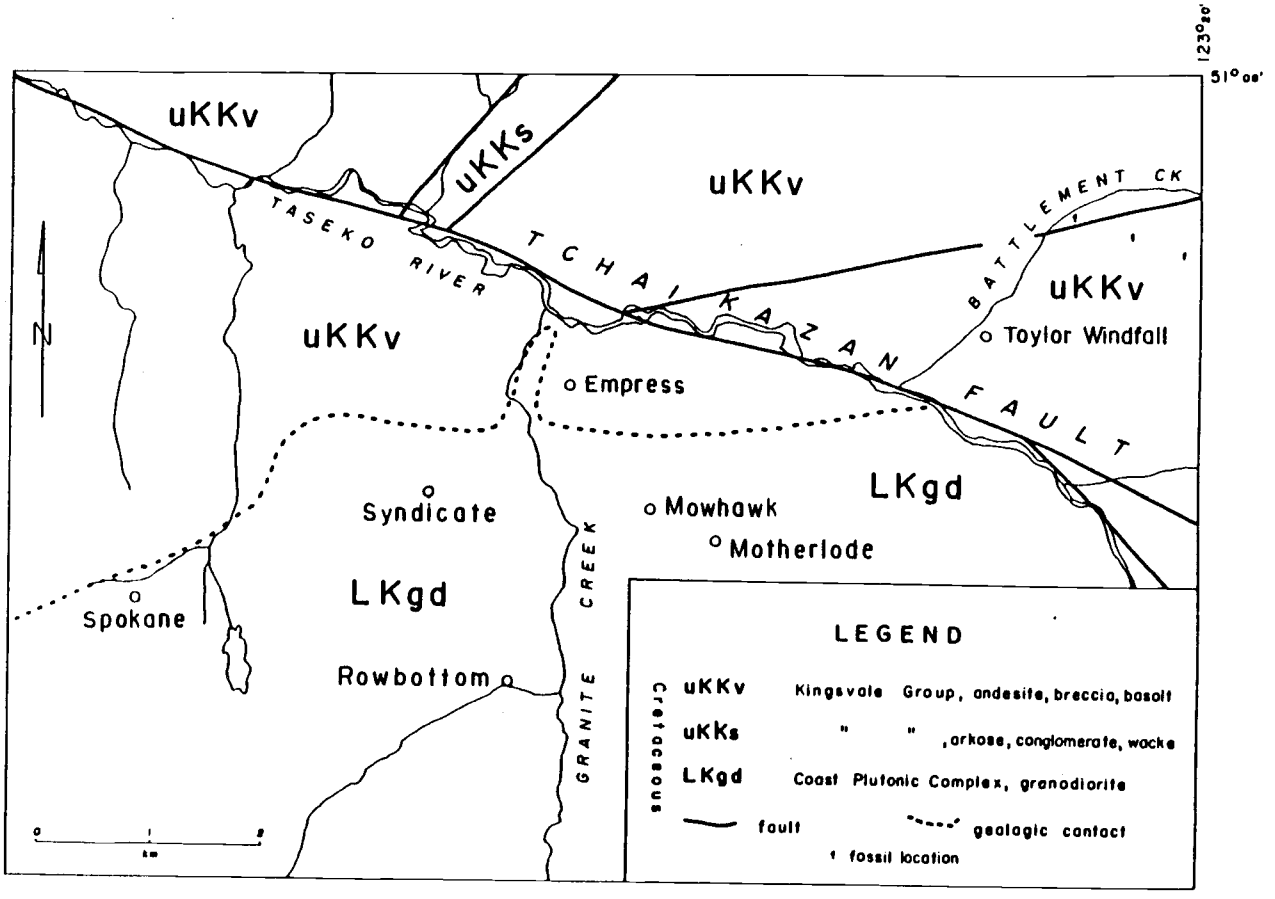

Figure 3. Regional geology and metal prospects. Modified after Bradford (1984) and Roddick et al.(1979).

workings and camp were then refurbished, and diamond drilling was undertaken, but the results of the drill program are not available.

A crew of three from Westmin Resources mapped (1:500) and sampled rock and soil in the immediate mine area for five weeks in 1983. Westmin returned for three months in 1984, as part of a joint venture with Esso Resources of Canada. Work completed during the 1984 field season included:

1) geophysical exploration that consisted of an induced polarisation survey, a very low frequency survey, and a magnetometer survey (grid spacing of 25 m by 50 m);

2) back hoe trenching;

3) diamond drilling (BQ and HQ) of approximately 800 m;

4) refurbishing of about 500 m of underground workings;

5) mapping (1:200) of 770 m of underground workings;

6) remapping (1:200) of the surface area in the immediate vicinity of the mine;

7) rock chip (panel) sampling of about 400 m^2 of the underground workings; and

8) property surface mapping (1:1000).

The results of these efforts will be described in forthcoming chapters where they are relevent to this study of the Taylor-Windfall prospect.

REGIONAL GEOLOGY AND TECTONIC SETTING

Taylor-Windfall is situated in the centre of the Tyaughton Trough, on the western flank of the Intermontane Belt, as displayed in Figure 1. The Tyaughton Trough is a successor basin, established after mid-Jurassic tectonism in the Omenica Crystalline Belt (Eisbacher, 1974). Closure of the Tyaughton Trough may have occurred after the final stage of accretion of the Wrangellia island arc terrane (Davis et. al, 1978), or after emplacement of the subduction-related Coast Plutonic Complex (Monger and Price, 1979). Both events would have occurred during mid-Cretaceous to mid-Jurassic times (Monger and Price, 1979).

The Tyaughton Trough trends northwest, subparallel to the contact between the Coast Plutonic Complex and the Intermontane Belt, and to the major faults of the area (Fig. 2). The trough is filled with a succession of immature sedimentary rocks, mafic volcanic flows, and pyroclastic deposits 4000 m in thickness (Wheeler et. al, 1972). Direction of sediment transport was from the northeast and southwest (Eisbacher, 1974). Relative and absolute timing of orogenic events such as faults, magmatism, uplift, erosion and deposition, is considered "obscure" by Monger and Price (1979). Souther (1967) states that the eruption of Cretaceous and Early Tertiary volcanic rocks in the Intermontane Belt and on eastern flank of the Coast Plutonic Complex is "approximately coincident" with the development of the Coast Plutonic Complex, and therefore intrusive and extrusive rocks are comagmatic.

At present, the Tyaughton Trough is bound on the southwest

by the Jurassic-Cretaceous Coast Plutonic Complex, and on the northeast by a thick succession of Cenozoic flood basalts (Fig. 2).

Intrusive history

Intrusive phases of the Coast Plutonic Complex are well-exposed over hundreds of square kilometers to the southwest of Taylor-Windfall (Fig. 2). McMillan (1976) described the plutonic rocks which outcrop to the immediate southwest of Taylor-Windfall as sparingly porphyritic quartz diorites and quartz monzonites. Alhough his petrographic descriptions are limited, incipient propylitic alteration is implied by mineral assemblages and alteration styles (chloritized biotite, carbonates, and sericite).

McMillan (1976) dated a suite of rocks consisting of biotite from a granodiorite, sericite from an "alteration zone", and biotite from a post-ore dyke, all collected from the Mohawk prospect that is about 4 km west-southwest of the Taylor-Windfall property (Fig. 3). The respective ages as obtained by the potassium-argon method are: 86.7 +/ 2.6 Ma; 84.9 +/ 2.5 Ma; and 84.7 +/ 2.5 Ma. It is probable that McMillan dated secondary alteration biotite and sericite, rather than primary magmatic minerals, and thus his ages may reflect post-intrusion alteration, rather than crystalisation of a magma. Therefore the ages of plutonic rocks in the area are not known with certainty.

The nature of the intrusive-extrusive contact in the Taylor-Windfall area is unclear from the literature. Dolmage (1929) described the contact as concordant to the strike and dip of the volcanic bedding which was confirmed by Quintana (1976), who drilled eight holes (100 to 250 m deep) over an area of about 800 square m at

the Granite Creek property (located in Fig. 3). Although it has been assumed that the pluton intruded the volcanic rocks, the evidence does not preclude the possiblity that the volcanic rocks were emplaced on top of the pluton.

Extrusive history

A succession of predominantly subaerial volcaniclastic rocks having a thickness of 1500 m overlies the pluton in the immediate mine area. The stratigraphic sequence consists of basal andesitic volcaniclastics intercalated with lesser amounts of vitric tuffs and and andesitic flows, which are overlain by a thick succession of coarsely crystalline andesite flows intercalated with lesser shaley mudstones, tuffaceous wackes and conglomerates that are capped by an agglomerate. Younger dykes of felsic and intermediate composition cut across all units except the upper flows.

All units are concordant, strike N090E, and dip 20 to 25^{o} to the north, except where they are locally structurally disturbed. Coarse andesite agglomerate, which has clasts up to 25 cm in diameter, is exposed in the upper reaches of Battlement Creek. The presence of coarse clasts indicates proximity to a vent that probably formed above a small intrusive body, such as the quartz diorite that crops out at the headwaters of Battlement Creek. Other evidence of a vent has been removed by glacial erosion.

Rocks that host the Taylor-Windfall prospect have been mapped as members of the "Eocene or Oligocene (?)" Sheba Group (Tipper, 1978), which is composed of buff, mauve, and brown dacitic and rhyolitic tuffs, breccias and flows. However, plant fossils from the shaley mudstones (Fig. 3), have been dated as Late Cretaceous in age (Esso

Minerals, per. comm., Appendix 5). Thus, the successions of chiefly volcanic rocks in the Taylor-Windfall area are more likely to be members of the Cretaceous Kingsvale Group, which consists of interbedded greywacke, conglomerate and shale, and basaltic to dacitic agglomerate, breccias and tuffs, minor flows and volcaniclastic sediments (Jeletzky and Tipper, 1968; Tipper, 1978). These rocks are also mapped as Cretaceous in the 1:1,000,000 scale compilation map (Roddick, et. al, 1979), and the author is unsure if Roddick assigned them to the Cretaceous System, or if the small scale of the map did not permit Roddick to differentiate between Cretaceous and Miocene rocks.

Structure

Deformation structures in the Tyaughton Trough consist of large scale broad open folds in the northern area, and northwest-trending dextral strike-slip faults and associated west-dipping northeast-directed thrust faults in the central area (Wheeler, et. al, 1972). Major dextral faults are the Fraser, Yalakom, Taseko, and Tchaikazan faults, as shown in Figure 2. Right lateral displacement along the Yalakom Fault is about 37 km for rocks of the Upper Cretaceous, and 220 km for those of the Middle Jurassic (Tipper, 1969). Oblique plate movement during island arc accretion and associated subduction probably were the causes of these fault movements (Wheeler et. al, 1972).

Taylor-Windfall is bound on the south by the Tchaikazan Fault. The trace of this fault is expressed by the west-northwest trends of the Taseko River and the contact between the Coast Plutonic Complex and the Kingsvale Group (Tipper, 1978). The age of the fault is not

clear (Tipper, 1978), although it is post-Kingsvale and has a displacement of about 14 km, as was measured 50 km to the northwest of the Taylor-Windfall property (Tipper, 1969).

Tipper (1978) mapped a major fault which trends N070E along the trace of Battlement Creek. It is truncated to the south by the Tchaikazan Fault, and to the north by another northwest-trending fault. Neither slickensides nor displaced bedding were observed along Battlement Creek, possibly because of removal by glacial and fluvial erosion, though a high density of fractures trend N060E and parallel to this fault at Taylor-Windfall.

Displacements along these large-scale faults occurred over an extended period of time, and were concurrent with intrusive activity, volcanism, and alteration-metalisation. These large-scale faults probably acted as conduits for ore-bearing hydrothermal fluids and their presence enhances the potential of the Tyaughton Trough as a metal-producing area.

Alteration and metalisation

Regional alteration of the contact area between the Coast Range Plutonic Complex and Kingsvale Group over a width of about 5 km and a length of about 12 km has been described in detail by MacKenzie (1920). All rocks are propylitically altered to mineral assemblages containing chlorite, magnetite, apatite, epidote, calcite, pyrite, quartz, and secondary biotite as a consequence of the destruction of primary feldspar and hornblende.

Esso Minerals of Canada conducted a reconnaissance survey of the area (Bradford, 1984). Although the results are confidential,

this work identified extensive areas are argillic alteration consisting of pyrophyllite, alunite, dickite, kaolinite, and quartz. Controls for the localization of this alteration are proximity to plutonic rocks, density and orientation of fractures and faults, and types of host rock. Pyrite and tourmaline are sporadically distributed but highly concentrated in the volcanic rocks (Bradford, 1984, per. comm.). Post-glacial supergene alteration of pyritic volcanic rocks has resulted in the formation of extensive and thick masses of surficial limonite (MacKenzie, 1920).

In addition to the Taylor-Windfall property, there are seven other metal prospects in the area (Fig. 3). These consist of the Buzzer, Motherlode, Mowhawk, Rowbottom, Syndicate, and Spokane properties that are hosted by plutonic rocks and are characterized by vein and disseminated types of metalisation. Ore minerals found at these prospects are chalcopyrite, pyrite, scheelite, tennantite, hematite, covellite, digenite, sphalerite, galena, arsenopyrite, molybdenite, native silver, and native gold (Bradford, 1984; McMillan, 1976). The Empress prospect is hosted by volcanic rocks, and has disseminated pyrite, chalcopyrite, magnetite, pyrrhotite, hematite, and molybdenite (Quintana, 1976). Concentrations of gold and silver at these properties are reportedly low.

PROPERTY GEOLOGY

Host rocks of the Taylor-Windfall property consist of a concordant succession of hydrothermally altered tuffaceous lithic and vitric andesites, that strike N090E and dip 25^{o} to the north, as shown in Figures 4 to 7b (in map pocket). Graded bedding implies that the succession is upright. Although seven volcanic units were identified in the field, fifteen alteration sub-units were subsequently identified in the laboratory, and all are described in the following text, under rock units.

Structures at the Taylor-Windfall property are not complex, and may be related to two phases of brittle deformation. An early, very dense set of high angle fractures, oriented at N060E is offset by a later set of high angle fault and shear zones that trend N030W. The younger faults display both right lateral and vertical movement. Detailed descriptions of these and other minor faults are presented in the following text, under structure.

All rocks at the prospect have undergone hydrothermal alteration, ranging from weak propylitic alteration, to near complete silicification. The discussion of alteration constitutes the bulk of this study, as the alteration mineralogy and distribution of assemblages define the hydrothermal system responsible for the deposition of metaliferous mineralisation.

An auriferous tourmaline vein (100 m by 150 m by 0.2 m) and an auriferous sulphide vein (dimensions unknown), oriented at N060E, located on the 1648 m level (Figs 4-7a), constitute the only sub-economic concentrations of metals, known at this time.

Rock units

Data from mapping (1:200), thin section examination, and X-ray diffraction (XRD) analyses have been used to identify five concordant volcanic units and single dykes of andesite and quartz diorite at the property. These are described in order from oldest to youngest below, and depicted on Figures 4, 5, and 6 which are 1:500 property maps, reduced from 1:200. Concordant flows, ash fall tuffs, tuffaceous sediments, and black shales which are located up section and to the east of the mine were mapped (1:1000) by the author, R. Lane, and, R. Britten. Descriptions of the eastern area are beyond the scope of this study.

The detailed mapping, confined to the mine and immediate area, was done in order to establish the controls of metal distribution, rock types, structure, and alteration. Properties that may control metal localization are porosity, permeability, mineralogical and chemical composition of host rocks, density and orientation of faults and fractures, and relative ages of rocks and structures. All of these properties determine the susceptability of the host rocks to alteration and metalisation.

All host rocks of the Taylor-Windfall property have been variably altered. The intensity of this alteration ranges from incipient sericitization of feldspars and chloritization of mafic minerals (propylitic alteration) to pervasive silicification. For this reason, alteration sub-units were mapped, based on the predominant mineral assemblages (ie. epidote-feldspar), and mineral percentages (ie. 30 to 50 percent quartz). Mineral percentages have been estimated visually from thin sections, except for those of quartz, kaolinite, and dickite

that were determined using quantitative XRD methods as described in Appendix 1. Alteration sub-units crosscut lithologies, but nomenclature is maintained in order to avoid confusion. For example, units 1A, 2A, 3A, 4A, and 5A have similar but not identical kinds and abundancies of alteration mineral assemblages. Each unit is given both a compositional and a textural or structural name. The composition stated is pre-alteration, determined either from the An-content of the plagioclase feldspar (Michel-Levy method), or by spatial associations with less altered rocks.

As the diffuse alteration contacts crosscut all units, mineral assemblages are merely listed for each unit, and a reference sample number is provided. Locations of reference samples are plotted on the 1:500 scale maps, and mineralogies of these samples are in Appendix 1. Mineral descriptions and associations are provided in the following section under alteration to avoid the redundancy of repeatedly describing some alteration minerals which were observed in almost every unit and sub-unit (ie. tourmaline).

Andesite lithic/crystal tuff (Unit 1) Unit 1 is well-exposed on surface, and at the 1648 m level portal. Hand samples are dark gray-green, and are locally mottled with aggregates of a subrounded dark mineral (0.5 cm diameter) comprising up to 15 percent of the host. This basal unit is more than 50 m in thickness (Lane, 1983).

Pyroclastic textures are evident in thin section, as shown in Plate 1. Subrounded lithic fragments (1.5 mm in diameter) constitute 30 to 50 percent of the rock. Andesine (An 37) crystals and crystal fragments constitute about 30 to 40 percent. Plagioclase feldspars

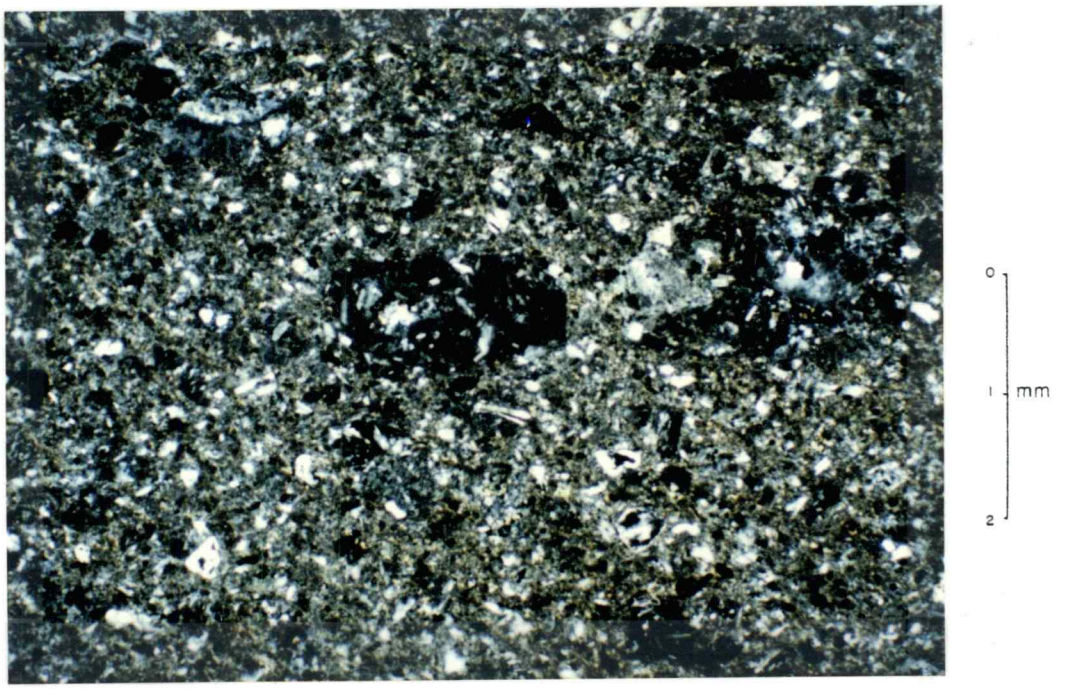

Plate 1 . Photomicrograph of unit 1 under crossed nicols. A lithic fragment is surrounded by feldspar crystals and crystal fragments. Sample GP 84 34D.

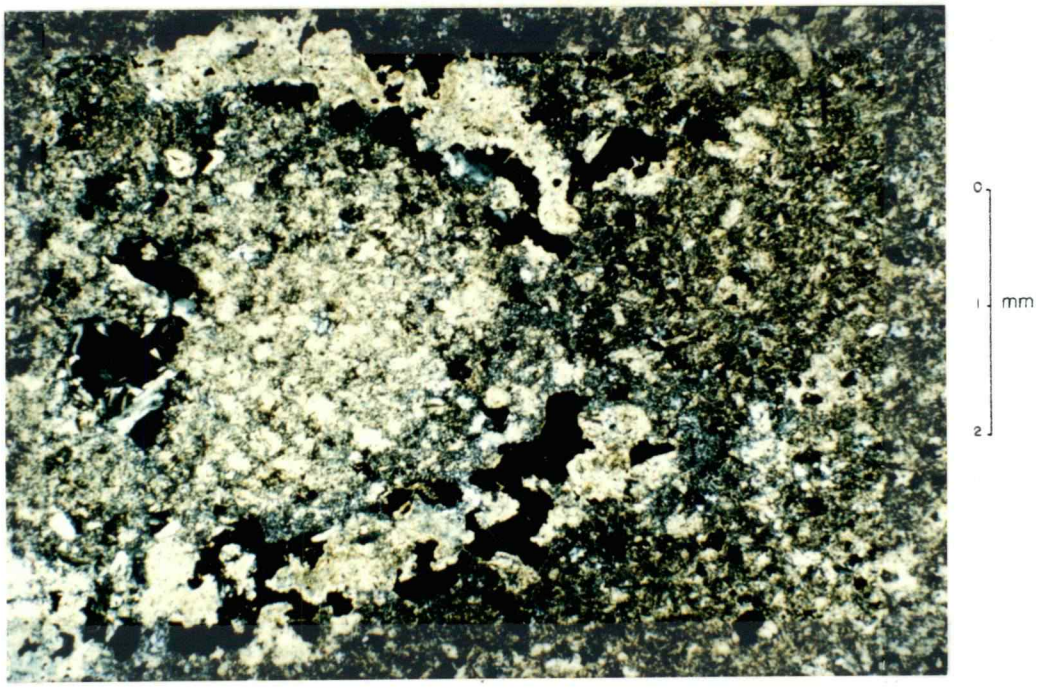

Plate 2. Photomicrograph of sub-unit 1A under crossed nicols. Orbicular texture overprints but has not destroyed the tuffaceous volcanic texture. Sample GP 84 31D.

are bimodal in size; 2 percent are as large (4.5 mm) phenocrysts which exhibit up to 80 percent replacement by sericite, and the remainder are as smaller (0.5 mm) pristine to weakly sericitized crystals and crystal fragments. Biotite, chlorite, and muscovite have replaced hornblende, and occur as 3 mm dark subrounded knots (5 percent of total rock). Groundmass, (less than 30 percent of the total rock) consists of chlorite, quartz, muscovite, dickite, kaolinite, pyrite, Fe-oxide, rutile, apatite, and epidote (sample GP84 34G).

The andesite tuff has been divided into four sub-units, 1A, $1A_1$, 1AA, and 1B. Sub-unit 1A is dominated by sericite (40 percent), and has combined kaolinite and dickite (3 to 13 percent), quartz (25 to 30 percent), chlorite (15 percent), and trace amounts of pyrite, tourmaline, corundum, apatite, iron oxide, and rutile (sample GP84 41D). Original volcanic texture is poorly preserved, and may be observed petrographically in reflected light.

An unusual alteration texture locally overprints, yet has not destroyed, the original volcanic textures as shown in Plate 2. The overprinting texture consists of spheres (0.5 to 2.5 cm in diameter) of various alteration minerals arranged as vague layers or radiating spokes. The author refers to these as "orbicules", and neglects the Bates and Jackson (1980) definition of orbicules which includes concentric layering. Not all orbicules at Taylor-Windfall have well-defined concentric layering. The mineralogy of the orbicules is variable and consist of tourmaline, quartz, sericite, koalinite, dickite, chlorite, pyrite, and tennantite. Orbicules locally define bedding as shown in Plate 3, and are cross-cut by N030W fractures.

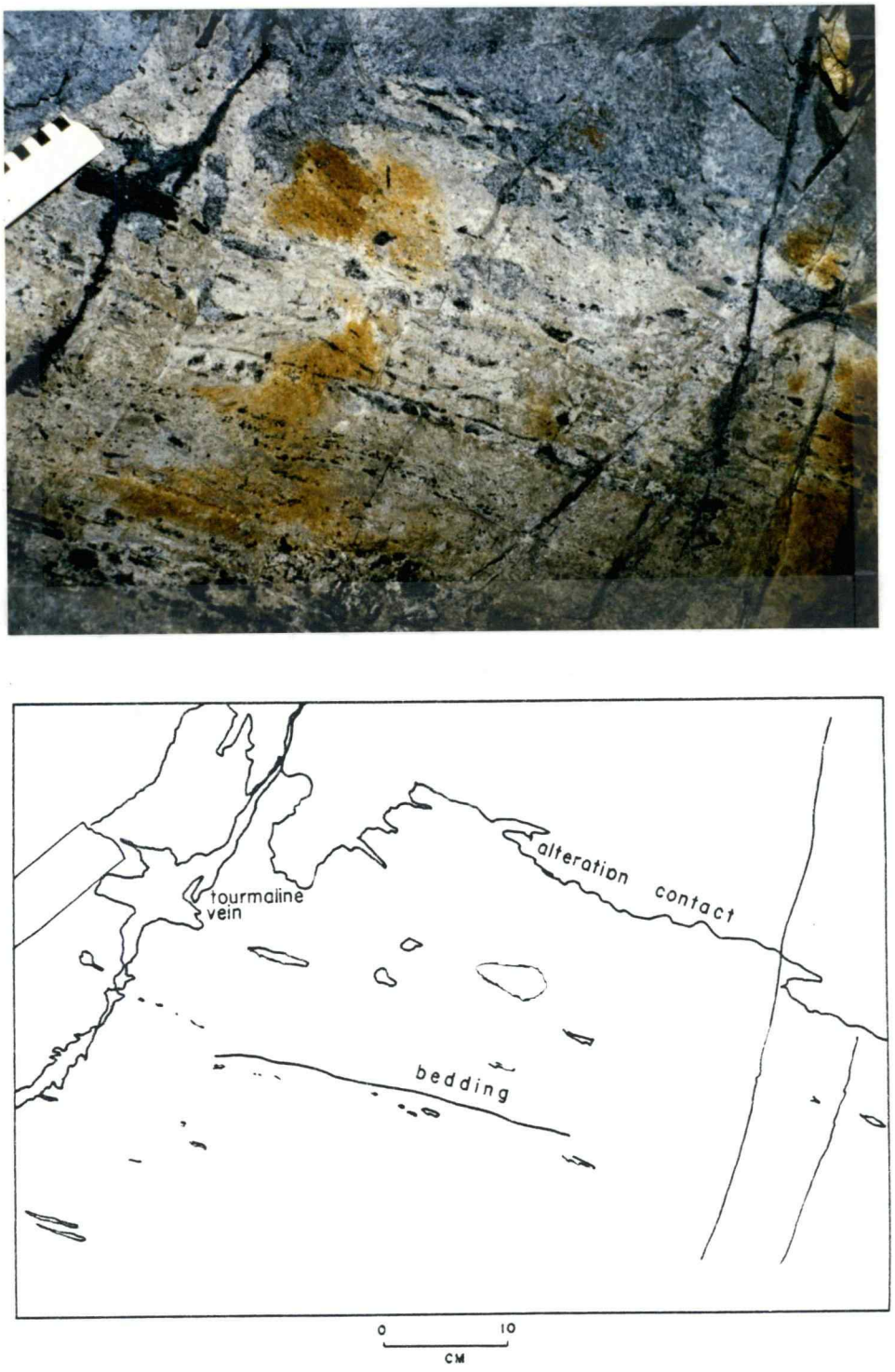

Plate 3. Photograph of sub-unit 1B in the 1648 m level. Orbicules are elongate parallel to the alteration contact and bedding.

They are confined to sub-unit 1A in the 1648 m level.

The mineralogy of remaining sub-units $1A_1$, 1AA, and 1B is similar to that of sub-unit 1A. However, sub-unit $1A_1$ has an additional 5 to 15 percent andalusite, and a lack of epidote (sample GP84 43C). Sub-unit 1AA has up to 5 percent epidote (sample GP84 33A). Sub-unit 1B is richer in quartz (30 to 50 percent), and has less combined kaolinite and dickite (less than 5 percent) and less sericite (25 to 45 percent) than sub-unit 1A (sample GP84 28A).

Welded andesite/dacite (?) vitric ash tuff (Unit 2) Unit 2 is best exposed in the 1763 m level, where it is strongly altered and original volcanic textures are preserved. Less altered rocks crop out on the north side of Battlement Creek, where the alteration minerals are more destructive of original textures. The rock is mottled pale gray to bleached white and has vague lineations of darker coloured elongate forms. Eutaxitic textures are observed in thin section. Shards, up to 2.0 mm long are moderately to strongly welded, as portrayed in Plate 4. The original composition of unit 2 is not known, as no primary volcanic minerals are present. A sharp, concordant contact between units 2 and 1 is observed on surface, and nowhere else. Unit 2 is 10 metres thick.

The welded andesite tuff has been divided into two sub-units. They consist of; sub-unit 2A, which has 20 to 35 percent quartz, and variable amounts of sericite, kaolinite, dickite, pyrophyllite, pyrite, chlorite, tourmaline, and possibly corundum (sample GP 84 6A), and sub-unit $2A_1$, which has an additional 5 to 15 percent andalusite (sample GP84 1B). Pyrite has formed a coarse dendritic arrangment of crystals up to 3 cm long, in local concentrations in sub-unit $2A_1$.

Plate 4. Photomicrograph of sub-unit $2A_1$ under plane polarised light. Poorly welded shards have been devitrified and replaced by andalusite, quartz, sericite, and dickite/kaolinite. Sample GP 84 3.

Andesite lithic/crystal tuff (Unit 3) The least altered sample of this andesite is mottled green, and has 80 percent subrounded to angular coarse ash (3 to 4 mm) lithic fragments as shown in Plate 5. Lithic fragments contain variable amounts of Fe-oxide, ghosts of feldspar microlites and larger feldspar laths, mafic phenocryst ghosts, and shards. Some lithics have up to 70 percent Fe-oxide, others, up to 70 percent shards, and others exhibit a pumiceous spongy texture. Devitrified and altered glass, identified by small scale flow textures, and amygdules defined by Fe-oxide rims are interstitial to the lithics. Composition of the matrix is; 20 to 40 percent andesine (An 49) which exhibits up to 80 percent alteration to sericite, 25 percent secondary biotite, 10 percent chlorite, and trace amounts of quartz, pyrite, tourmaline, sericite, rutile, and apatite (sample GP84 29B).

Sharp concordant contacts between units 3 and 4, and 3 and 2 are observed from surface exposures that are peripheral to the area of most intense alteration. Within unit 3, faults and sharp contacts between alteration sub-units are parallel to subparallel to bedding as shown in Plates 6 and 7.

Unit 3 is of interest as it exemplifies a possible stratigraphic control over the distribution of alteration minerals and associated metals. It was originaly mapped as a rhyolite (Dolmage, 1932) because of the high SiO_2 content of some beds. It is 110 m thick (Lane, 1983).

This tuffaceous andesite has been divided into six sub-units, 3, 3AA, 3A, $3A_1$, 3B, 3C, and 3Cl. Sub-unit 3AA is similar to unit 3, and has an additional 5 percent epidote. Sub-unit 3A is comprised of

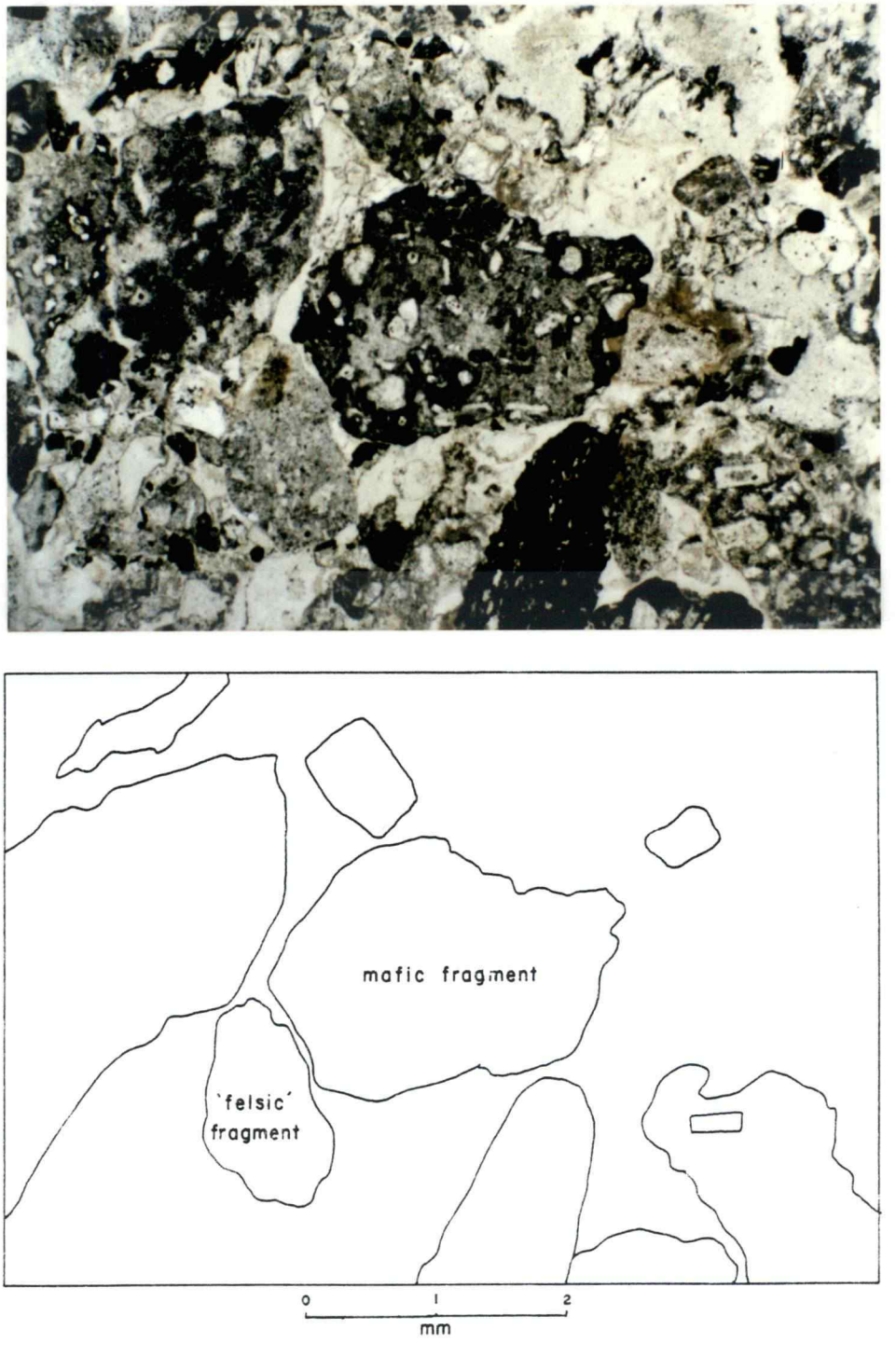

Plate 5. Photomicrograph of sub-unit $3A_1$ under plane polarised light. Subrounded lithic fragments are of variable composition. Sample GP 84 44E.

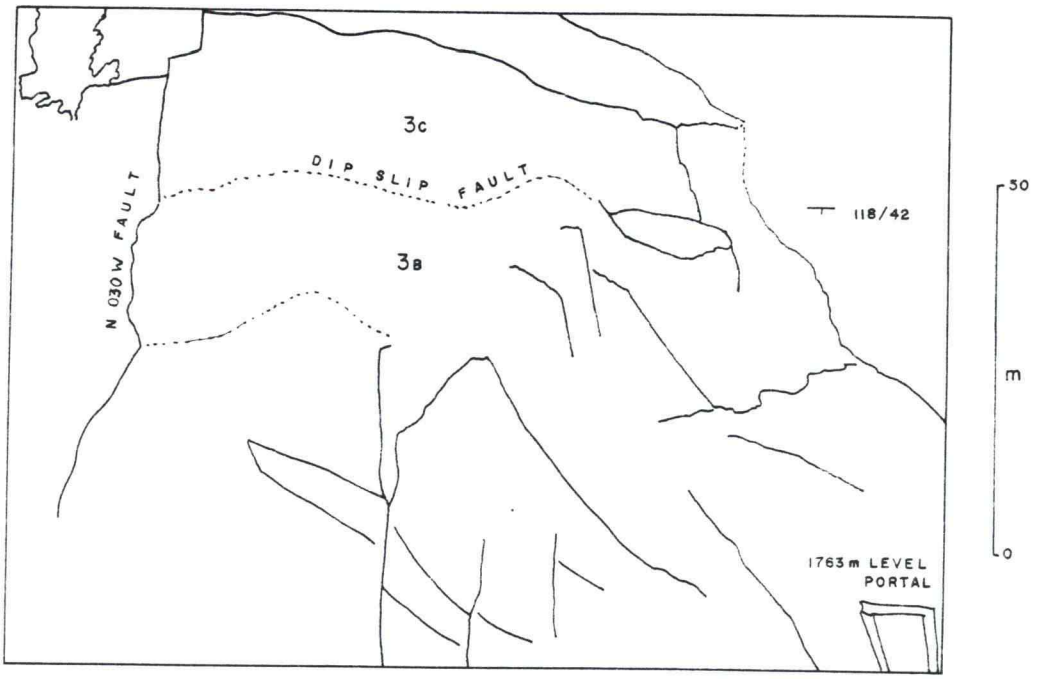

Plate 6. Photograph taken facing south on the south bank of Battlement Creek. Alteration contacts and a fault plane are parallel to bedding.

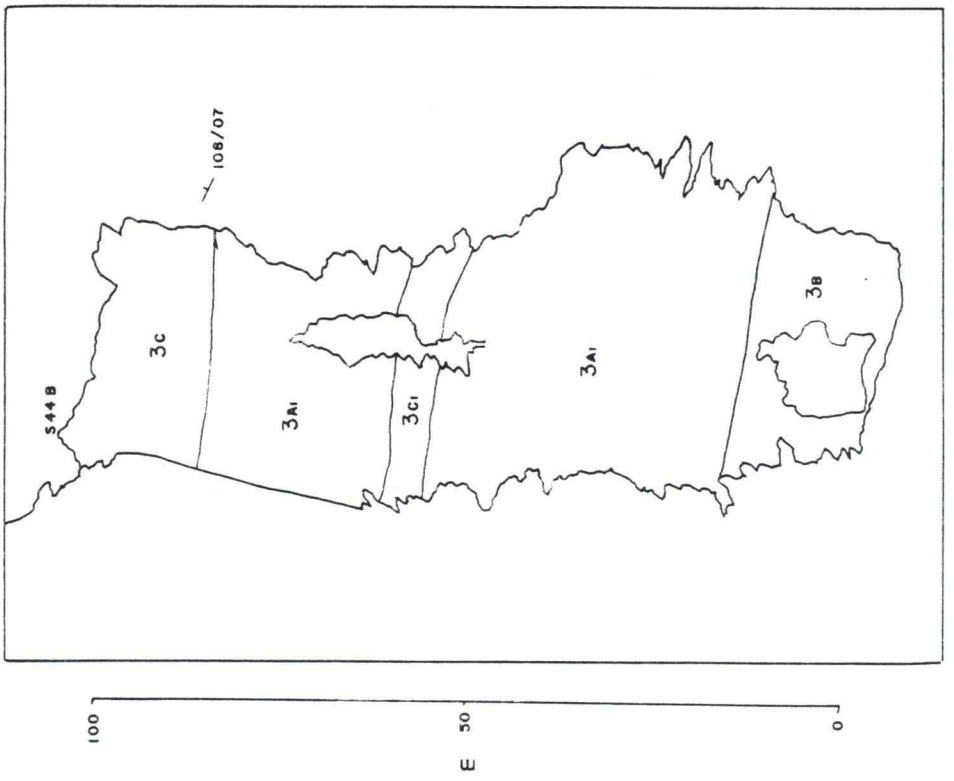

Plate 7. Photograph taken facing north on the north bank of Battlement Creek. Alteration contacts are parallel to bedding.

sericite (40 percent), quartz (25 to 30 percent), chlorite (15 percent), kaolinite and dickite (3 to 13 percent) and trace amounts of pyrite, tourmaline, corundum, apatite, iron oxide, and rutile. Original volcanic textures are poorly preserved. Sub-unit $3A_1$ is similar but has 5 to 25 percent andalusite, and possibly pyrophyllite (sample GP 84 44C). Sub-unit 3B has a higher percentage of quartz (30 to 50 percent), variable amounts of sericite (25 to 45 percent), less combined dickite and kaolinite (5 percent), and trace amounts of pyrite, tourmaline and rutile (sample GP84 41A). Sub-unit 3C is the erosionally resistant "siliceous ridge" (a term used by the property geologist), which has greater than 50 percent quartz, less than 1 percent kaolinite, and a remainder of tourmaline, pyrite, and sericite (sample GP 84 37B). Sub-unit $3C_1$ has a similar mineralogy to the "siliceous ridge", and in addition has 5 to 15 percent andalusite.

Andesite lithic/crystal tuff (Unit 4) Unit 4 was easily identified in the 1648 m level, where it is peripheral to the areas of most intense quartz-sericite alteration. Contacts are sharp, and it is only about 3 m thick. The tuff is dark green, and has subrounded to angular lithic fragments (up to 1.2 mm diameter) and crystals (0.5 mm). The lithics are of variable original composition and have different proportions of sericite and Fe-oxide, as observed in thin sections and illustrated in Plate 8. Lithics constitute 40 to 60 percent of the rock, and are comprised of feldspar laths set in a fine-grained chlorite-sericite-quartz-Fe-oxide groundmass. The remainder of the rock is composed of: 30 percent andesine (An 43) as 0.03 mm laths and crystal fragments, some of which are zoned, and all of which exhibit sericite replacement of 1 to 30 percent; 40 percent

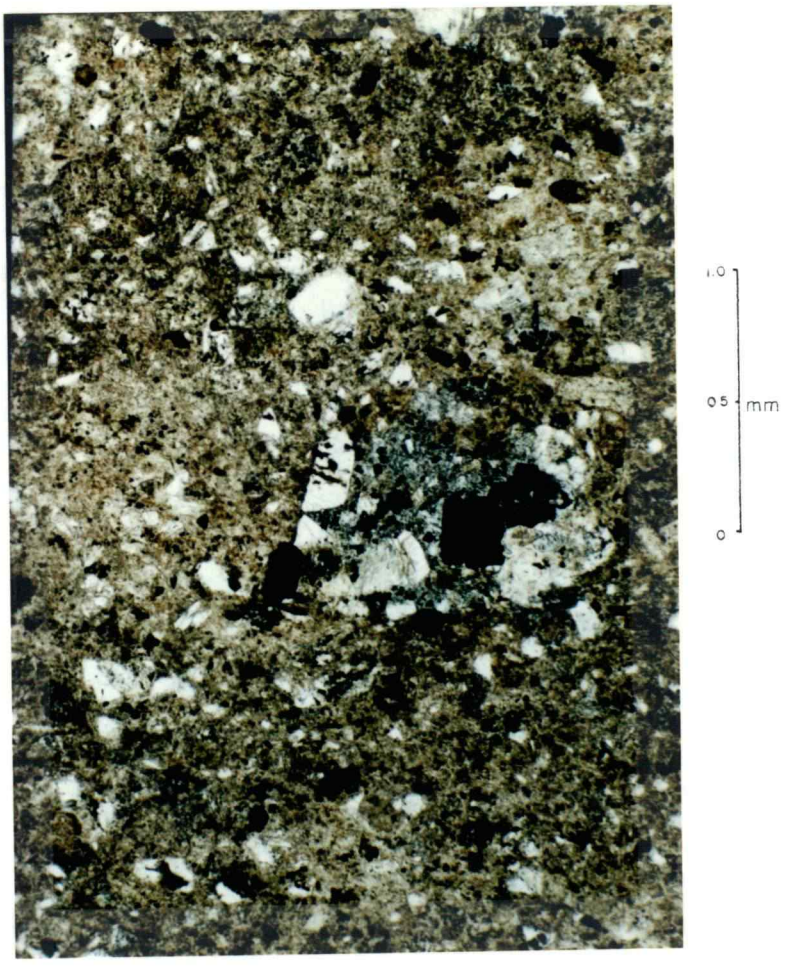

Plate 8. Photomicrograph of unit 4 under plane polarised light. A poorly defined chlorite- pyrite-rich lithic fragment is surrounded by feldspar fragments, and a sericite-rich matrix. Sample GP 84 20I.

combined sericite and quartz as a fine grained matrix; 20 percent chlorite as replacement of euhedral laths and as matrix; and traces of pyrite, biotite, rutile, tourmaline, apatite, and possibly clinozosite (sample GP84 20I).

This lithic tuff has only one sub-unit (4A) which is comprised of 15 percent sericite, 15 percent combined dickite and kaolinite, 25 percent chlorite, 25 percent quartz, and trace amounts of tourmaline, pyrite and rutile (sample GP 84 24G).

Andesite flow (Unit 5) This medium to dark green andesite flow is easily recognized by its porphyritic texture. Contacts are sharp, and the thickness is about 20 m thick (Lane, 1984).

Unit 5 is comprised of: 40 percent andesine (An 49) laths of bimodal size (2.0 mm 0.4 mm) that range in alteration from 10 to 50 percent replacement by sericite, and are locally resorbed; 30 percent combined sericite and chlorite as pseudomorphs of pyroxenes (1.5 mm), and as matrix replacement; and trace concentrations of pyrite, dickite, kaolinite, tourmaline, quartz, clinozoisite, apatite, and rutile (sample GP84 21C). Plate 9 illustrates a weakly altered sample.

The andesite flow has been divided into two sub-units, 5A and 5AA. Sub-unit 5A is comprised of 20 percent sericite, 15 percent combined dickite and kaolinite, 15 percent chlorite, 30 percent quartz, and trace amounts of pyrite, tourmaline and rutile (sample GP84 20B). The original texture is well preserved, as shown in Plate 10. Sub-unit 5AA exhibits strong magnetism, but appears to be similar in mineralogy to sub-unit 5A (sample GP 84 21C).

Andesite dyke (Unit 6) The dyke is exposed only in the main drift

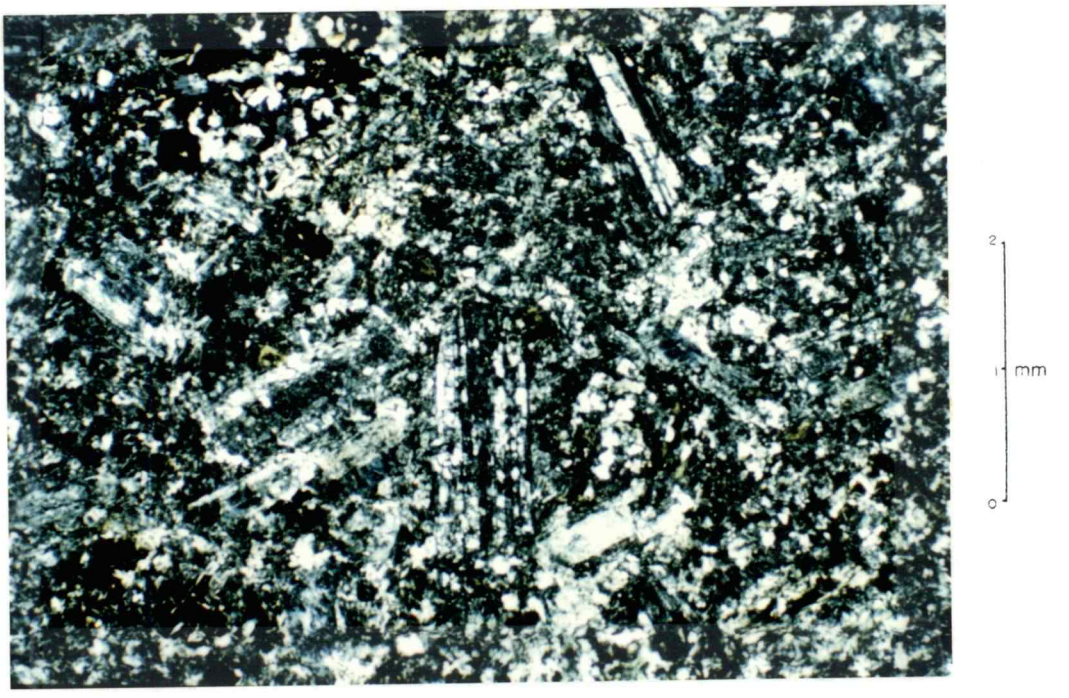

Plate 9. Photomicrograph of unit 5 under crossed nicols. Feldspar phenocrysts exhibit 15 to 30 percent replacement by sericite, chlorite, and quartz. Sample GP 84 21C.

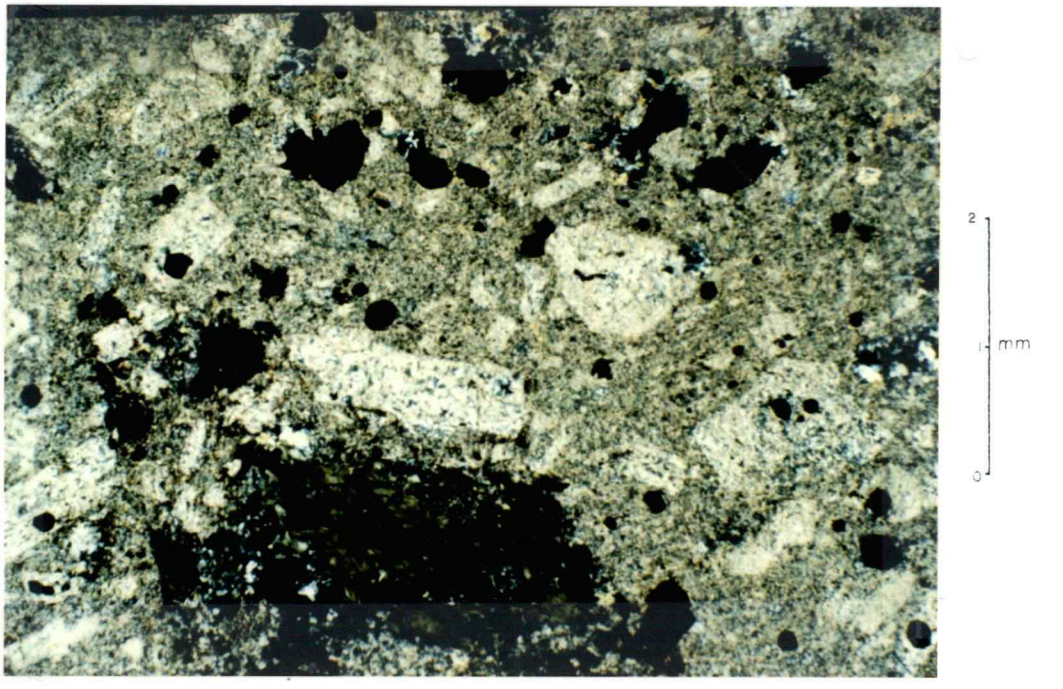

Plate 10. Photomicrograph of sub-unit 5A under crossed nicols. Feldspars have been totally replaced by sericite, quartz, kaolinite/dickite, and amphiboles replaced by chlorite. Sample GP 84 20B.

of the 1648 m level. Rocks are bleached pale green, and have 8 percent amygdules which are filled with laumontite and traces of epidote as was observed in hand samples. Amygdules are elongate, well-aligned, and range from 1 to 10 cm in length. Laumontite also occurs as aggregates that replace euhedral lath-shaped feldspars. Quartz eyes (1 percent) are also visable in hand sample. A weak trachytic texture is evident in thin section, as shown in Plate 12.

The andesite dyke is comprised of 60 percent andesine (An 36) as euhedral laths which are weakly altered to epidote and sericite, 20 percent epidote as ragged anhedral aggregates that have replaced interstitial material, 5 percent combined secondary biotite and chlorite as feathery anhedral crystal aggregates that have completely replaced poorly to well defined amphibole crystals (0.1 mm), 5 percent quartz as eyes (1.8 mm) and fine-grained matrix, and trace amounts of apatite, dickite, kaolinite, and rutile (sample GP84 21C). The dyke is about 8 m thick and has sharp contacts. It intruded the volcanic rocks after the period of brittle deformation that resulted in northeast-trending fractures and after metal deposition, as the dyke does not host veins, and the N060E fractures do not cut across it.

Quartz diorite (?) dyke (Unit 7) Two quartz diorite dykes (8 m thick) are exposed in the 1648 m level, and on surface. Dyke rocks are bleached white, and have a mylonitic-like texture defined by alternating quartz-rich and sericite-rich bands approximately 0.5 cm in width, as shown in Plate 11. Contacts are sharp and parallel to foliation, which implies that banding is a secondary tectonic feature. The quartz diorite dyke is comprised of 55 percent sericite, 40 percent fine grained quartz, 2 percent euhedral to subrounded

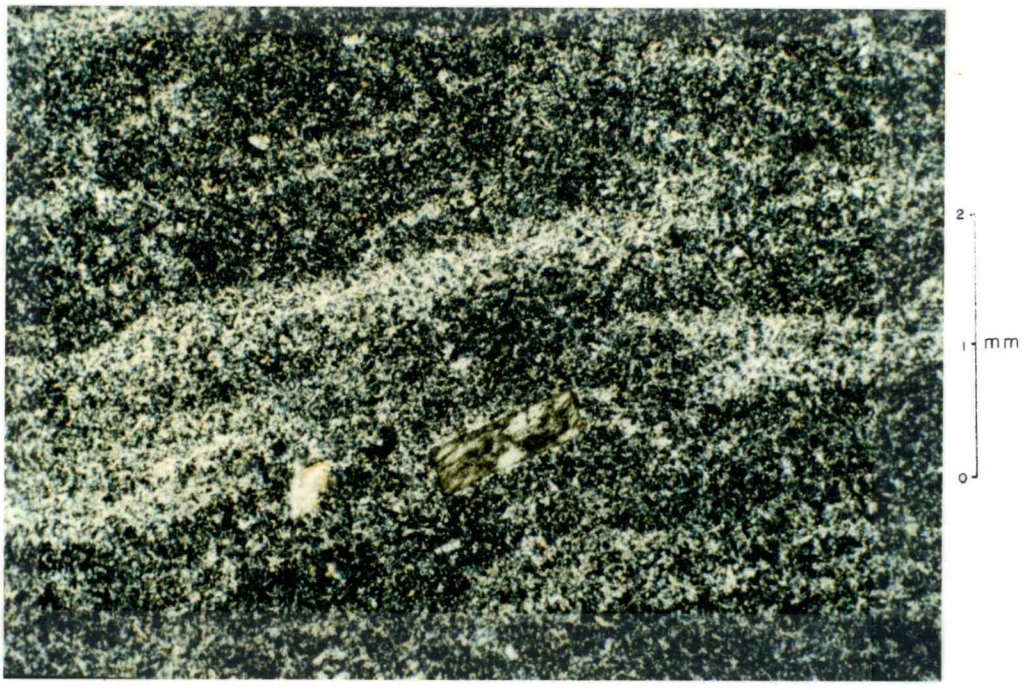

Plate 11. Photomicrograph of unit 7 under crossed nicols. Foliation is defined by quartz-sericite bands. Sample GP 84 23D.

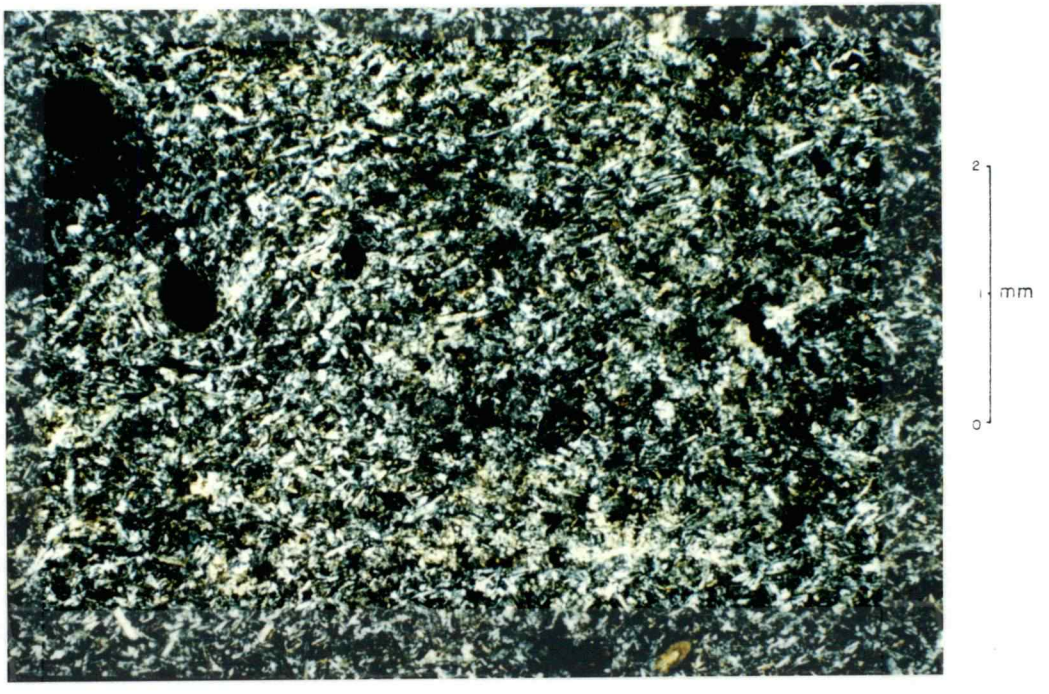

Plate 12. Photomicrograph of unit 6 under crossed nicols. Feldspars exhibit weak alignment. Sample GP 84 33D.

quartz eyes (1.8 mm), and trace amounts of plagioclase and rutile (sample GP 84 23D).

Structure

Two phases of brittle deformation are present in the Taylor-Windfall area. The first phase resulted in a predominant set of east-northeast fractures (N060E/75S), and a weak set of faults that trend parallel to bedding (N090E/20N). The second phase of deformation resulted in a conjugate pair of faults that trend north-northwest (N030W/88E) and northeast (N045E/85S). These structures are described below in order from oldest to youngest.

East-northeast set: These fractures have a consistently high density of 10 to 15 fractures per metre in the underground workings. Steep dips and their common association with volcanic rock suggest that they may have been volcanic cooling joints which were opened during a period of tension. Although offsets were not observed on any of these fracture planes local displacement is implied by the presence of gouge in a one of the fractures (referred to as the Shaft Shear Zone in old reports; Dolmage, 1932). The gouge is exposed in the 1707 and 1648 m levels and was identified in drill cores of DDH 85 03 and DDH 85 05 (Fig. 7b in map pocket). The majority of N060E fractures are coated by a 1 to 5 mm thick layer of dickite/kaolinite, sericite, chlorite, quartz, tourmaline, and/or pyrite. Poles to fracture planes that are coated by predominantly tourmaline and quartz are plotted on the stereoographic projections (Figs. 8a and 8b, respectively). Most tourmaline- and quartz-bearing fractures trend N060E, although quartz-bearing fractures exhibit a greater variability in orientation. Auriferous tourmaline-bearing fractures trend N060E and

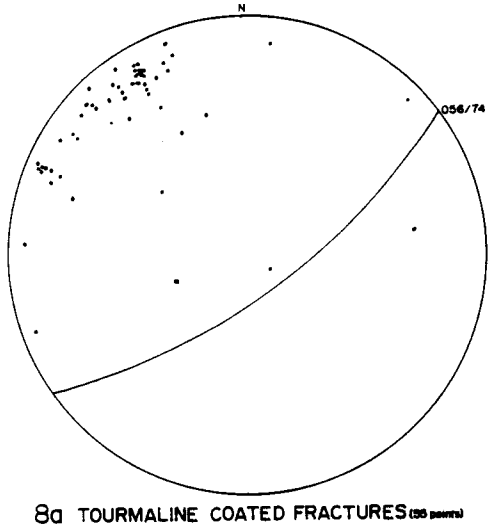

8a TOURMALINE COATED FRACTURES (55 points)

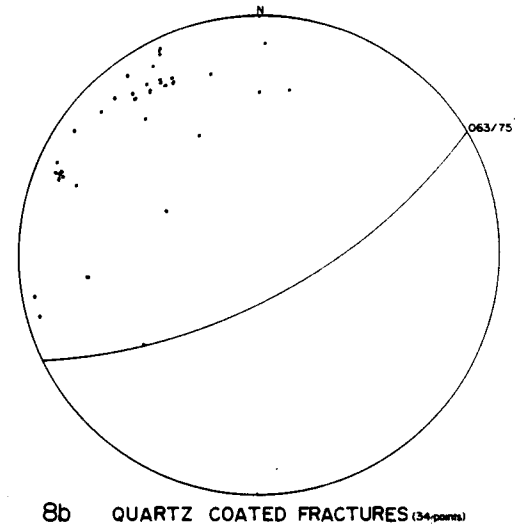

8b QUARTZ COATED FRACTURES (34 points)

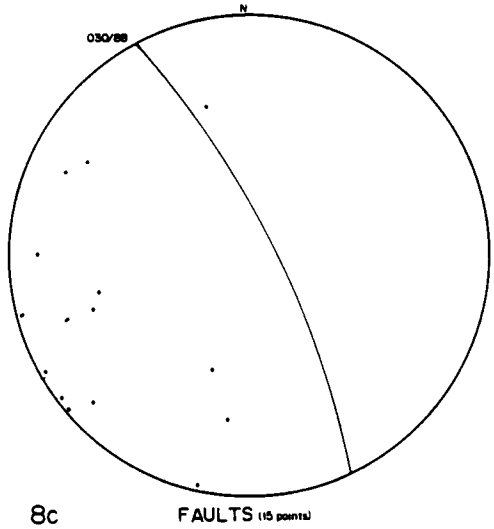

8c FAULTS (15 points)

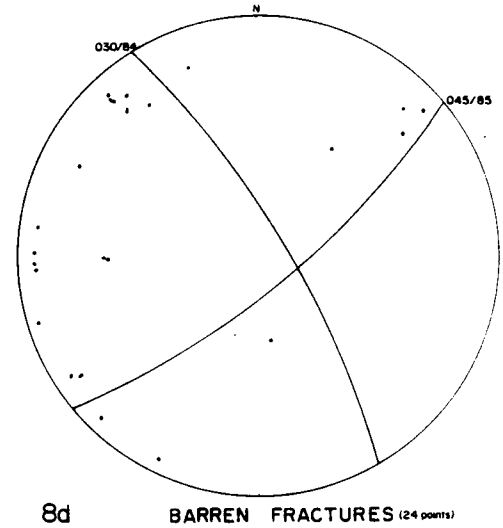

8d BARREN FRACTURES (24 points)

Figure 8. Stereographic projection of poles to the planes; 8a) tourmaline coated fractures, 8b) quartz coated fractures, 8c) faults, and 8d) barren fractures.

are described in a subsequent section of the text under metalisation.

East-west set: Displacement is minor on these bedding-parallel faults; rarely exceeding 2 m (Plate 6). Slickensides trend N060E, parallel to the dominant set of first phase fractures. A gold-bearing admixture of chlorite and tourmaline was noted in several fault planes on surface exposures above the 1707 m level. The mixture was removed in early days of mining, and now only boxwork after tourmaline remains.

North-northwest set: These faults are the dominant member of the conjugate pair that is associated with the second phase of brittle deformation. There are four major fault zones up to 10 m wide that trend N030W (Figs. 4, 5, 6, 7a, and 7b in map pocket). These faults exhibit 1 to 2 m of dextral displacement, and 100 to 200 m of vertical displacement. Evidence for vertical displacement is the juxtaposition of volcanic flows (Unit 5) and ash tuffs (Unit 1), and the vertical separation of an andalusite-bearing zone at depth from a similar zone at surface (Fig. 7a). Evidence for strike-slip displacement is the offset of the east-northeast set of faults, as was observed in the 1648 m level. Densely spaced planar structures that define the fault zones are coated by dickite/kaolinite, sericite, and tourmaline. Dykes of andesite and quartz diorite (Units 6 and 7) are oriented parallel to the faults, and are sheared parallel to their contacts; thus N030E faults predate and postdate dyke emplacement. Dykes and N030E faults crosscut the N060E and N090E structures. Poles to fault planes are plotted on the stereoographic projection in Figure 8c, and most planes where displacement was observed are oriented N030W. Poles to fractures that do not exhibit displacement are plotted on Figure 8d, and some planes are oriented N030W.

Northeast set: Poles to the planes of this weak set of faults are plotted on Figures 8d, and the conjugate relationship to the N030W fractures is shown on the summary projection in Figure 9. They exhibit offset of less than 5 cm, and are coated by dickite/kaolinite, sericite and chlorite.

In summary, an early tensional and densely spaced set of locally auriferous tourmaline-bearing fractures (N060E) and bedding plane faults (N090E) have been offset dextrally and vertically by a late set of faults (N030W).

Alteration

The discussion of alteration is presented in three sections; mineralogy, major oxides, and summary. In the first section mineral colours, textures, associations, and spatial distributions are discussed. Occurrences in known ore-related alteration systems are documented, to assure the reader that these minerals are common. Minerals are presented in the order in which they formed. Analytical techniques that are referred to in this chapter are discussed in detail in the appendices. All mineral modes were determined by visual estimation from thin sections, except for those of quartz, dickite, and kaolinite that were determined by quantitative XRD analyses. In the second section major oxide data are interpreted and alteration reactions are proposed on the basis of mineral associations and distributions. The third section is a summary of alteration, put in a space-temperature-time framework.

Mineralogy

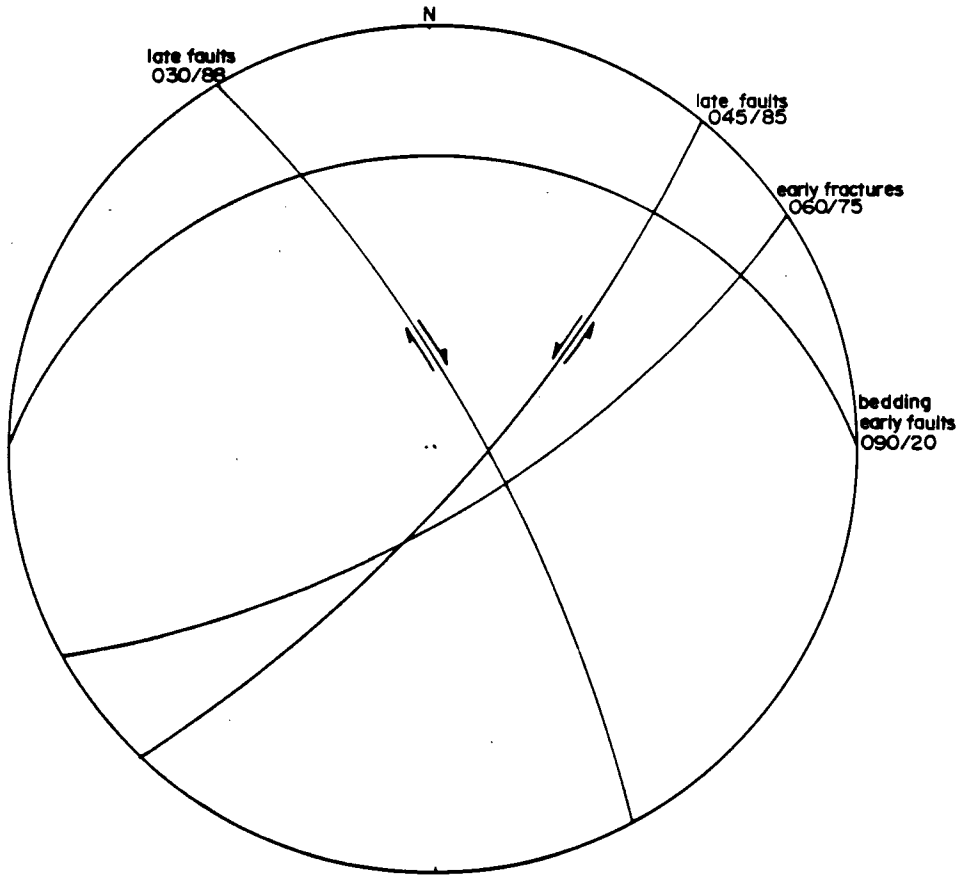

Figure 9. Summary stereographic projection.

Pyroxene-Amphibole These minerals have been totally replaced by chlorite, but pseudomorphs of both are recognized in thin section by their distinctive habit and cleavage.

Anorthoclase [$(K,Na)AlSi_3O_8$] Primary anorthoclase phenocrysts (2v of 55°) occur in one sample in sub-unit 2A1. Crystals are euhedral, about 0.2 mm long, and exhibit variable alteration from pristinely unaltered to totally replaced by coarse (0.05 mm) muscovite crystals. They constitute less than 1 percent of the rock.

Secondary orthoclase also is present in one vein sample of sub-unit 2A1.

Andesine (An 30-50) [$NaAlSi_3O_8 - CaAl_2Si_2O_8$] Primary andesine is a major phase in concentrations of up to 65 percent in eleven samples. Another ten samples formerly contained abundant feldspars as indicated by distinctive pseudomorphs. Compositions were determined using the Michel-Levy method, and a minimum of ten crystals were examined per slide. Composition varies as a function of the original rock type and extent of albitization (Deer, Howie, and Zussman, 1962; V. 5 p.95-165). Alteration intensity varies from 2 to 3 percent replacement by sericite to complete replacement by sericite, dickite, kaolinite, chlorite, and pyrite. Crystal habits are preserved as euhedral laths and broken fragments, up to 3 mm in length.

Secondary pristine andesine was noted in one sample of sub-unit 3B; a quartz vein, enveloped by sericite, kaolinite, quartz, pyrite, muscovite, chlorite, and tourmaline.

Quartz [SiO_2] Quartz is ubiquitous and ranges in abundance from 1 to 95 percent, and in size from 1.8 mm to less than 0.001 mm. Primary quartz was found only in dyke units 6 and 7 as coarse euhedral

phenocrysts. All other forms of quartz are secondary and occur as fine grained replacements and alteration products, vein and cavity linings and fillings, and cores and rims of orbicules. The crystalisation of secondary quartz has not destroyed original volcanic textures.

Secondary quartz is a definitive constituent of the potassic and phyllic alteration assemblages of porphyry copper deposits as defined by Lowell and Guilbert (1970), and its occurrences are well documented (Titley, 1982).

Biotite $[K_2(Mg,Fe)_{6-4}(Fe,Al,Ti)_{0-2}[Si_{6-5}Al_{2-3}O_{20}]O_{0-2}(OH,F)_{4-2}$ Secondary biotite in concentrations of up to 25 percent is present in ten samples of the least altered rocks. Crystals range in size from 0.001 to 0.4 mm in diameter. They form fine-grained feathery shredded aggregates, which have replaced the matrix, and ragged anhedral laths, which have replaced hornblende, pyroxene, and feldspar crystals. Larger crystals exhibit resorbtion, alteration to chlorite, rutile, and iron oxide, and local replacement by tourmaline. Larger biotite crystals display green and red-brown pleochroism, and smaller crystals have only green pleochroism. This variation in pleochroism indicates ranges in the Fe^{2+}, Fe^{3+}, and Ti^{4+} content (Deer, Howie, and Zussman, 1962; v.3, p. 69). All biotite is believed to be secondary because of its replacement habit. The presence of secondary biotite in the potassic alteration zone of porphyry copper deposits is well-documented in the literature.

Chlorite $[(Mg,Fe,Al)_{12}(Si,Al)_8O_{20}(OH)_{16}]$ Chlorite is widespread, and occurs in 42 samples as was determined using XRD analyses, and in an additional 9 samples using thin section examination only.

Concentrations range from 35 percent to trace, and crystal sizes from 0.001 to 0.8 mm. The majority of the chlorite crystals exhibit dark green pleochroism, although some crystals exhibit anomalous 'Berlin Blue' interference colours, which indicates a high Fe^{2+} content. Lack of pleochroism in some chlorite (sub-unit 3B) is probably caused by acid leaching of both Fe and Mg (Deer, Howie, and Zussman, 1962; v. 3, p. 150).

Chlorite forms aggregates of euhedral to anhedral feathery laths and mats that replace feldspars, pyroxenes, amphiboles, and tourmaline. It rims and embays pyrite, rims and replaces the cores of orbicules, and lines vugs. Iron oxide is found locally on cleavage planes. Chlorite crystalisation has not destroyed original volcanic textures. Crystal habits suggest at least two generations; an early one that has replaced pyroxenes, amphiboles, and feldspars, and a later one that has replaced tourmaline and filled void spaces. In hand specimen, fine-grained chlorite is easily mistaken for sericite and dickite, and vice versa.

Chlorite is member of the propylitic alteration assemblage of porphyry copper systems as defined by Lowell and Guilbert (1970), and occurrences are well documented (Titley and Hicks, 1966).

Epidote - Clinozosite $\{Ca_2FeAl_2O\text{-}OH\text{-}Si_2O_7\text{-}SiO_4$ - $Ca_2Al\text{-}Al_2O\text{-}OH[Si_2O_7][SiO_4]\}$ The presence of epidote-clinozosite has been documented in eight samples by recognition in thin section and confirmation by XRD analyses where concentrations are greater than about 5 percent. Epidote-clinozosite ranges in concentration from trace to 20 percent, and both are confined to units 1 and 6 in areas peripheral to the most intense alteration.

Crystals are anhedral, fine-grained (less than 0.1 mm) and are present as ragged individual laths and grainy indistinct agglomerates. They appear to replace matrix and feldspars, although petrographic relationships are not readily evident. Their growth has not destroyed original volcanic textures.

Epidote is a definitive member of the propylitic alteration assemblage of porphyry copper systems (Lowell and Guilbert, 1970).

Calcite [$CaCO_3$] Calcite was recognized in one sample (DDH 84 03, 141.5 m), where it forms a fracture filling with hematite in propylitically altered rock. It is a common mineral in propylitically altered rocks of porphyry copper deposits (Titley, 1982).

Laumontite [$Ca(Al_2Si_4)O_{12}\text{-}4H_2O$] Laumontite was identified using XRD analysis, and it is present only as a vesicle filling in the andesite dyke. It is an alteration product of feldspars and probably interstitial volcanic glass. Laumontite is found in hydrothermally altered rocks at the Island Copper porphyry deposit, B.C. (Cargill et al., 1976) and many others.

Apatite [$Ca_5(PO_4)_3(F,Cl,OH)$] Apatite was recognized by thin section examination in 15 samples. It was not identified in routine whole rock XRD analyses because of its low concentration. The root word for apatite is the Greek **apate**, which means deceit and accordingly, it has in the past been confused with colourless tourmaline, andalusite, and clinozosite. It is present as subhedra in crystal aggregates, and in association with epidote as an alteration product of plagioclase feldspars.

Magnetite [Fe_3O_4] Magnetism was detected in four samples, and a filmy Fe-Ti-Mn (?) dark brown to black oxide coats the majority of

samples. Magnetite occurs locally as subhedral crystals, and as fine grained aggregates which rim mafic ghosts and lithic fragments. Magnetite is a common constituent of the propylitic alteration assemblage of many hydrothermally altered deposits.

Rutile [TiO_2] Rutile is ubiquitous in concentrations up to about 3 percent, and ranges in size from about 0.2 to 0.001 mm. Euhedral crystals are rare, and the majority are anhedral filmy aggregates. Presumably it originated from the destruction of biotite, hornblende, and pyroxene, although these paragenetic relationships are only observed locally.

Corundum [Al_2O_3] Blue corundum (sapphire) was identified macrocopically by its hardness of 9 (Mohs scale). As shown in Plate 13, microscopic corundum has very high relief and forms grainy aggregates of subhedral small crystals, less than 0.001 mm in diameter. Tourmaline and dickite/kaolinite are interstitial to these aggregates. Pleochroism was not observed although the blue colour of the hand samples indicate trace amounts of Fe and Ti (Deer, Howie and Zussman, 1962; V. 5, p. 11-20). Corundum growth has obliterated original volcanic textures.

Corundum was positively identified in 14 samples using XRD analyses, and another 10 samples may contain corundum. In the latter samples there were problems with the XRD analyses in that two of the four high intensity peaks overlapped those of tourmaline (I=75, d=2.48 A^{O}; I=90, d=2.55 A^{O}). The remaining peaks (I=100, d=2.085 A^{O}; I=80, d= 1.601 A^{O}) were low and indistinct in the traces from the 10 samples. Corundum was recognized in a thin section made from a macroscopically identifiable sample. It was not observed in other

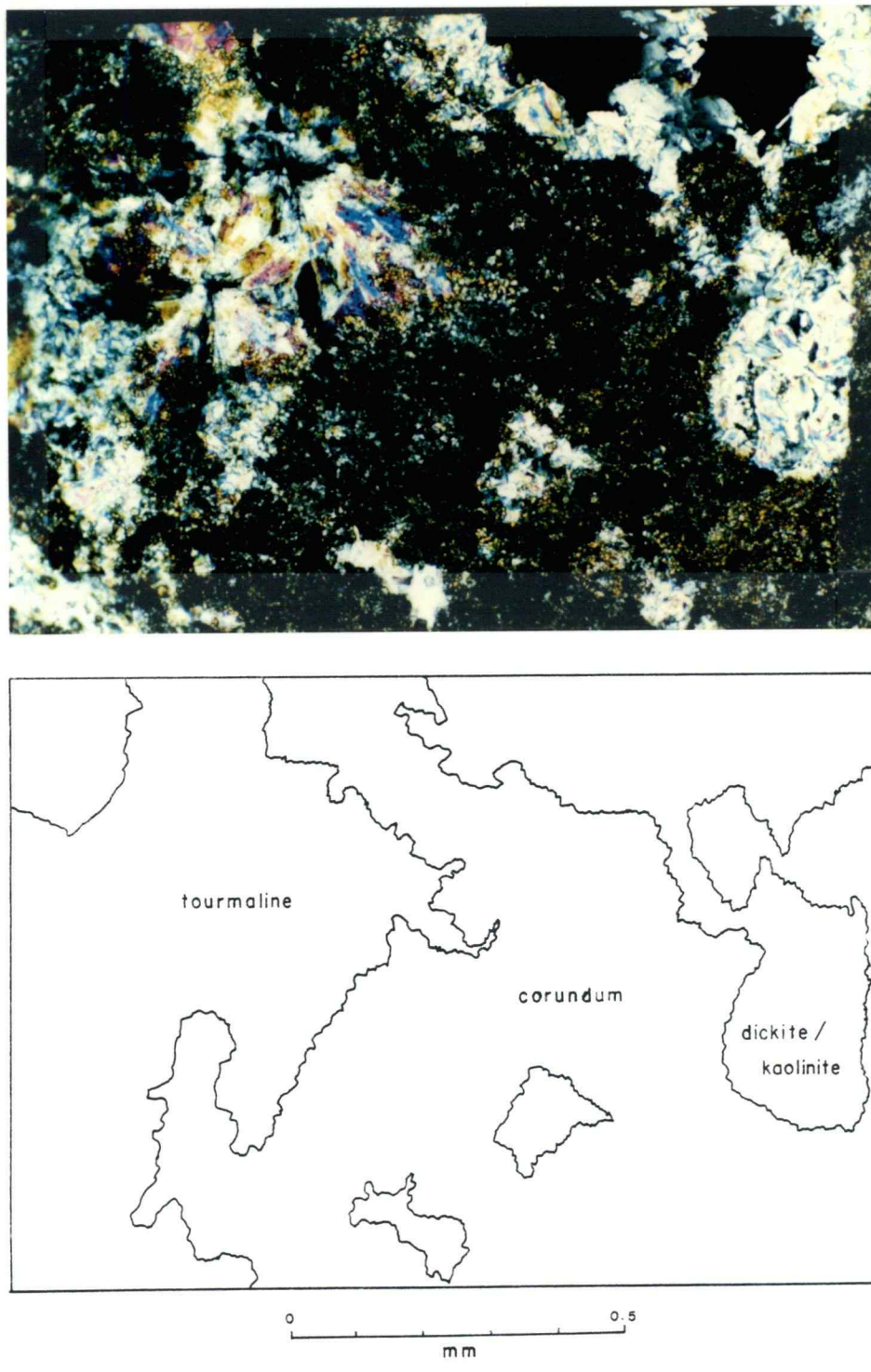

Plate 13. Photomicrograph of grainy corundum, tourmaline and dickite/kaolinite under crossed nicols. Paragenetic relationships are unclear.

thin sections as it is very fine-grained, and because of hardness, most corundum was plucked out during polishing.

The occurrence of corundum in association with hydrothermal alteration is documented at porphyry copper deposits at El Salvador, Chile (Gustafson and Hunt, 1975) Sulawesi, Indonesia (Lowder and Dow, 1978), and Butte, Montana (Brimhall, 1977). It also occurs at Equity Silver Mine, B.C. (Wojdak and Sinclair, 1984).

Andalusite [$Al_2O(SiO_4)$] Andalusite in concentrations of greater than about 5 percent was identified using XRD analyses, then recognized in thin section. It is mottled in appearance and good optical figures are rare. Concentrations range from trace to 35 percent, and size ranges from 0.01 to 0.4 mm. In hand specimen it is coulourless, and in thin section nonpleochroic which implies a lack of the commonly occurring carbonaceous impurities and trace amounts of ferric iron (Deer, Howie, and Zussman, 1962; V.3, p. 129-136).

Andalusite is present as ragged subhedral aggregates, and locally as mottled radiating sprays. Crystals are fractured and host inclusions of quartz, sericite, kaolinite, dickite, and locally pyrite and chlorite, and possibly corundum and pyrophyllite.

All samples of the vitric tuff (unit 2) contain moderate to high proportions of andalusite as a replacement of devitrified welded tuff. Here, the morphology of andalusite is after the original flattened and stretched forms of the volcanic glass. The growth of radiating andalusite sprays in sub-unit $1A_1$ destroyed the original volcanic texture, as shown in Plate 14.

The occurrence of andalusite in association with hydrothermal alteration has been documented in porphyry copper deposits at

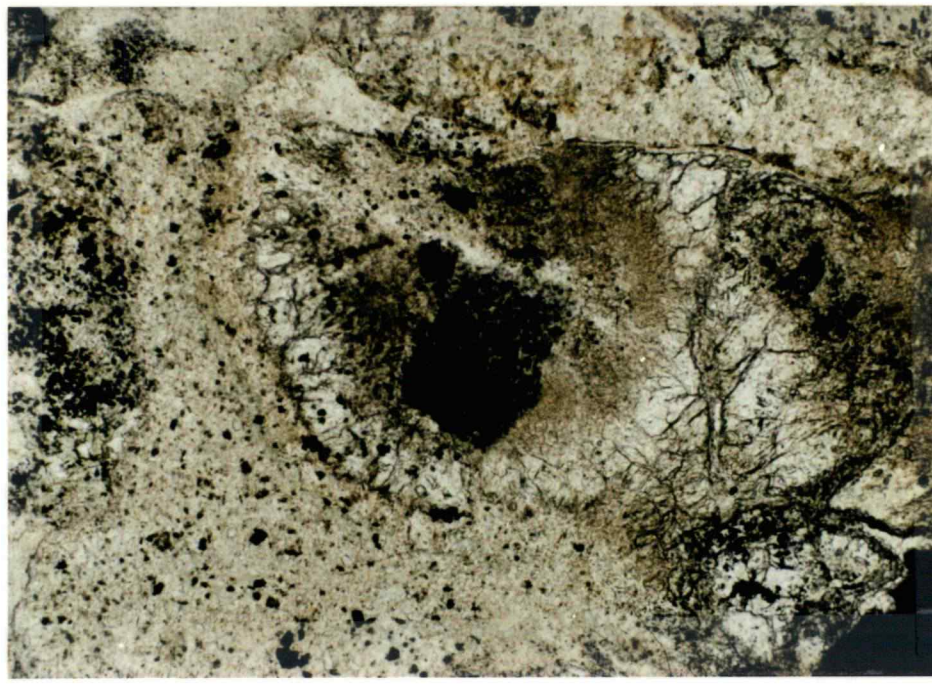

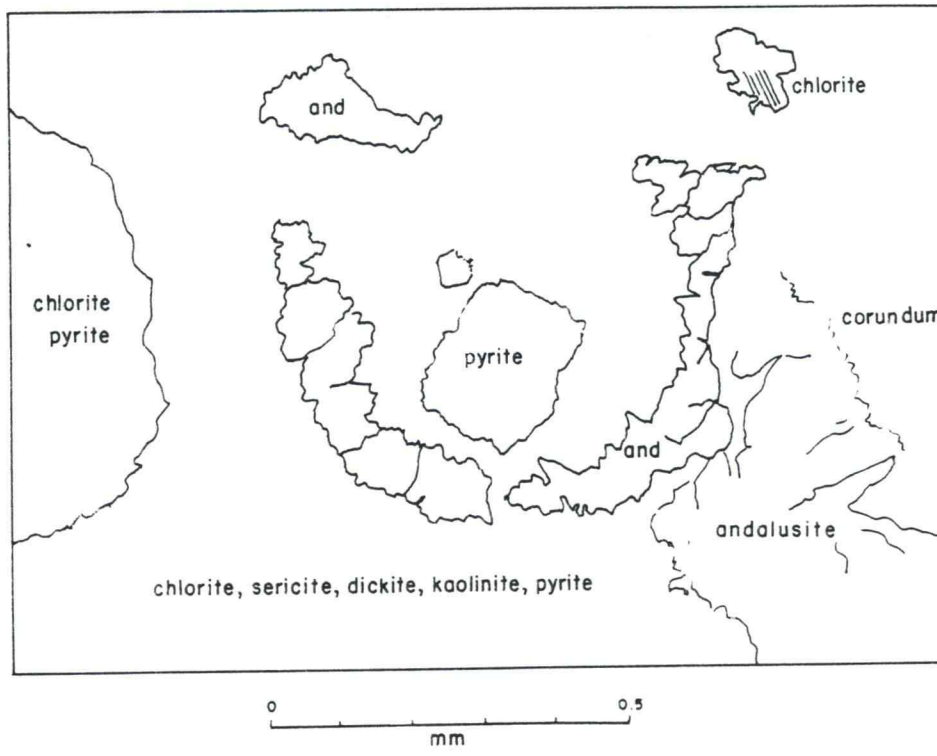

Plate 14. Photomicrograph of andalusite under plane polarised light. Original texture of the vitric tuff has been destroyed.

Papau-New Guinea (Britten, 1980), El Salvador, Chile (Gustafson and Hunt, 1975), Sulawesi, Indonesia (Lowder and Dow, 1978), and Butte, Montana (Brimhall, 1977).

Muscovite [$KAl_2AlSi_3O_{10}(OH)_2$] Muscovite/sericite is ubiquitous. Modes have been visually estimated in thin section, and range from a trace to 60 percent. The author refers to sericite as being chemically, morphologically, and structurally identical to very fine-grained muscovite. However, Deer, Howie, and Zussman (1962; V. 3, p. 14) state that sericite has higher SiO_2, MgO, and H_2O, and a lower K_2O content than muscovite.

Muscovite forms plates of individual crystals and aggregates, up to 1 mm in length. The coarsest crystals occur in veins, and at alteration fronts such as directly under sub-unit 3C. Coarse crystals embay pyrite, are locally altered to kaolinite and dickite, and have iron oxide along cleavage traces. Finely crystalline sericite is an alteration product of feldspars and mafic minerals. Sericite also has totally replaced lithic fragments and shards, and occurs as cores and rims of orbicules. Original volcanic textures are preserved, even after complete replacement by quartz-sericite-dickite-kaolinite. Local pale green colouration is due to Fe^{2+} and Mg^{2+} impurities (Deer, Howie, and Zussman; V. 5, p. 21).

Muscovite is a dominant member of the phyllic alteration assemblage of porphyry copper systems as summarized by Lowell and Guilbert (1970). Muscovite is also found in great concentrations in the phyllic alteration zones of epithermal hotspring-related precious metal deposits (Berger and Eimon, 1983).

Pyrophyllite [$Al_4(Si_8O_{20})(OH)_4$] Pyrophyllite was positively

identified in five samples using XRD, and subsequently identified in thin section by its tabular form, high birefringence (0.048). parallel extinction, one perfect cleavage, moderate relief, and 2v of 55°.

Pyrophyllite forms subhedral tabular crystals up to 0.1 mm in length. Though petrographic relationships are not clear, it may have altered from andalusite. It contains inclusions of sericite, kaolinite, and dickite, and disequilibrium conditions are suggested by the presence of brown reaction rims. Pyrophyllite growth has destroyed original volcanic textures, as shown in Plate 15. It is restricted to the vitric tuff (unit 2) and areas of units 1 and 3 near their contacts with unit 2.

The occurrence of pyrophyllite in association with hydrothermal alteration is documented at porphyry copper deposits at Freida, Papau-New Guinea (Britten, 1980), El Salvador, Chile (Gustafson and Hunt, 1975), and others (Meyer and Hemley, 1967). Pyrophyllite is also present the Pueblo Viejo epithermal gold deposit (Kesler et al., 1981).

Pyrite [FeS_2] Pyrite is ubiquitous and ranges in abundance from trace to 20 percent, and in size from 0.001 mm to 2 cm. It forms euhedral pristine to embayed crystals, rimmed and crosscut by tourmaline, muscovite, and chlorite. Pyrite is present as large (1 cm diameter) dodecahedrons, dendritic aggregates, orbicule rims and radiating spokes, and as vein material. Variability in the intensity of oxidation within individual rock samples suggests that there are at least two generations of pyrite, or there was continuous crystalisation over a long time span relative to that of other minerals. Original volcanic texture were mostly preserved.

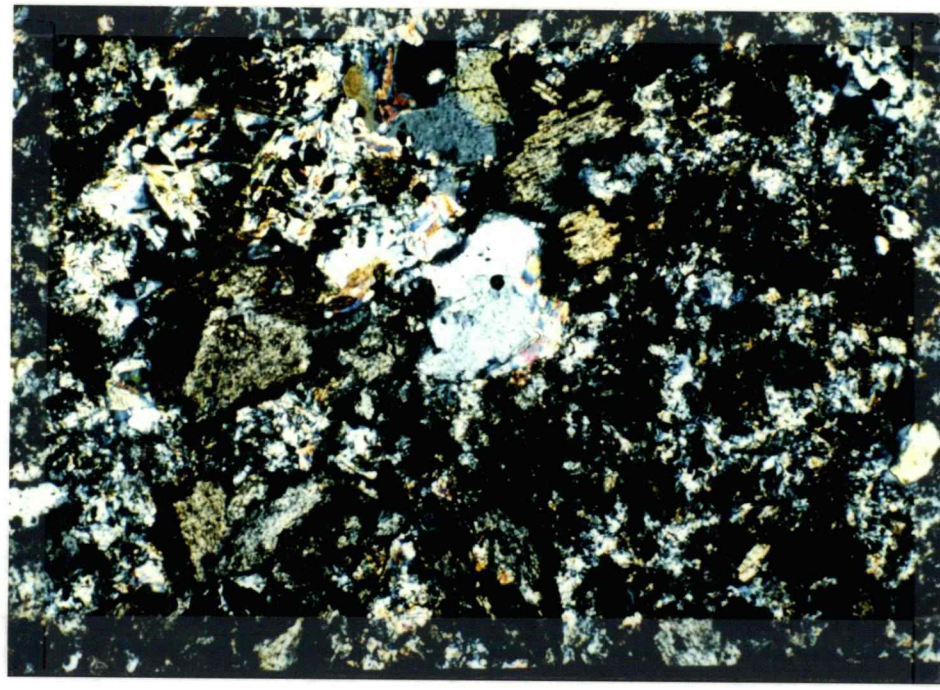

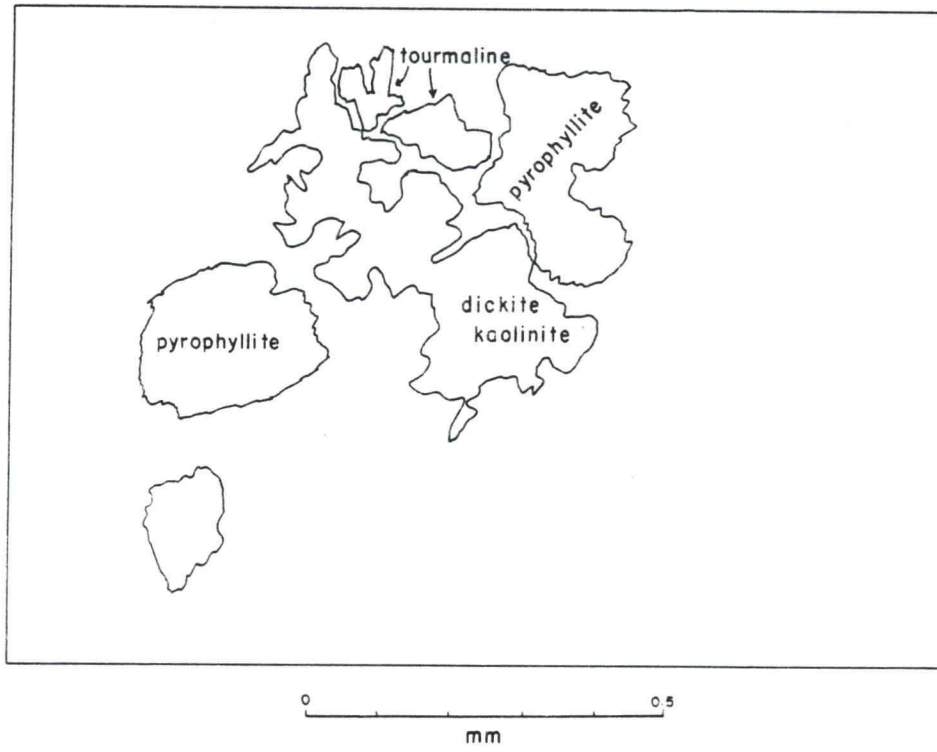

Plate 15. Photomicrograph of pyrophyllite under crossed nicols. Pyrophyllite crystals have reaction rims, and have altered to dickite/kaolinite.

Examples of the high concentrations of pyrite that commonly occur at the phyllic-argillic alteration zone contact at porphyry copper deposits are documented in the summary by Lowell and Guilbert (1970).

Tourmaline; Schorl $[NaFe_3B_3Al_3(OH)_4(Al_3Si_6\ O_{27})]$, Dravite $[NaMg_3B_3Al_3(OH)_4(Al_3Si_6\ O_{27})]$, Elbaite $[Na_2Li_3B_6Al_9(OH)_8(Al_3Si_6\ O_{27})]$ Tourmaline ranges in abundances from trace to 80 percent, and 90 percent of the samples have 3 to 5 percent. Pleochroism varies from colourless to a deep blue-green. Tourmaline forms euhedral crystals in aggregates and sunbursts. Fine acicular needles of less than 0.01 mm in length are pristine, and larger laths of up to 1.0 mm are commonly mottled and altered to chlorite as shown in Plate 16. Larger crystals are zoned which indicates changes in fluid composition during crystalisation. Tourmaline forms rims and embayments on pyrite, in both veins and aggregates, with quartz-chlorite-sericite as diffusion haloes around veins, as orbicule rims and cores, and as knots up to 15 cm in diameter. Tourmaline crystalisation has destroyed original volcanic textures.

The occurrence of tourmaline in association with hydrothermal alteration has been documented at porphyry deposits at El Salvador, Chile (Gustafson and Hunt, 1975), Bolivia (Sillitoe et al., 1975), Sierrita-Esperanza, Arizona (West and Aiken, 1982), and Bell Copper, B.C. (Carson et al.,1976). Tourmaline is also present at the Equity Silver Mine, B.C. (Wojdak and Sinclair, 1984).

Dumortierite $[(Al, Fe^{3+})_7(B_3)(SiO_4)_3$ Massive dumoriterite was found in float at the eastern boundary of the area mapped. XRD analyses revealed that two samples contain dumortierite.

Dumortierite exhibits rose colour pleochroism in radiating sprays

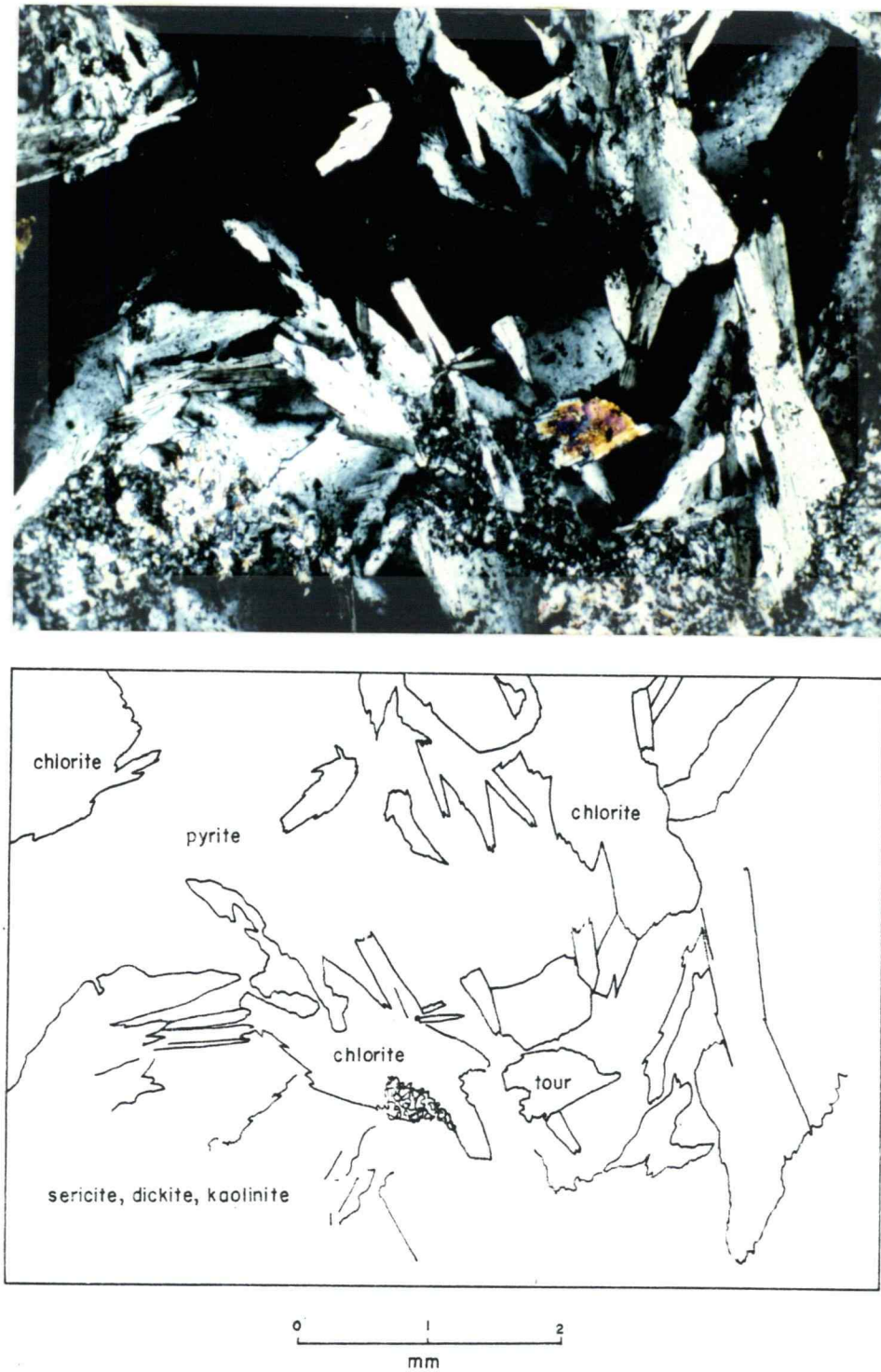

Plate 16. Photomicrograph of cholorite as an alteration product of tourmaline, under crossed nicols.

of feathery to acicular crystals. Associated minerals are quartz, dickite, kaolinite, rutile, and iron oxide.

Dumortierite has been observed in association with andalusite at Equity Silver, B.C. (Wodjak and Sinclair, 1984), and at Oreana, Nevada (Kerr, 1935). Dumortierite is also associated with pyrophyllite, kaolinite, quartz, and muscovite at the Island Copper porphyry deposit (Cargill et al., 1976).

Diaspore [AlO(OH)] and Gibbesite [$AlO(OH)_3$] The presence of diaspore was inferred in 15 samples using XRD analyses. It was not positively identified in thin section or hand sample. XRD identification was not completely satisfactory due to the overprint of diaspore peaks by those of feldspars. Britten (1984) has positively identified diaspore elsewhere on the property, using XRD analyses.

Gibbesite was positively identified in one sample using XRD analysis. It was not identified in thin section.

Diaspore is present in porphyry copper deposits at El Salvador, Chile (Gustafson and Hunt, 1975), Sulawesi, Indonesia (Lowder and Dow, 1978), and Papau-New Guinea (Britten, 1980).

Alunite [$KAl_3(SO_4)(OH)_6$] Alunite was identified in one sample using XRD analysis (Britten, 1984). It was not recognized in thin section. The occurrence of alunite as an alteration product associated with epithermal precious metal deposits is well-documented (Berger and Eimon, 1983; Harvey and Vitaliano, 1963; and, Hemley et al., 1969). Alunite is also common in the leached cappings associated with supergene alteration of porphyry copper deposits (Anderson, 1982).

Kaolinite/Dickite [$Al_4Si_4O_{10})(OH)_8$] Quantitative XRD analyses

revealed the ubiquitous presence of kaolinite/dickite in abundances ranging from trace to 16 percent. Please refer to Appendix 1 for raw data and a discussion of analyses. Massive fine-grained, unctuous pale blue-green dickite was recognized macrocopically in veins and at local alteration fronts. Coarse-grained dickite/kaolinite was recognized in thin section as an alteration product of muscovite.

Kaolinite/dickite is a dominant member of the argillic alteration assemblage of hydrothermal systems.

Major oxides

A suite of twenty rock samples (representative of thirteen sub-units) was analysed for the major oxides; SiO_2, Al_2O_3, TiO_2, Fe_2O_3, FeO, MnO, CaO, MgO, K_2O, Na_2O, and P_2O_5. The resulting weight percentages were converted to grams per 1000 cm^3 by multiplying,

1000 x wt% x measured density. (1)

The values of mass of oxide per unit volume have been used by other authors to interpret the chemical data of hydrothermally and diagenetically altered rocks (Creasey, 1959; Hemley and Jones, 1964; Krauskopf, 1967; Pettijohn, 1975; and Ford, 1978). The g/1000 cm^3 values are particularly useful for determining the additions and depletions of oxides that occur during hydrothermal alteration. Discussion of the analytical method, and presentation of the analyses, densities, and resulting g/1000 cm^3 values are given in Appendix 2.

All rocks within and peripheral to the area mapped have been hydrothermally altered, thus fresh samples from each unit were not available for comparison. In order to quantify additions and depletions of oxides that resulted from hydrothermal alteration,

the oxide data (g/1000 cm^3) from host rocks at Taylor-Windfall are compared with those calculated for "average orogenic andesite" from Gill (1981) that is assumed to be of similar pre-alteration composition, density and tectonic setting. The least altered rocks at Taylor-Windfall are andesitic (as determined by plagioclase feldspar compositions), have similar densities to Gill's andesite, and all rocks at the property were formed in an orogenic environment.

Calculated gains and losses with respect to "average orogenic andesite" are presented in Figure 10. Values are in a general order from maximum depletion of SiO_2 (-67 g/1000 cm^3) to maximum addition of SiO_2 (+753 g/1000 cm^3), from left to right. Gains and losses of SiO_2 have been used as a crude measure for the extent of alteration. However, the samples are also grouped according to their sub-units. Correlation coefficients (r) of gains and losses of oxides are presented in Table 1, and plots of oxide versus oxide that yield an r of greater than 0.75 (CaO versus Na_2O, Al_2O_3 versus TiO_2, and Fe_2O_3 versus MgO) are in Figure 11. Correlations of less than 0.75 reflect a wide and meaningless scatter of points, as is shown in the CaO versus MgO plot (Fig 11d).

Additions, depletions, and correlations of the major oxides are discussed below in the order of oxides that are presented in Figure 10. Some of the gains and losses may in fact reflect pre-alteration compositions that were different from that of Gill's "average orogenic andesite".

Rocks at Taylor-Windfall contain from 62 to 95 percent SiO_2. Gains are large (+753 g/1000 cm^3) relative to losses (-67 g/1000 cm^3) because of the influx of hydrothermal fluids, and to a lesser extent,

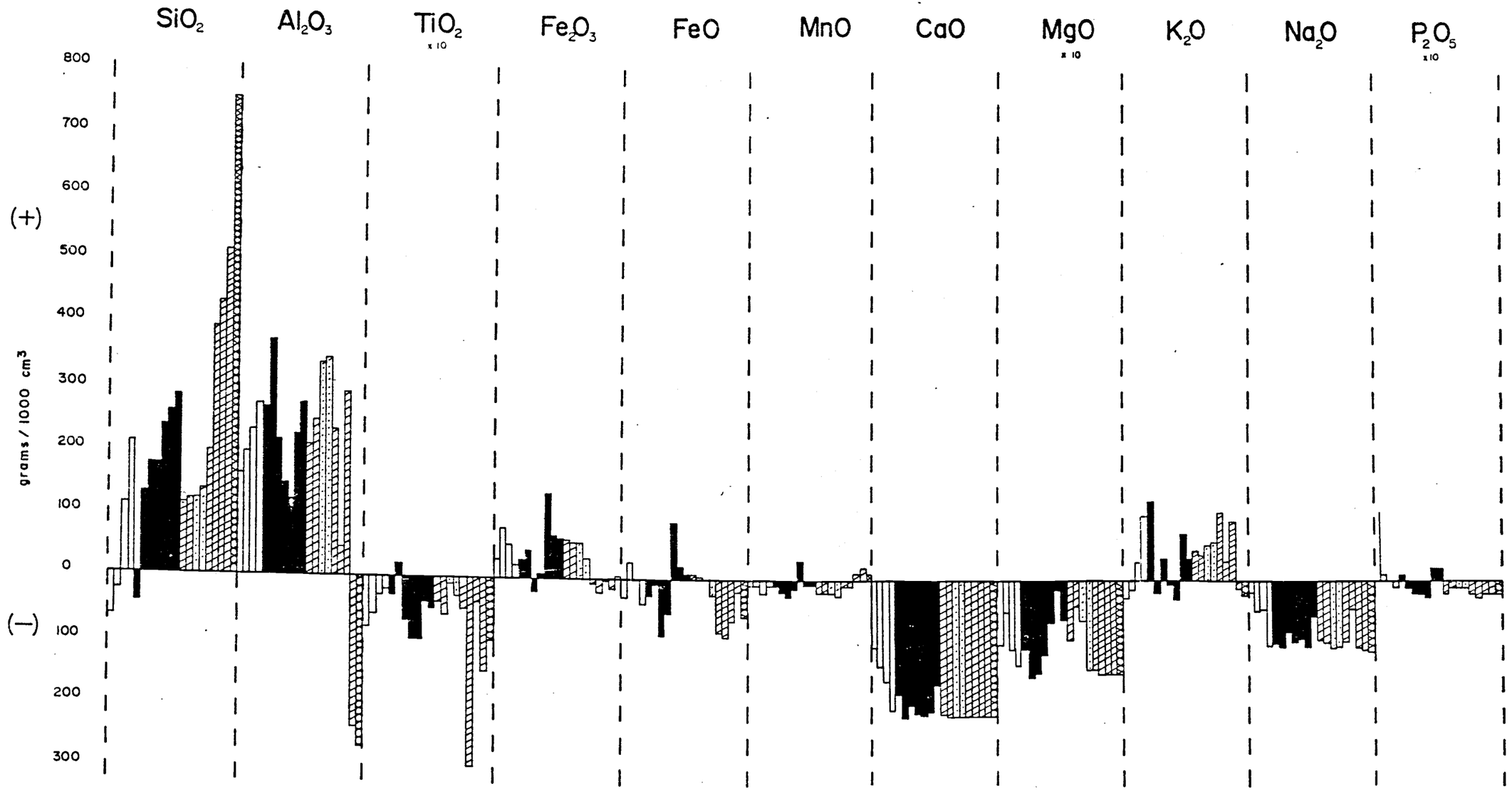

Figure 10. Gains and losses of major oxides (gm/1000cm^3) of altered andesites of Taylor-Windfall, relative to the oxide concentrations of average orogenic andesite as defined by Gill (1981).

TABLE 1

CORRELATIONS OF GAINS AND LOSSES OF MAJOR OXIDES

	SiO2	Al2O3	TiO2	Fe2O3	FeO	MnO	CaO	MgO	K2O	Na2O	P2O5
SiO2	1.00	-0.24	-0.42	-0.38	-0.29	+0.52	-0.53	-0.42	-0.18	-0.38	+0.28
Al2O3		+1.00	+0.77	+0.37	+0.32	-0.25	+0.24	+0.40	+0.48	+0.05	+0.07
TiO2			+1.00	+0.38	+0.36	-0.33	+0.47	+0.19	+0.30	-0.55	+0.15
Fe2O3				+1.00	+0.58	+0.18	+0.28	+0.77	-0.21	-0.02	+0.26
FeO					+1.00	-0.24	+0.20	+0.77	-0.27	+0.06	+0.16
MnO						+1.00	-0.15	-0.03	-0.38	-0.17	-0.03
CaO							+1.00	+0.71	+0.27	+0.63	+0.87
MgO								+1.00	-0.30	+0.15	+0.31
K2O									+1.00	-0.28	-0.16
Na2O										+1.00	+0.62
P2O5											+1.00

covariance = Sxy = 1/n-1 (SUMx1y1 - 1/nSUMx1y1)

standard deviation = S = square root [(SUM x12 - nx2)/n-1]

correlation coefficient = R = (Sxy)/(SxSy)

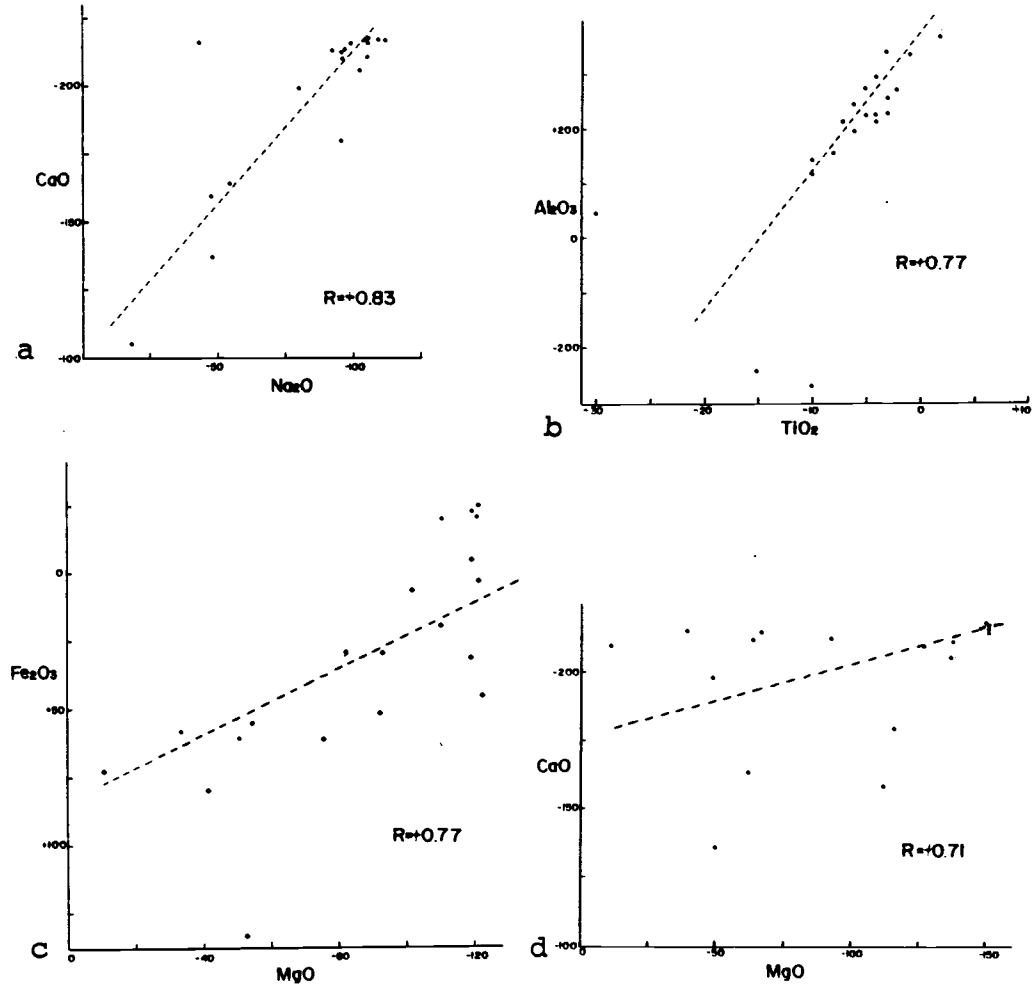

Figure 11. Gains and losses of; a) CaO versus Na_2O, b) Al_2O_3 versus TiO_2, c) Fe_2O_3 versus MgO, and d) CaO versus MgO.

the alteration of primary and secondary minerals that released SiO_2, which was redeposited elsewhere as quartz by replacement processes.

The amounts of Al_2O_3 in the altered host rocks range from less than 1 percent to 25 percent. Alumina is added (+46 to +369 g/1000 cm^3) to all samples except for those of sub-units $3A_1$ and 3C, which exhibit the largest additions of SiO_2 (where 240 and 273 g/1000 cm^3 of Al_2O_3 are lost). Because of the low solubility of Al_2O_3 in many supercritical fluids and immobility during weathering, this oxide is assumed to be immobile during hydrothermal alteration (Krauskopf, 1967; Frantz et al., 1974; and Dudas et al., 1983). Thus the gains and losses may be reflect compositional inhomogeneities of the rocks prior to alteration. However, 335 and 369 g/1000 cm^3 of Al_2O_3 have been added to sub-units $3A_1$ and 2A respectively, and 273 g/1000 cm^3 have been depleted from the extremely siliceous sub-unit 3C. Therefore the major oxide data suggests that Al_2O_3 is mobile to some extent, or was in high concentrations in the host rocks prior to alteration. It is possible that the vitric tuff (Unit 2) is a tuffaceous sediment and thus the source of alumina could be detrital clay minerals.

Additions and depletions of TiO_2 with respect to Gill's "average orogenic andesite" are small and range from +2 to -15 g/1000 cm^3. There is a high correlation between gains and losses of Al_2O_3 and TiO_2 (+0.77 in Fig. 11b). Immobility of TiO_2 during weathering has been documented (Webber and Jellema, 1965), and as is the case with Al_2O_3, it may also be somewhat immobile during hydrothermal alteration. Thus TiO_2 concentrations may reflect primary (or original) compositional variations of the volcanic host rocks.

Gains and loses of iron oxides relative to Gill's "average orogenic andesite" range from +134 to -90 g/1000 cm_3. As amphiboles, pyroxenes, biotites and chlorites were hydrothermally destroyed the iron oxides were released and then either redeposited as tourmaline, chlorite, pyrite, epidote and magnetite, or released by groundwaters during processes of extreme acid leaching and supergene weathering.

All samples contain less than 0.3 percent MnO, and additions and depletions of MnO are small (-1 to +3 g/1000 cm^3) and correlate poorly with those of all other oxides.

Of the twenty samples analysed, seven have less than 0.03 percent CaO. Lime is depleted in all samples (-105 to -217 g/1000 cm^3) because of the hydrothermal destruction of plagioclase feldspars which altered to sericite. Complete replacement of plagioclase by sericite is shown in Plate 10. Calcium ions are evolved as a result of the reaction proposed by Hemley and Jones (1964),

$$3Na_2CaAl_4Si_8O_{24} + 8H^+ + 4K^+ \rightleftharpoons 4KAl_2AlSi_3O_{10}(OH)_2 + 6Na^+ + 3Ca^{2+} + 12SiO_2 \quad (2)$$

which illustrates that feldspar alter to sericite. The calcium ions were taken up in apatite, epidote, calcite, clinozoisite, and laumontite.

All samples exhibit losses of MgO with respect to "average orogenic andesite" (-12 to -151 g/1000 cm^3), and four samples do not contain MgO. Losses of iron oxides correlate with those of magnesia ($r=+0.77$) and reflect the destruction of amphiboles, pyroxenes, and biotite. There are minimal depletions of less than 65 g/1000 cm^3 of MgO in samples of sub-units 5A, 5AA, 4A and 3B where biotite is preserved.

Additions and depletions of K_2O range from -26 to +128 g/1000 cm^3. The additions presumably were derived from a magmatic hydrothermal fluid source. Correlations between gains and losses of K_2O and those of other oxides are low ($r < 0.48$), and the behavior of potash appears erratic. Although in the least altered rocks (units 6, 5AA and 1 in Fig. 10), K_2O and SiO_2 are mutually depleted. Their losses may be attributed to the alteration of biotite to chlorite according to the equation proposed by Meyer and Hemley (1967),

$$2K(Mg,Fe)_3AlSi_3O_{10}(OH)_2 + 4H+ \rightleftharpoons (Mg,Fe)^{2+} + 2K^+ + Al(Mg,Fe)_5AlSi_3O_{10}(OH)_8 + 3SiO_2 \quad (3)$$

and as was observed in thin sections of samples that contain biotite.

Primary potassium feldspar has been preserved in only one sample, and elsewhere pseudomorphs were not observed. Thus, it was probably all altered to sericite,

$$3KAlSi_3O_8 + 2H^+ \rightleftharpoons KAl_2AlSi_3O_{10}(OH)_2 + 6SiO_2 + 2K^+ \quad (4)$$

as shown in this equation, from Hemley and Jones (1964).

The alteration of sericite to kaolinite was observed in thin sections, and takes place according to the reaction,

$$2KAl_2AlSi_3O_{10}(OH)_2 + 2H^+ + 3H_2O \rightleftharpoons 3Al_2Si_5(OH)_4 + 2K^+ \quad (5)$$

as suggested by Creasey (1959).

Pyrophyllite has a reaction rim of unknown composition where it is in contact with sericite and kaolinite, as shown in Plate 15. Thus pyrophyllite may form as a result of sericite destruction,

$$2KAl_2AlSi_3O_{10}(OH)_2 + 6SiO_2 + 2H^+ \rightleftharpoons 3Al_2Si_4O_{10}(OH)_2 + 2K^+ \quad (6)$$

which results in the liberation of potassium ions (Creasey, 1959).

Although alunite was identified using XRD, it was not observed in thin sections, and petrographic relationships are not known.

Perhaps alunite also may have formed as a result of sericite destruction by the reaction,

$$KAl_2AlSi_3O_{10}(OH)_2 + 3H^+ + 2SO_4^{2-} \rightleftharpoons 3SiO_2 + KAl_3(SO_4)(OH)_6 \quad (7)$$

as proposed by Harvey and others (1963) for the alteration of sericite to alunite.

Therefore, from the textural relationships that were observed in thin sections as corroborated by the aforementioned equations, one may conclude that K_2O is mobile in a hydrothermal system, and its behavior is complex.

Of the twenty samples analysed, 14 have less than 1 percent Na_2O, and all samples exhibit depletion of soda relative to Gill's "average orogenic andesite" (-18 to -112 g/1000 cm^3). Losses of Na_2O correlate with those of CaO (r=+0.87 in Fig 11), which reflects a concommitent depletion of oxides because of plagioclase feldspar destruction. Where some plagioclase is preserved (quartz diorite and andesite dykes and sub-units 5AA and 4A) depletions of Na_2O are lowest (<55 g/1000 cm^3). Chlorite has formed as a result of the destruction of feldspar,

$$2NaAlSi_3O_8 + 4(Mg,Fe)^{2+} + 2(Fe,Al)^{3+} + 10H_2O \rightleftharpoons \quad (8)$$
$$(Mg,Fe)_4(Fe,Al)_2Si_2O_{10}(OH)_2 + 4SiO_2 + 2Na^+ + 12H^+$$

according to the equation proposed by Meyer and Hemley (1967). Chlorite replacement of plagioclase feldspar is shown in Plate 9.

Gains and losses of P_2O_5 are low (-2 to +2 g/1000 cm^3) except in one sample of the andesite dyke (+11 g/1000 cm^3).

In summary, an extreme quantity of SiO_2 and possibly lesser amounts of Al_2O_3 and K_2O have been added to the rocks by an external source, presumably a hydrothermal fluid. Plagioclase feldspar

destruction resulted in depletion of Na_2O and CaO, and mafic mineral destruction involved the loss of MgO and iron oxides. Titanium oxide is probably immobile, and thus concentrations of TiO_2 in the hydrothermally altered rocks are the same as those of the unaltered precursor. Manganese oxide and P_2O_5 are of too low concentrations to show any trends. In the following text, the mobilities of these oxides are discussed with respect to specific alteration events.

Summary of alteration events

The five spatially and temporally discrete alteration events that took place at Taylor-Windfall are in order of earliest to latest; 1) propylitic, 2) high temperature (>350°c), 3) retrograde, 4) argillic, and 5) supergene. Each event resulted in the formation of spatially restricted mineral assemblages that replaced primary minerals and those of previous alteration events. Therefore, the alteration events were elucidated on the basis of recurrent associations of spatially restricted minerals. The five alteration events are described below in terms of mineral associations, the mobility of critical oxides, and stratigraphic and structural controls governing the distribution of alteration assemblages.

The initial alteration event consisted of widespread regional propylitization over tens of square kilometers. It has been locally overprinted by high temperature, retrograde, argillic and supergene alteration assemblages. This propylitic event, which immediately followed the intrusion of a magma into a reactive host, involved the destruction of primary amphiboles, pyroxenes and feldspars, and the associated depletion of CaO, Na_2O, and MgO. The resultant alteration assemblage contains chlorite, biotite, epidote, calcite,

clinozoisite, zeolites, magnetite, apatite, rutile, pyrite and quartz. Distributions of the propylitic assemblage on a large scale are determined by proximity to the Coast Plutonic System, as the rocks in contact with plutonic heat sources exhibit propylitic alteration, whereas those farther to the east in the Williams Lake area (Fig. 3) do not. At the Taylor-Windfall property, distributions of individual replacement minerals such as zeolites are attributed to ranges in the pre-alteration compositions of the volcanic host rocks.

The high temperature alteration event resulted in destruction of all pre-existing minerals, both primary and secondary, and in the formation of corundum, andalusite, tourmaline, muscovite, pyrite, pyrophyllite, chlorite, and quartz. During this event, there was an influx of hydrothermal fluids enriched in SiO_2 and probably K_2O into the N060E fractures, bedding plane faults, and adjacent wall rocks. The highest concentrations of these alteration minerals are in the N060E fractures, the vitric tuff (unit 2), and at the contact area between sub-units 2A1 and 3B.

The corundum-andalusite assemblage formed at a minimum temperature of 395+/-10^{o}c according to the experimental work by Hemley et al. (1980) as shown in Figure 12b. In response to falling temperatures and (or) increasing SiO_2 and K_2O activity, the hydrothermal fluid became saturated with respect to silica and potash, and large volumes of quartz and sericite were deposited (arrows on the plots indicate probable paths of crystalisation, Fig. 12). Fluid saturation of SiO_2 and K_2O is implied by the sharp alteration contact between sub-units 3B and 3C, which consists of a thin continuous 1 to 3 cm thick layer of almost pure coarsely crystalline muscovite that is

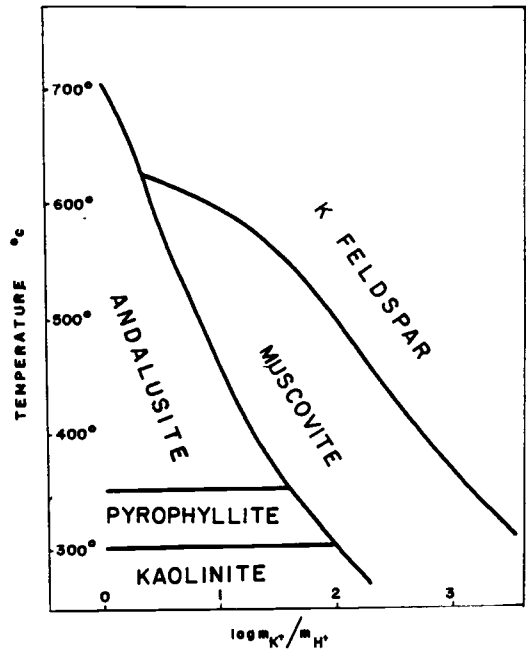

a

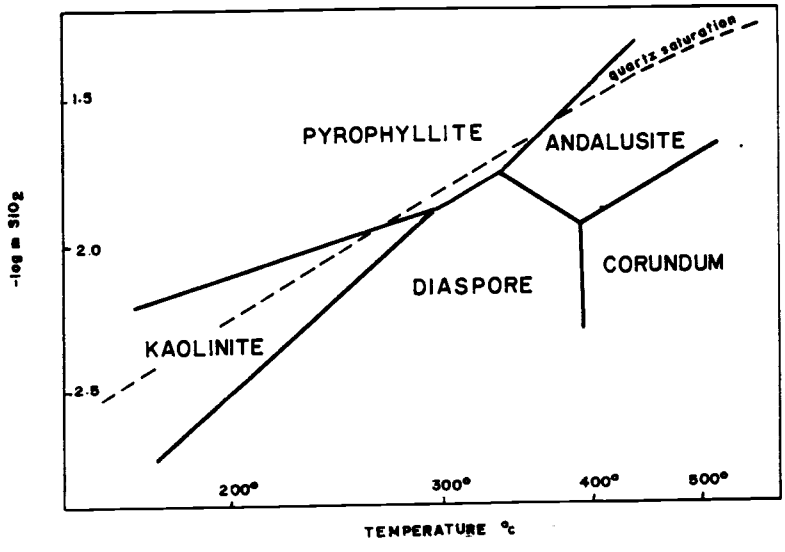

b

Figure 12. Mineral equilibria in the systems; a) K_2O-Al_2O_3-SiO_2-H_2O at 1 kilobar H_2O, after Wojdak and Sinclair, 1984, and b) Al_2O_3-SiO_2-H_2O at 1 kilobar H_2O, after Hemley et al., 1980.

locally altered to pure dickite. Highly siliceous rocks of sub-unit 3C, up to 30 m thick, are above the muscovite layer. This contact is parallel to bedding, and thus the alteration front is in part stratigraphically controlled. It is interpreted to represent the horizon at which the fluids became saturated with respect to K_2O and SiO_2.

There probably was a massive influx of boron contained in the hydrothermal fluid during the high temperature alteration event, because tourmaline formed abundantly in veins and envelopes during this stage. All plagioclase feldspar and most chlorite altered to very finely crystalline sericite concurrently with vein formation. Tourmaline veins, rocks deficient in chlorite and plagioclase, and the corundum-andalusite assemblage are restricted in space to a funnel shaped area in sub-units 5A, 4A, 3A, 3A1, 3B, 2A, 2A1, 1B and 1A (Figs. 7a and 7b). Fine-grained sericite crystals indicate that this event was rapid, and the funnel shape indicates that the high-temperature fluids were limited in their mobility. In summary, this high temperature event may have been related to the fluids which evolved from a deep seated magma. These fluids ascended to the surface along conduits related to large scale structures such as the Tchaikazan Fault.

Retrograde reactions such as chloritisation of tourmaline (Plate 16) and the alteration of aluminosilicate minerals to sericite took place in response to falling temperatures, and diminishing pH. Pristine crystals of tourmaline and pyrite also formed at this time as they crosscut mottled tourmaline. The orbicules probably formed during retrograde alteration, because they are composed of tourmaline,

quartz, sericite, chlorite and sulphides, and not of high temperature corundum and andalusite.

An influx of acid meteoric waters into the hydrothermal system probably caused the formation of advanced argillic alteration. A large volume of sericite was altered to kaolinite due to the addition of H^+ ions (supplied by magmatic fluids). This alteration path is illustrated in Figure 11a. The resulting assemblage mostly consists of dickite and kaolinite, and locally distributed smaller amounts of alunite, dumortierite, diaspore, gibbesite, quartz, pyrite, chlorite, and tourmaline. Massive dickite/kaolinite formed on all late stage northwest-trending fractures, and replaced chlorite in most early stage veins that trend northeast. The argillic assemblage in wall rocks is restricted to a funnel-shaped area consisting of parts of sub-units 1A, 1B, 2A, $2A_1$, 3A, $3A_1$, 3B, 4A, 5A and 7.

Supergene oxidation took place because the ubiquitous disseminated pyrite is unstable in an oxidizing environment. The result was the formation of ferricrete that is exposed in Battlement Creek and elsewhere in the Taseko area (MacKenzie, 1921).

A summary of the paragenesis of alteration minerals is presented in Figure 13. Minerals are given in the order that they formed as deduced from petrographic relationships, and they are listed in groups of assemblages. The mineral abundancies are depicted by the thicknesses of the bars. The initial propylitic alteration is widespread, and its assemblage consists of clinozoisite, quartz, biotite, chlorite, epidote, calcite, laumontite, apatite, magnetite and rutile. High temperature alteration is confined to a narrow funnel-shaped area, and corundum, andalusite, sericite, pyrite, and

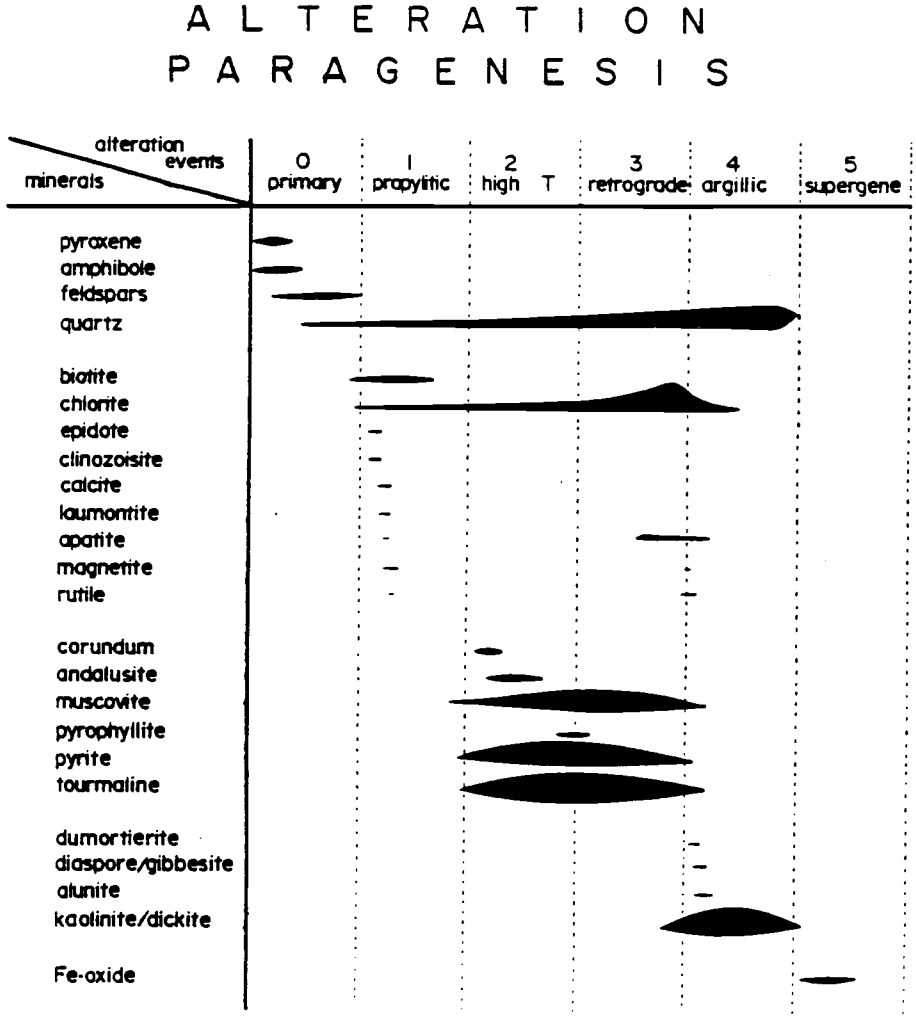

Figure 13. Alteration paragenesis.

tourmaline constitute this assemblage. The retrograde assemblage that formed in this same general area consists of quartz, pyrophyllite,sericite, pyrite, tourmaline, and chlorite. Argillic alteration overprints and surrounds the area of high temperature and retrograde alteration. The resulting assemblage contains kaolinite/dickite, quartz, chlorite, alunite, dumortierite, diaspore, gibbesite, and tourmaline. Local ferricrete formed because of supergene oxidation of pyrite-rich rocks.

Metalisation

Metals at the Taylor-Windfall prospect are concentrated largely in two veins; one is tourmaline-rich and the other is sulphide-rich. Both are oriented at about N060E, and are exposed only in the 1648 m level. Quartz veins, pyrite-tourmaline fracture coatings and wall rocks were also analysed and examined for their economic potential, but were found to be lacking in metals. Results are presented below in five sub-sections; vein descriptions, vein mineralogy, trace elements in veins, trace elements in wall rocks, and summary.

Vein descriptions

A single tourmaline vein is exposed in and oriented parallel to the 1648 m level drift (N060E). As the vein is only 10 to 20 cm wide, it was not mappable at a scale of 1:500, and thus is not shown in Figure 5 (Geology of the 1648 m level, in map pocket). In exaggerated width the main tourmaline vein is plotted on Figure 14. Strike length is about 110 m, and down dip extension is about 130 m (as determined by diamond drill hole intersections, Fig. 7a in map pocket). Up dip extension is about 70 m to the 1707 m level. The vein pinches, swells, bifurcates, and has been shifted southwest by

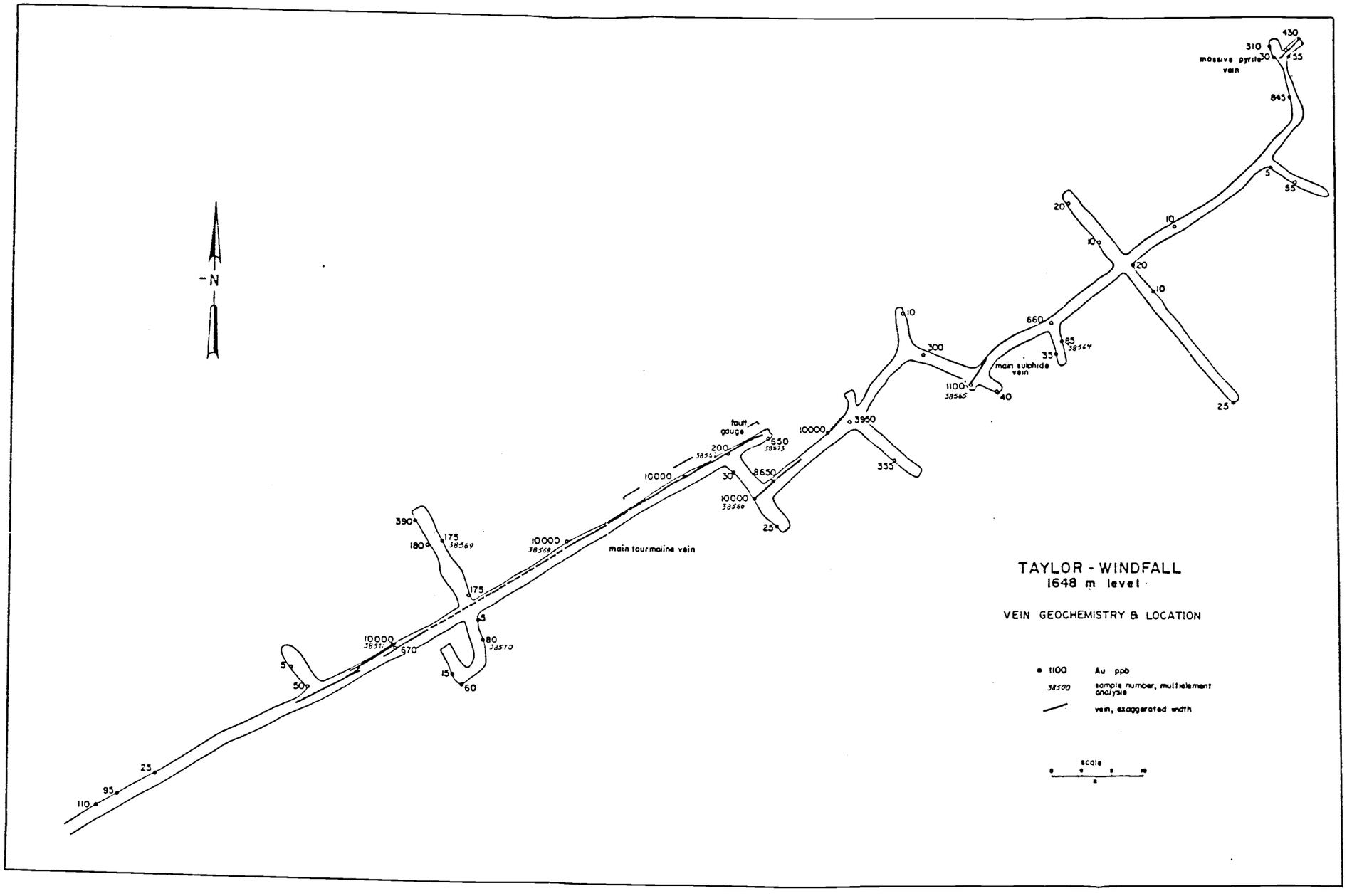
N
430
310
massive pyrite vein
30
55
845
5
55
20
10
10
20
10
10
660
300
85
38564
35
main sulphide vein
1100
38565
40
25
fault gauge
10000
3950
200
38551
630
38573
10000
353
30
8650
10000
38560
25
390
180
175
38569
10000
38548
main tourmaline vein
175
5
80
38570
10000
38571
670
5
50
15
60
25
95
110
TAYLOR - WINDFALL
1648 m level
VEIN GEOCHEMISTRY & LOCATION
1100 Au ppb
38500 sample number, multielement analysis
vein, exaggerated width
scale

Figure 14.

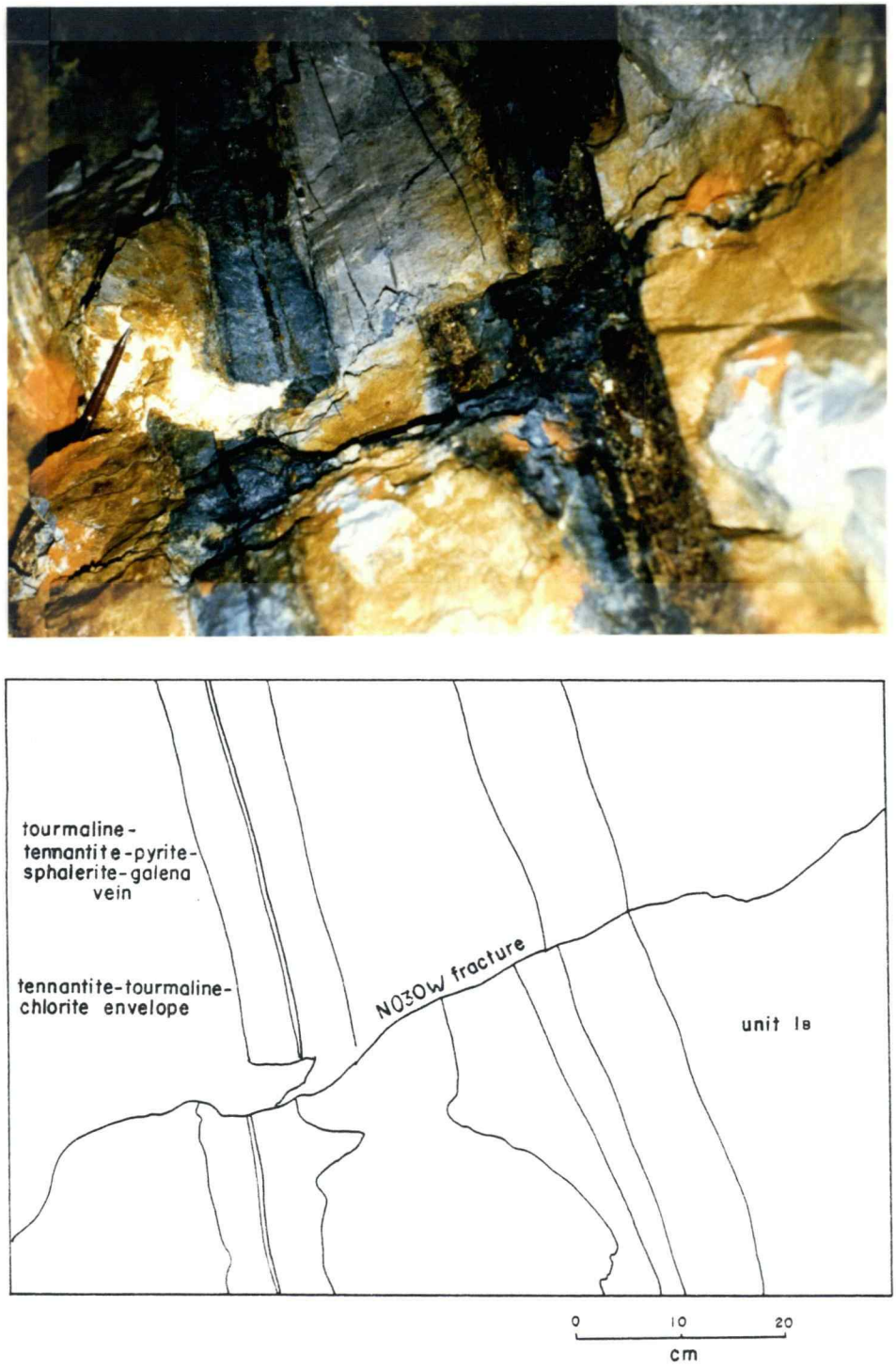

Plate 17. The main tourmaline vein, 1648 m level. The vein is displaced by a N030W fault.

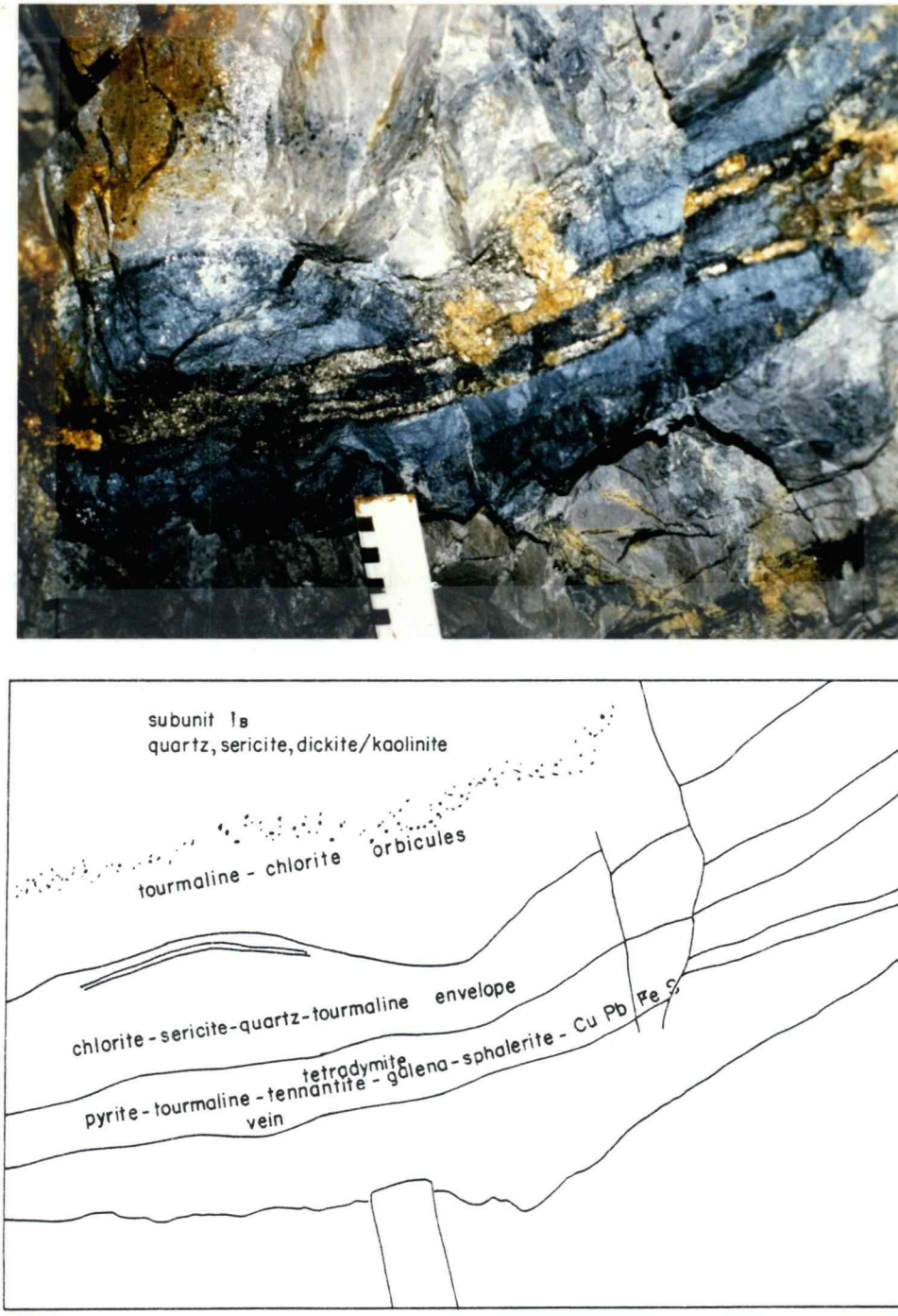

Plate 18. The main tourmaline vein, 1648 m level. The vein lacks symmetry, and has a broad diffusion envelope.

N030W faults, as shown in Plates 17 and 18.

The open space filling (less than 5 cm wide) is comprised of tourmaline (20-50 percent), chlorite (10-30 percent), pyrite (1-30 percent), tennantite (5-20 percent), sphalerite (5-10 percent), chalcopyrite (1-5 percent), an unnamed Cu-Pb-Fe-S phase (2-5 percent), galena (1-2 percent), a rare earth element-bearing phosphate (1-2 percent), and less than 2 percent tetradymite, gold and enargite. Colours of the vein and selvage range from dark blue-green to black as a function of variable proportions of minerals. A dark blue-green diffusion envelope, comprised of tourmaline, chlorite, tennantite, and the Cu-Pb-Fe-S phase, defines the remainder of the 10 to 20 cm vein, as depicted in Plates 17 and 18. Pyrite is the only sulphide that forms discrete mineral layers in the veins (Plate 18).

The main tourmaline vein is sheared on the 1707 m level (15 m west of sample site S6A, Fig. 6 in map pocket), and down dip on the 1648 m level (sample site S27F, Fig. 5 in map pocket). Vein minerals have been totally replaced by coarse (1-3 mm) muscovite plates and pyrite dodecahedrons (0.5-1.0 cm). This sheared portion of the main tourmaline vein is called the 'Shaft Shear Zone'in old reports (Dolmage, 1932). Sub-units 1A and 1B on the 1648 m level host the main vein, and sub-units 1B and $2A_1$ host the sheared portion on both the 1648 and 1707 m levels.

A myriad of fractures also trend N060E and they are coated with layers 0.1 to 2.0 mm thick of tourmaline (20-80 percent), pyrite (2-80 percent), sericite (1-50 percent), and chlorite (1-50 percent), as shown in Plate 19. Fracture intensities range from 2 to 15 per linear metre perpendicular to strike. A few massive pyrite veins,

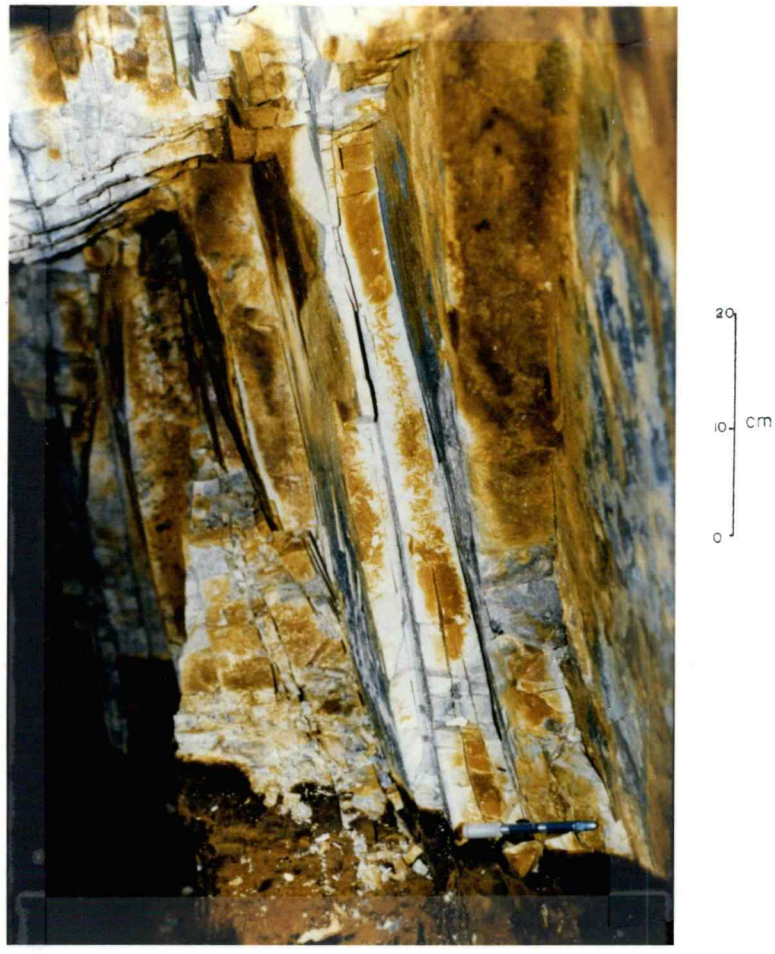

Plate 19. Photograph of the N060E fractures on the 1648 m level. Fractures are coated by a thin layer of tourmaline and chlorite.

(up to 20 cm wide) are also oriented N060E, parallel to the fractures, as depicted in Plate 20. All units except the dykes host coated fractures and pyrite veins.

The bulk of the main sulphide vein has been mined, thus dimensions are not known. It trends N057E/84S and exhibits a width of 20 cm and a strike length of 10 m on the 1648 m level. The vein is truncated to the northwest by a fault, and to the southeast it extends into a caved stope. Although differing in proportions, the mineralogy of the sulphide vein is similar to that of the tourmaline vein. The sulphide vein has greater amounts of the REE phosphate, sphalerite, tennantite, and in addition has coarse siderite crystals and a malachite coating. Alteration selvages and mineral layering are lacking. The main sulphide vein is hosted in sub-unit 1B in an area that is strongly faulted. This sulphide vein is plotted on Figure 14 in exaggerated width.

Quartz veins are present only on the 1648 m level between the two exposures of the quartz diorite dyke. Vein orientations are variable and range from N005E/90 to S007E/52W. They are up to 20 cm wide, and up to 5 m in strike length. The quartz veins pinch, swell, birfurcate, and are sheared at all angles from parallel to perpendicular to their strike. Veins are comprised of 90 percent quartz, and a remainder of rutile, pyrite, sericite, dickite, and kaolinite. They are banded open space fillings that lack diffusion haloes. Vugs lined with drusy quartz are also present in the same area between the two dyke exposures. Quartz veins are hosted in sub-units 1A, 1B, 4A, and 5A, in an area of intense fault disruption (Fig. 7a in map pocket).

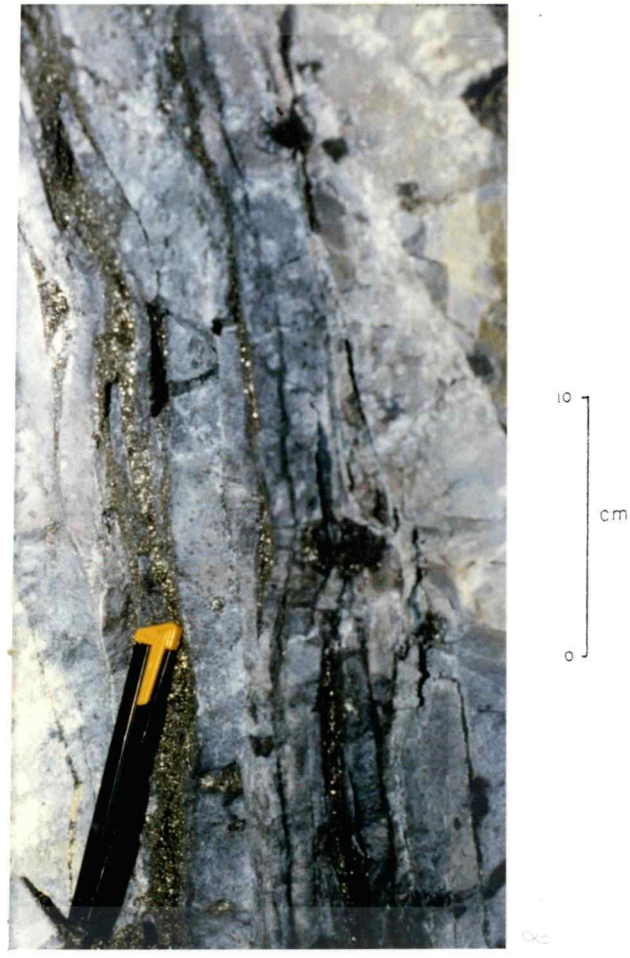

Plate 20. Photograph of pyrite veins that trend N 060 E, on the 1707 m level. Other sulphide minerals, tourmaline, and chlorite are absent.

Vein mineralogy

Vein minerals are described below in the paragenetic order in which they were deposited. Mineral identification and textures were obtained from reflecting microscope and scanning electron microscope-energy dispersive system (SEM-EDS) examinations.

Pyrite [FeS_2] Pyrite comprises up to 30 percent of both main veins, where it is pristine to strongly oxidized, coarsely crystalline (1.0 mm), and interstitial to tourmaline. It hosts inclusions of chalcopyrite, shares mutual grain boundaries with tetradymite, enargite, galena, tennantite, sphalerite, and a Pb-Cu-Fe-S phase, and is embayed by the REE phosphate. As shown in Plates 17 and 20, pyrite is present as open space filling and as replacements in the diffusion envelopes.

Tetradymite [Bi_2Te_2S] The main sulphide vein contains minor amounts of tetradymite (less than 2 percent). It was identified by SEM-EDS analysis. This early-forming mineral exhibits a mottled, finely crystalline (0.8 mm) appearance, and is surrounded and replaced by the Cu-Pb-Fe-S phase and tennantite, as shown in Plates 21 and 22. Tetradymite has irregular grain boundaries, and because of its softness of 1.5 (Mohs scale) it is pitted and crosscut by a myriad of scratches. Tetradymite is present in hypothermal to mesothermal gold-bearing quartz veins, subvolcanic metalliferous veins, and skarn deposits (Ramdohr, 1980, p. 438).

Enargite [Cu_3AsS_4] (Sb can substitute for As: Ramdohr, 1980, p. 583)

Enargite is similar to tetradymite in habit, size, and amount present. It formed early, has irregular mottled boundaries, and is surrounded by tennantite, sphalerite, and the Cu-Pb-Fe-S phase. As it

has a hardness of 3 (Mohs scale) it is pitted and scratched. Enargite is spatially associated with tetradymite, although mutual grain boundaries were not observed. As it alters to tennantite, enargite loses its bright green and red colours in reflected polarised light, and becomes isotropic. Mottled remnants of enargite hosted in tennantite are present in the main sulphide vein, as shown in Plates 23 and 24.

Enargite is present in porphyry copper systems (Butte, Montana, and Chuquicamata, Chile; Ramdohr, 1980, p. 588), as well as in some epithermal precious metal deposits (El Indio, Chile; Walthier et al., 1983).

Galena [PbS] Galena is an early-formed mineral of low concentration. It is similar in habit and texture to tetradymite and enargite, although grain boundaries are angular because of crystal structure (Plates 21 and 22). Galena hosts inclusions of sphalerite and chalcopyrite.

Gold [Au] Native gold is present in trace amounts spatially associated with tennantite, as was observed by B.C.D.M. (1935) and Payne (1983). Native gold was not observed (by the author) in polished sections, and concentrations of gold did not exceed about 1 ppm in the lattices of sulphide minerals as was deduced from SEM-EDS analyses. However, the author found a clot (2mm) of free gold in elluvium near the portal of the 1707 m level.

Gold may be present in some porphyry copper systems in sub-economic quantities such as at Bougainville, Papau-New Guinea (Ford, 1978), and Island Copper, B.C. (Cargill et al., 1976). By definition, gold is concentrated in economic quantities at many

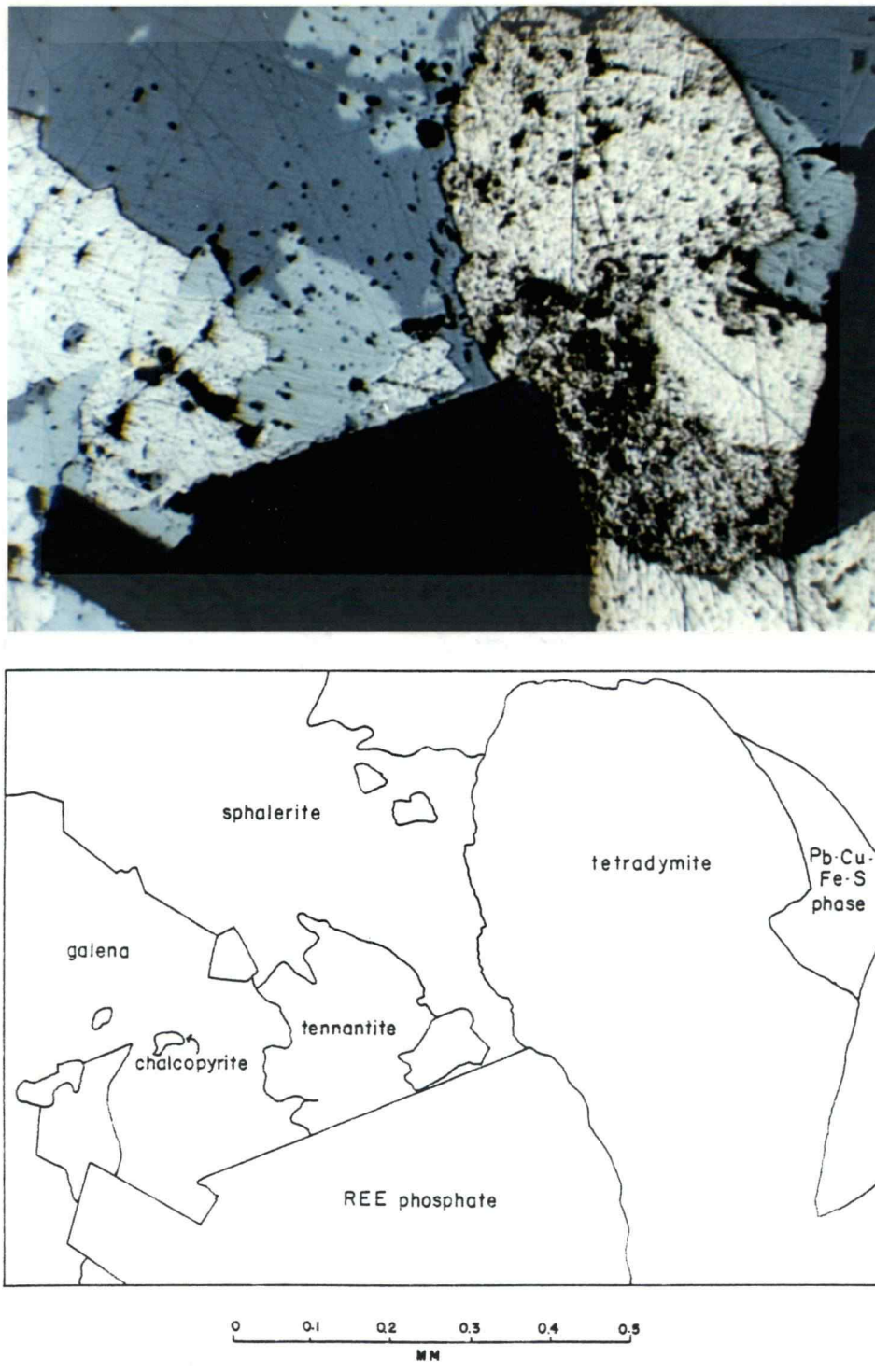

Plate 21. Photomicrograph of tetradymite under reflected light, from the main sulphide vein. This early mineral is ragged, pitted, and embayed by later crystallising minerals.

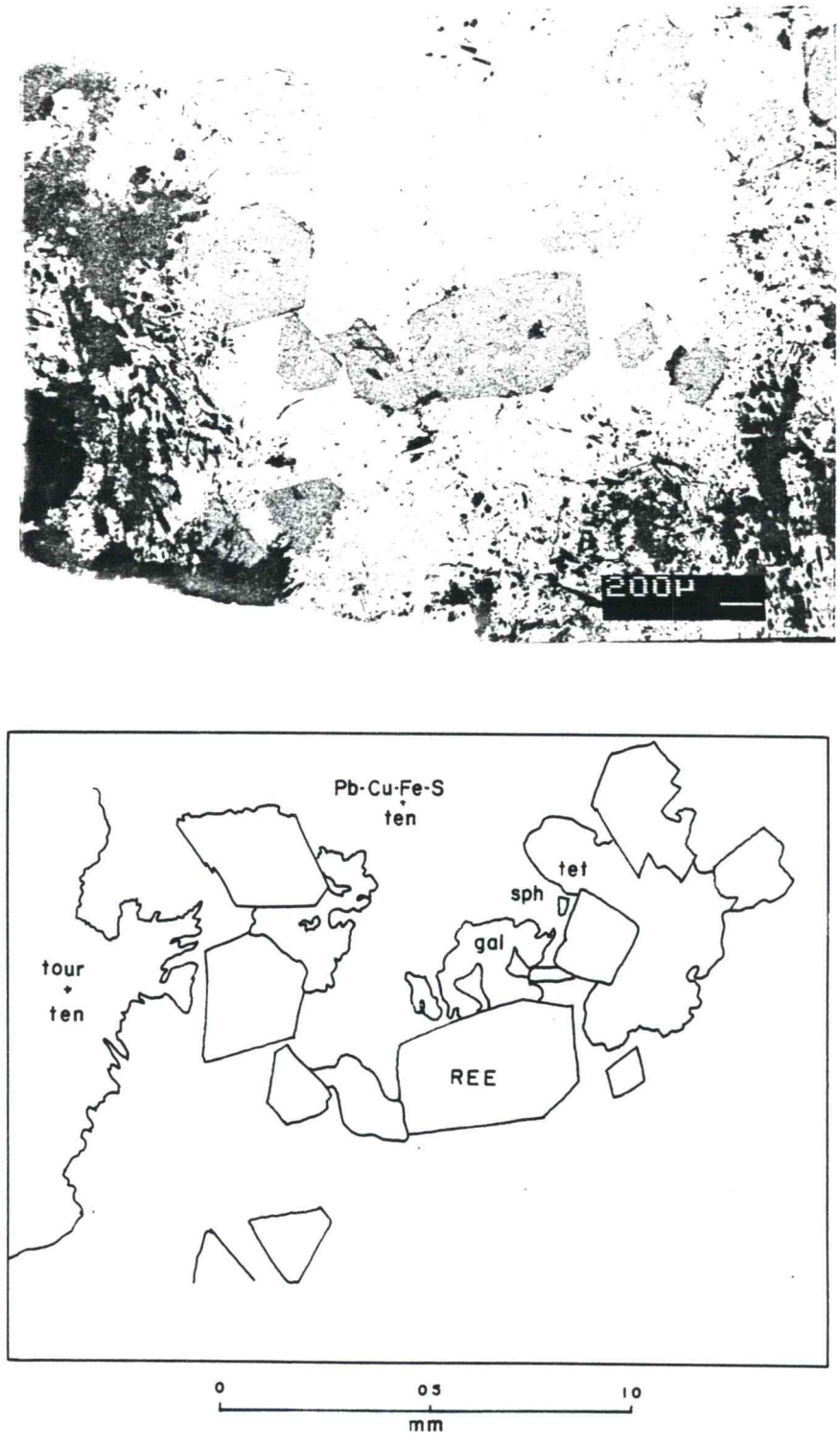

Plate 22. S.E.M. photo image of backscattered electrons of the sulphide phases in the main sulphide vein. Tennantite and the Cu-Pb-Fe-S phase are late matrix minerals.

precious metal epithermal deposits.

Tennantite [$Cu_{12}As_4S_{13}$] (with possible replacement of Cu by Ag, Hg, Zn, Fe, and, of As by Sb, Bi, Ge, and Sn: Picot et al., 1982, p. 139)

The tourmaline and sulphide veins have 5 to 20 percent tennantite as matrix material. Anhedral tennantite crystals (0.06-0.1 mm) form aggregates that are interstitial to pyrite, enargite, tetradymite, galena, and tourmaline, and are embayed by tourmaline and the REE phosphate (Plates 21 and 22). Tennantite exhibits emulsion textures with sphalerite, the Cu-Pb-Fe-S phase, and chalcopyrite. Some crystals of tennantite exhibit up to 80 percent replacement by chalcopyrite, yet veinlets of tennantite also cut across chalcopyrite. Payne (1983) and B.C.D.M. (1935) observed inclusions of chalcopyrite and galena in the tennantite. As antimony was not found using SEM-EDS analyses, it is assumed that tetrahedrite ($Cu_{12}Sb_4S_{13}$) is not significantly present in solid solution with tennantite at Taylor-Windfall.

Tennantite is present in the porphyry copper deposits at Chuquicamata, Chile, and Butte, Montana (Ramdohr, 1980, p. 570), and in epithermal precious metal deposits at Pueblo Viejo, Dominican Republic (Kesler et al., 1981), El Indio, Chile (Walthier et al., 1983), Goldfield, Nevada (Buchanan, 1981) and, Julcani, Peru (Buchanan, 1981).

Sphalerite [ZnS] Sphalerite is associated with tennantite and the Cu-Pb-Fe-S phase as matrix material (Plates 21, 22, and 23). Anhedral crystals (0.01 to 0.08 mm) of sphalerite are present as intergrowths and exsolved phases of tennantite and the Cu-Pb-Fe-S phase.

Cu-Pb-Fe-S phase This unnamed mineral is matrix material that is

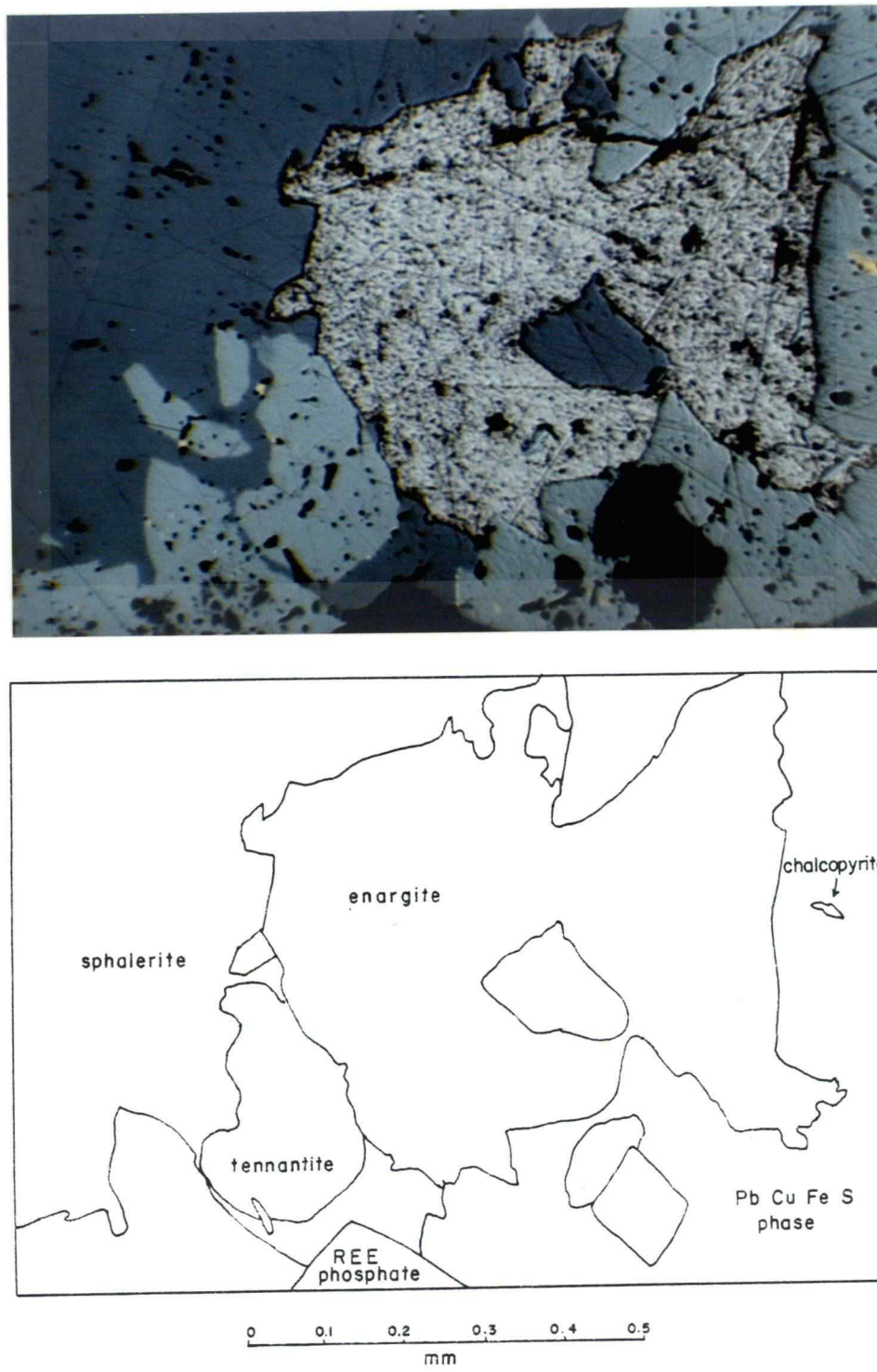

Plate 23. Photomicrograph of enargite under reflected light, from the main sulphide vein. Enargite is embayed and has a reaction rim.

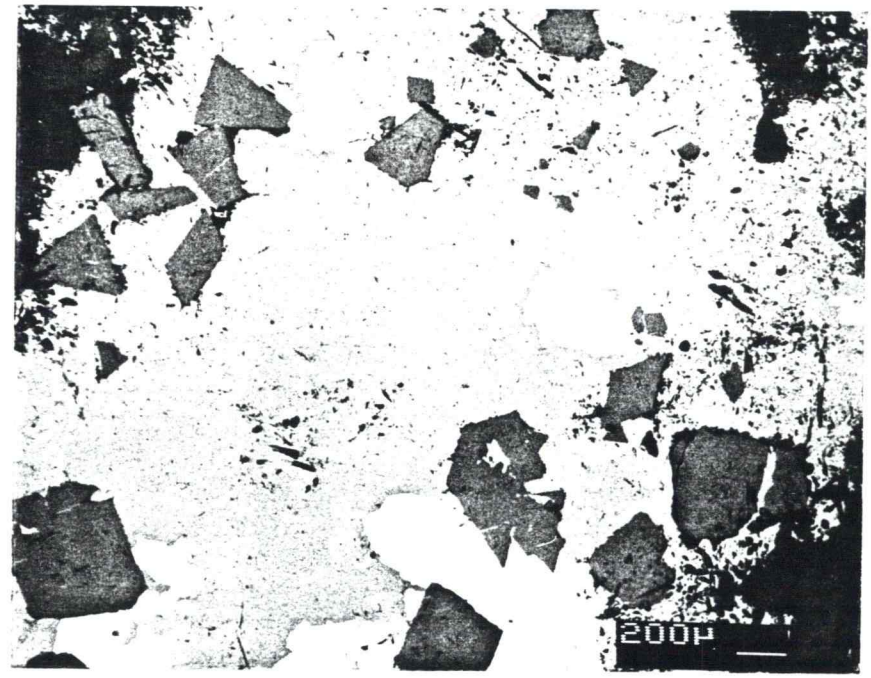

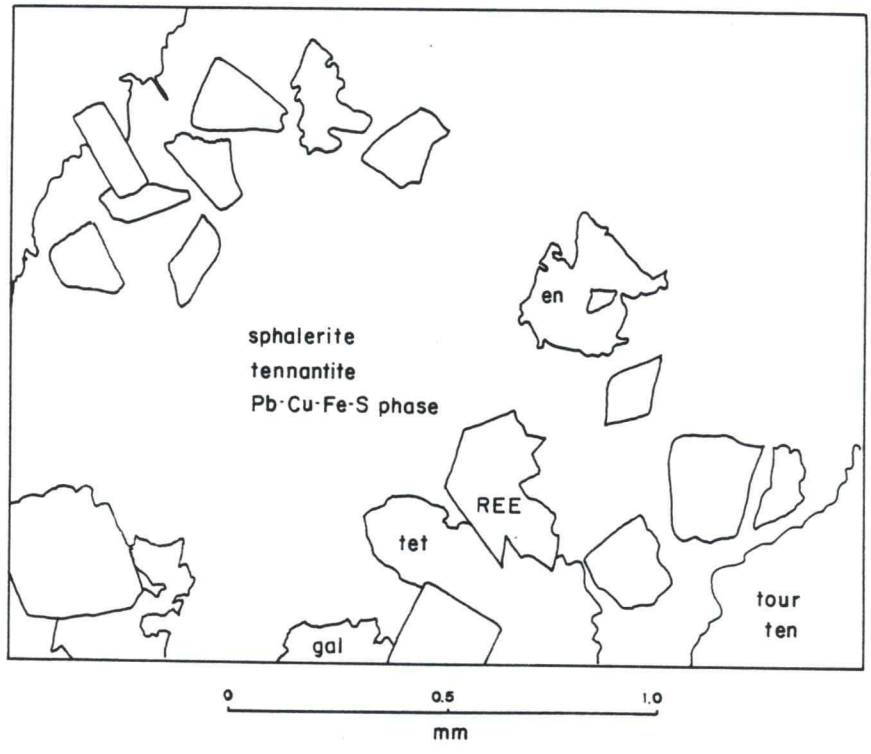

Plate 24. S.E.M. photo image of backscattered electrons of the sulphide phases in the main sulphide vein. Enargite and tennantite exhibit similar brightness because of their similar chemistry.

p.81 missing from original. Author unavailable to supply.

There are two p.72's. p.81 may not exist???

similar to sphalerite and tennantite in habit and mineral associations. It may be an mixture of galena and chalcopyrite. The phase was detected using SEM-EDS analyses and is indistinguishable from tennantite in reflected light.

Chalcopyrite [$CuFeS_2$] Chalcopyrite is present in concentrations of up to 5 percent in the main veins. It forms predominantly as an exsolved phase of small (0.05 mm) rounded to angular crystals hosted in tennantite. Chalcopyrite is both an early- and late-forming mineral as suggested by its habits as veinlets that crosscut late REE phosphate crystals, blebs interstitial to tourmaline, inclusions in tennantite, sphalerite, and pyrite, and as hosts for inclusions of these three minerals.

REE phosphate (La, Ce, Al, P, Nd? Pr?) A rare earth element phosphate was found using SEM-EDS analyses. Partial composition is shown in the EDS scan on Figure 15. Because of peak overlaps, Nd and Pr were not identified with absolute certainty. This mineral is hosted in both of the main veins at concentrations of up to 5 percent. It forms late phase pristine, rhombohedral crystals, up to 5 mm in length (Plates 21 to 24). Microveinlets of chalcopyrite cut across it, and a dark reaction rim surrounds the phosphate where it is in contact with tennantite.

Siderite [$(Fe,Mg)CO_3$ to $FeCO_3$] Siderite was identified using XRD analysis. Similar to the REE phosphate, it formed late as rhombohedrons.

Hematite [Fe_2O_3] Bladed specular hematite is hosted in a quartz vein (GP 84 25B), and forms vein material in association with pyrite, chalcopyrite, tourmaline, and calcite (DDH 84 03, 141.5 m).

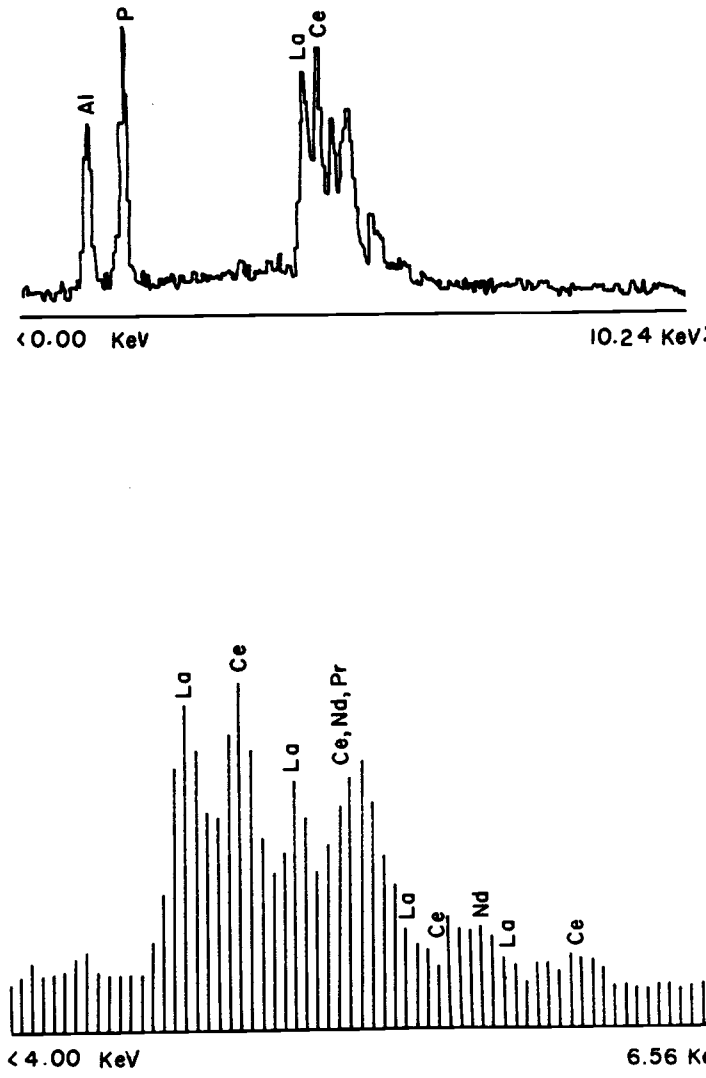

Figure 15. S.E.M.-E.D.S. peaks for the REE phosphate. The upper scan ranges from 0 to 10.24 KeV, and the lower more detailed scan ranges from 4.00 to 6.56 KeV. Total counts are 26,103 and 24,000 respectively.

Covellite [CuS] This fine-grained blue mineral has formed as replacement films on pyrite at crystal boundaries and on fractures in the main sulphide vein.

Malachite [$Cu_2CO_3)(OH)_2$] Macroscopic malachite occurs as an oxidation replacement rind on the main sulphide vein.

Trace elements in veins

All forty-six samples of vein material collected from the two underground levels were analysed for gold. Additional analyses for Cu, Pb, Zn, Ag, As, Hg, and Sb were made of nine of these samples, and results and vein mineralogies are given in Table 2. Sample locations, main vein locations, and results from gold analyses are plotted on Figure 14. Analytical methods and detection limits are in Appendix 3. Results are discussed below in the order of precious metals to base metals (Au, Ag, Hg, As, Sb, Cu, Pb, and Zn).

The main tourmaline and sulphide veins have concentrations of gold that range from 0.021 troy ounces per metric ton (650 ppb) to 0.9 oz/T (27,990 ppb). Of the seven samples collected from the main veins, four have greater than 0.32 ounces of gold per ton (10,000 ppb, which is the upper detection limit of one of the analytical methods used). Where the main tourmaline vein has been tectonically comminuted to fault gouge, the only sample collected returned a value of 0.006 oz/T (200 ppb).

Mineral coatings on 30 of the N060E -trending fractures (Plate 19) were analysed for gold. Values range from 5 ppb (the lower detection limit) to 845 ppb. The mean value is 144 ppb, and nineteen of the samples contain less than 100 ppb of gold. The range in gold concentrations from the five samples of quartz vein material collected

is 5 to 85 ppb, and the mean is 38 ppb. Only one sample from a pyrite vein was analysed (185 ppb).

Although native gold was not detected using SEM-EDS analysis, the author, Payne (1984), and early mine workers have observed discrete particles of native gold in polished sections and eluvium. Thus, gold is sporadically distributed, in greater concentrations in both main veins relative to the quartz and pyrite veins. Gold has been depleted in the faulted section of the main tourmaline vein, and was either depleted or originally of lower concentrations in minerals of the fracture coatings.

Only nine samples were analysed for silver (and Hg, As, Sb, Cu, Pb, and Zn). Descriptions of the nine samples, and analytical results are presented in Table 2. Because samples of the gouge zone, pyrite vein, fracture coating, and quartz vein have lower concentrations of silver, relative to the main veins, the distribution of silver appears to be similar to that of gold.

Mercury is distributed in the same pattern as gold and silver, although the quartz vein is slightly enriched (500 ppb) relative to the gouge zone (110 ppb), pyrite vein (120 ppb), and fracture coating (140 ppb). Arsenic, antimony, copper, lead, and zinc are also only in high concentrations in the main veins, and in low concentrations in the gouge zone, fracture coating, pyrite vein, and quartz vein.

Trace elements in wall rock

The underground workings were sampled in order to determine the open-pit large-tonnage mining potential of the Taylor-Windfall prospect. Each of the 206 panel samples consists of 1 to 2 kilograms

TABLE 2

VEIN DESCRIPTIONS AND MULTI-ELEMENT RESULTS

Sample number	Composition	Description	Cu ppm	Pb ppm	Zn ppm	Ag ppm	As ppm	Hg ppb	Sb ppm	Au ppb
38566	tour, py, sulph	main tour vein	>10000	4300	9100	19.0	>10000	26000	1000	>10000
38568	" " "	" " "	"	2700	10000	6.7	8300	27000	950	>10000
38571	" " "	" " "	4200	810	810	4.4	48	1900	800	670
38573	" " "	" " " (gouge zone)	150	19	32	0.3	32	110	25	650
58567	" " "	" " " " "	500	63	124	1.0	150	300	105	200
38565	sulph, tour	main sulphide vein	>10000	1450	10000	>100	5700	24000	100	1100
38569	py, chl, tour	massive py vein	240	37	452	0.7	81	250	26	175
38570	tour, py, chl, ser	fracture coating	158	22	155	0.4	53	140	1	80
38564	quartz, rutile	quartz vein	10	12	22	0.2	6	500	3	85

abbreviations: tour:tourmaline
py:pyrite
sulph:sulphide minerals (tennantite, tetradymite, enargite, galena, sphalerite, chalcopyrite, and Cu-Pb-Fe-S phase
chl:chlorite
ser:sericite

of approximately 1 cm^3 rock chips, collected every 10 cm over a panel area of 1 square metre. Panel sample locations and gold values equal to or greater than 45 ppb are shown in Figure 16 (in map pocket). Results from Cu, Pb, Zn, Ag, As, Hg, Sb, and Au analyses are in Appendix 3. Diamond drill core from DDH-84-03, 05, and 06 was split, and about 250 samples were analysed for Au. Values greater than or equal to 45 ppm are plotted on Figure 7b (in the map pocket), and other lower values are given in Westmin's 1985 report. Perusal of these results indicates that the Taylor-Windfall prospect would be uneconomic at current metal prices as an open pit mine for any of the trace elements listed. As the purpose of the analyses was to determine the mining potential and not to define target areas for further exploration, the anomalous high values (>98%) are not calculated for each trace element, and such data are not contoured. The target is already defined as the underground workings and immediate environs, and any smaller target area is regarded as uneconomic from the onset.

To better understand the mineralisation process and metal associations, element concentrations were correlated with each other, as shown in Table 3. All correlations are good to excellent (r=0.792 to r=0.982), with the exception of silver-element correlations. Good correlations indicate that the elements exhibited geochemical coherence as they diffused through the wall rock and underwent deposition.

These high correlation coefficients are misleading as some panel samples include vein material, and a number of vein sample results were erroneously included in the computations. A second correlation

TABLE 3

Correlation matrices, means, and ranges for trace element data

(111 samples of both wall rock and vein material)

	Cu	Pb	Zn	Ag	As	Hg	Sb	Au
Cu	1.000	0.890	0.979	0.664	0.951	0.957	0.982	0.835
Pb		1.000	0.872	0.456	0.903	0.923	0.868	0.855
Zn			1.000	0.697	0.969	0.951	0.933	0.820
Ag				1.000	0.521	0.672	0.644	0.255
As					1.000	0.931	0.899	0.885
Hg						1.000	1.000	0.815
Sb							1.000	0.972
Au								1.000

	Mean	Range
Cu	494 ppm	3-10000 ppm
Pb	105 "	1-4300 "
Zn	398 "	4-10000 "
Ag	1.6 "	0.1-100 "
As	339 "	3-10000 "
Hg	0.997 "	0.01-27 "
Sb	49.7 "	0.1-1000 "
Au	0.40 "	0.002-10 "

(96 samples of only wall rock)

	Cu	Pb	Zn	Ag	As	Hg	Sb	Au
Cu	1.000	0.078	0.394	0.029	0.451	-0.010	0.224	0.021
Pb		1.000	0.393	0.229	0.468	0.278	0.433	0.229
Zn			1.000	0.317	0.429	0.140	0.371	0.307
Ag				1.000	0.091	0.266	0.100	0.158
As					1.000	0.067	0.616	0.199
Hg						1.000	0.182	0.280
Sb							1.000	0.215
Au								1.000

	Mean	Range
Cu	60 ppm	3-340 ppm
Pb	8.4 "	1-57 "
Zn	29 "	4-155 "
Ag	0.2 "	0.1-0.6 "
As	11 "	3-72 "
Hg	0.1 "	0.01-1.8 "
Sb	2.4 "	0.1-21 "
Au	0.02 "	0.002-0.2 "

Numbers are faded on original.

matrix was constructed, and results from 15 samples that include vein material were deleted from the computation. Correlations are all low, as shown in Table 3. The extreme difference between the two correlation computations is shown in the plots of Cu versus Hg, in Figures 17a and 17b, where a few extremely large values produced a high correlation coeffecient.

In conclusion, the consistently high concentrations of Au, Ag, As, Sb, Cu, Pb, and Zn in the main tourmaline and sulphide veins suggest that these elements displayed similar characteristics in mobility and fixation as the hydrothermal fluid flowed through and mineralised these two structures. Mercury was more mobile, perhaps because it may have been transported as a vapour phase, as it is also concentrated in the quartz veins. These elements were in very low concentrations in the fluid that diffused through the wall rock, and they display a wide range of mobility as shown by the low correlation coefficients.

Metalisation paragenesis

Mineral (and metal) paragenesis is illustrated on Figure 18. In summary, these minerals were concentrated in a confined planar area during the high temperature and retrograde alteration events. Early forming minerals are enargite, tetradymite, galena, and probably native gold. Late crystalising matrix minerals are tennantite, sphalerite, the Cu-Pb-Fe-S phase, and chalcopyrite.

During argillic alteration, sulphide minerals were leached out of the main tourmaline vein in the gouge zone where the active fault movement permitted the access of acid supergene fluids. Sulphide

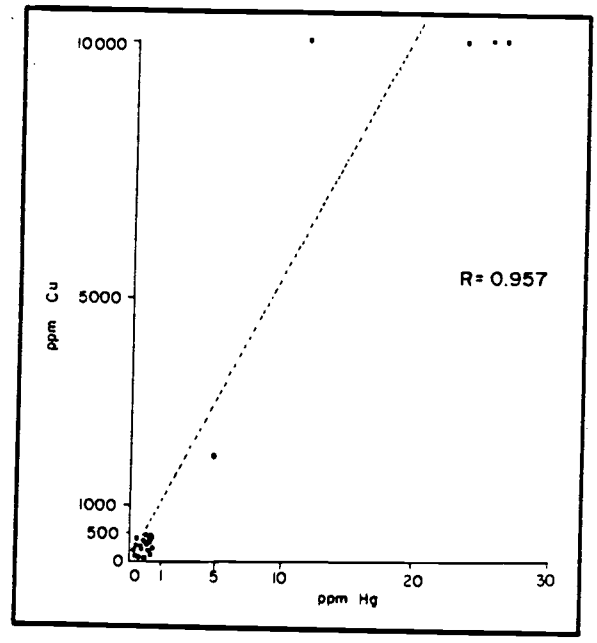

Figure 17a. Cu versus Hg for vein and panel samples.

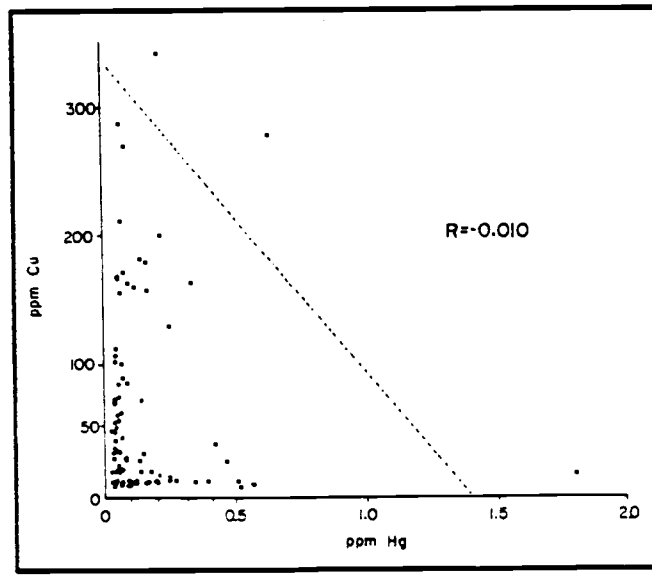

Figure 17b. Cu versus Hg for panel samples only.

minerals, if they were present, may also have been leached from the fracture coatings and wall rocks. Massive impermeable tourmaline may have blocked the movement of the acid fluid, and resulted in the preservation of sulphide minerals in the main tourmaline vein. The main sulphide vein has a lower proportion of tourmaline, and may have been sufficiently impermeable to prevent acid leaching.

In conclusion, ore grade vein and wall rock material is lacking possibly because; 1) the hydrothermal fluids initially had low amounts of metals, 2) sulphide minerals were concentrated in only a few anomalous structures that originated at great depth, 3) metals were concentrated only during a high temperature alteration event and 4) sulphide minerals may have been removed by subsequent supergene acid leaching.

PARAGENESIS

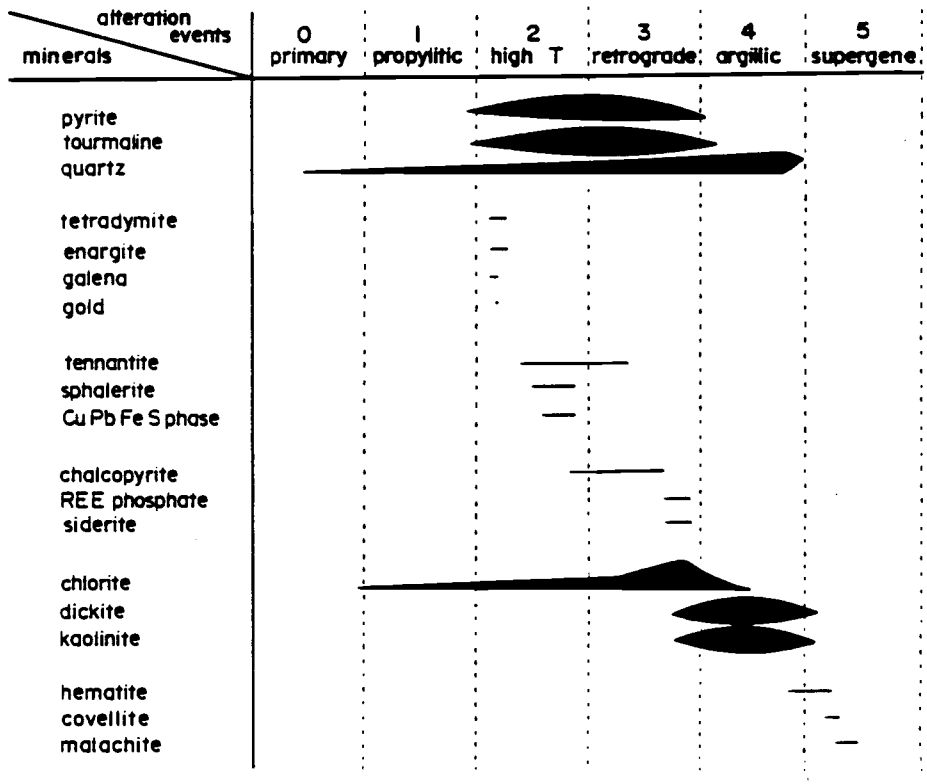

Figure 18. Paragenesis of economic minerals.

GENETIC MODEL

The Taylor-Windfall prospect bears similarities to both porphyry copper and epithermal precious metal hot spring-related deposits. In the following text the ages and tectonic settings, structures, host rocks, assemblages and distributions of alteration minerals, and styles of metalisation of the two types of deposits are described, and generalized models are proposed. The Taylor-Windfall prospect is compared to the porphyry and epithermal models, and in summary the genesis of the prospect is postulated.

Porphyry Model

Many authors have noted a clustering of plutonic activity and related porphyry copper deposition within specific temporal intervals; one appropriate and representative interval is from 50 to 80 million years ago (Sillitoe, 1972; Hollister, 1978; Meyer, 1981; Titley, 1982). Examples of porphyry deposits that formed about 50 million years ago in western British Columbia are the Granisle, Ajax, Berg, and Red Bird deposits (Field et al., 1974). Sillitoe (1972) states that the emplacement of copper-bearing plutons is contemporaneous with subduction at plate boundaries. In western British Columbia at the eastern margin of the Coast Range Plutonic Complex, the aforementioned porphyry deposits formed in spatial and temporal association with strike-slip and subduction-related tectonism (Hollister, 1978).

Porphyry deposits have a centrally located intrusive heat source and possibly one of metals, as shown in the model of Figure 19. These plutonic and (or) batholithic rocks are commonly quartz dioritic to

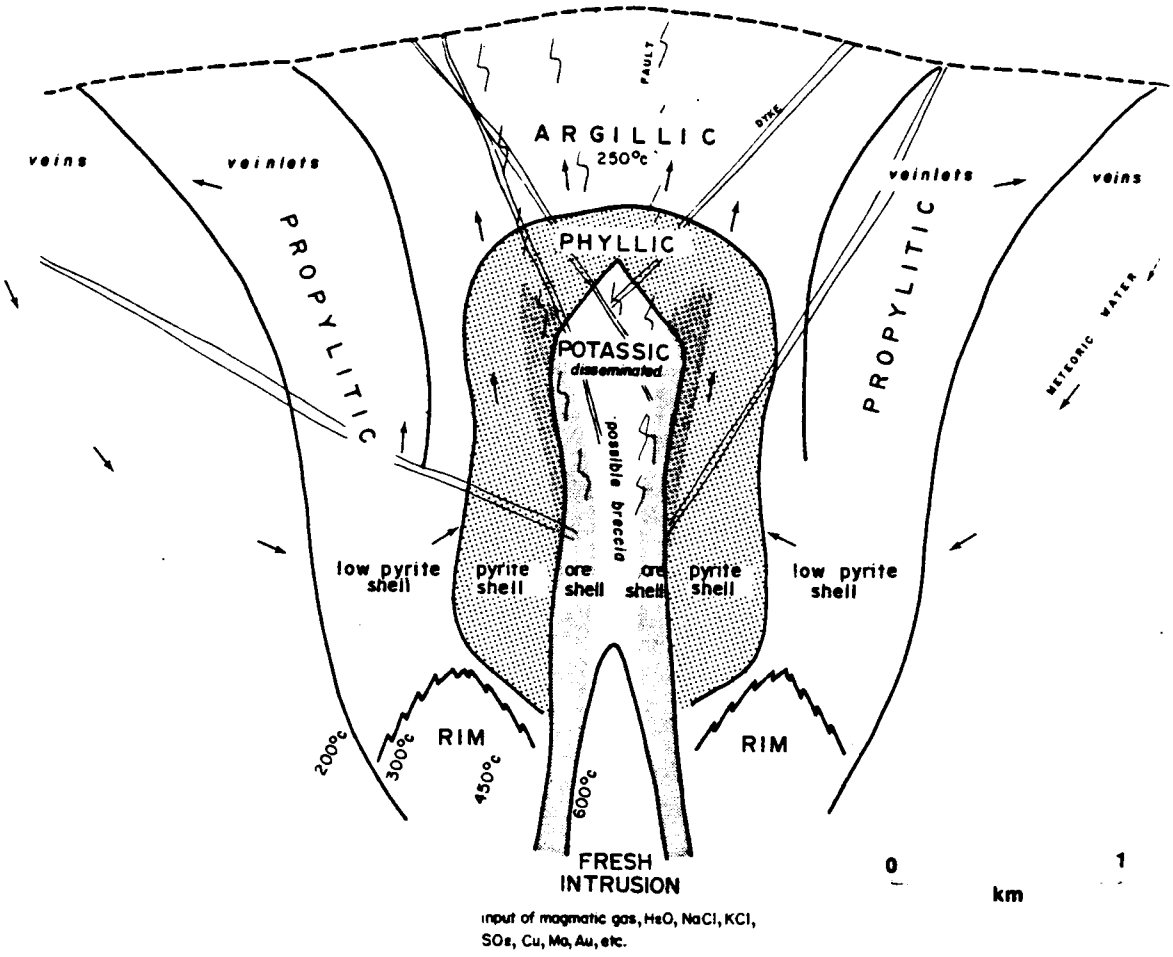

1) ALTERATION ZONES

PROPYLITIC: chlorite, epidote, carbonate, adularia, albite, sericite, montmorillonite, zeolites, quartz, pyrite, magnetite.
PHYLLIC: quartz, sericite, pyrite, chlorite, anhydrite, andalusite, tourmaline.
ARGILLIC: quartz, kaolinite, chlorite, montmorillonite, dickite, pyrophyllite, alunite, andalusite, gypsum, barite.
POTASSIC: quartz, orthoclase, biotite, sericite, anhydrite, albite, chlorite, tourmaline,.
FRESH INTRUSION: diorite, granodiorite, monzonite, quartz monzonite, ...

2) METALISATION ZONES

peripheral ore: chalcopyrite, galena, sphalerite, Au/Ag-bearing minerals.
low pyrite shell: 2% pyrite.
pyrite shell: 10% pyrite, <3% chalcopyrite, molybdenite.
ore shell: 1% pyrite, 1-3% chalcopyrite, molybdenite.

3) ORE TEXTURES

veins, veinlets, disseminations, breccia.

Figure 19. Hypothetical model of alteration zones, metalisation zones, ore textures and fluid flow at a porphyry copper deposit. Modified after: Lowell and Guilbert (1970); Gustafson and Hunt (1975); Henley and McNabb (1978); Hollister (1978); and, Beane (1982).

dioritic in composition (Titley, 1982). The intrusions are commonly overlain by comagmatic volcanic rocks, and both rock types may host ore (Sillitoe et al., 1984). Dykes may also be present.

The distributions of assemblages of hydrothermal alteration minerals in a generalized porphyry system are illustrated in Figure 19. Minerals contained in the various assemblages are listed below the figure. Individual minerals and (or) complete assemblages (ie. potassic) may be absent from some porphyry deposits (Gustafson and Hunt, 1975). During the formation of particular alteration assemblages specific oxides are gained or lost, such as Na_2O, CaO, MgO and iron oxides which are depleted during phyllic and argillic alteration, and SiO_2, MgO and K_2O which are probably added during potassic alteration (Beane, 1982). Magmatically derived hydrothermal fluids may cause alteration and metalisation by adding volatiles, oxides and the metals Cu, Mo, Zn, Au, Ag, As, Sb, (and others) to the host rocks (Gustafson and Hunt, 1975). Meteoric waters, rich in oxygen may percolate down into the porphyry system (Fig. 19) and argillic and supergene alteration may result from the oxidation of H_2S to H_2SO_4 (Beane, 1982).

Economic concentrations of Cu and Mo contained in chalcopyrite, bornite, chalcocite, covellite, native copper and molybdenite are present in veins and breccias, and disseminated throughout porphyry deposits. Lesser amounts of other base and precious metals may form in vein and replacement deposits peripheral to the porphyry ore. As illustrated in the model, ore commonly forms disseminations and breccias in the core, and veins in the surrounding area. The range in grades and tonnages of porphyry copper deposits is from about 10 to

1000 million tons of 0.4 to 1.0 percent copper, and recoverable amounts of Mo, Au, Ag, and other metals (Field et al., 1974).

Epithermal (hot spring-related) Model

The majority of epithermal precious metal deposits are Mesozoic to Tertiary in age, although some active geothermal systems are currently forming metals (Buchanan, 1981). These deposits may be spatially associated with large scale faults that have been related to subduction at convergent plate boundaries (Giles and Nelson, 1982). Epithermal deposits are commonly hosted by aphanitic, pyroclastic, scoriaceous and pumiceous andesitic to rhyolitic volcanic rocks (Buchanan, 1981).

A hypothetical model of an epithermal precious metal system is presented in Figure 20. The distribution of assemblages of alteration minerals in these deposits is somewhat similar to that in porphyry environments. Sillitoe and Bonham (1984) have noted that the argillic alteration which forms in active geothermal systems has a similar mineralogy to the the argillic assemblage found in the upper levels of porphyry copper systems, and thus epithermal precious metal deposits may be found above some porphyry deposits. The potassic zone is absent from epithermal deposits and the sericitic and propylitic assemblages are asymmetrically distributed around high angle faults. Also, epithermal (hot spring-related) deposits generally have a silica cap or sinter, that formed in and around the margins of hot spring pools as SiO_2-rich fluids breached the surface.

Metalised rocks in the epithermal model have been subivided into three groups based on depth of formation and mineral associations (Fig. 20). The silicified horizon may host veins and disseminations

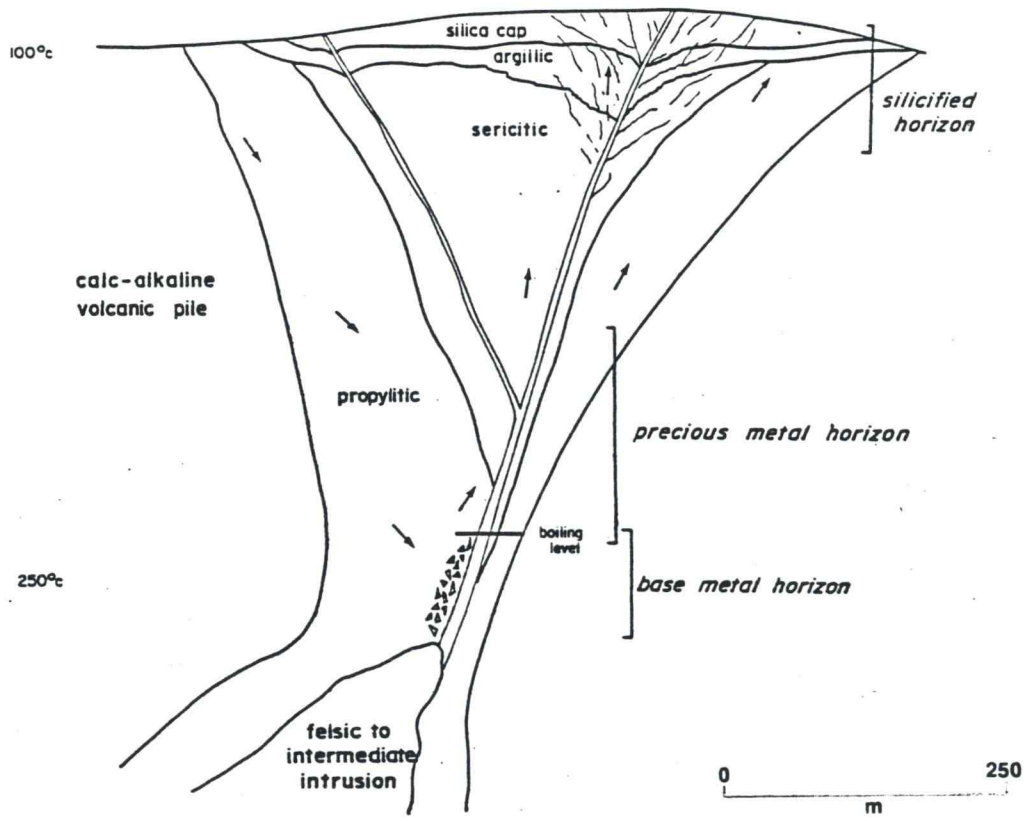

1) ALTERATION ZONES

silica cap: opal, cristobalite, quartz, anatase, pyrite, illite, cinnibar.

argillic: alunite, kaolinite, pyrite, zeolites, calcite, quartz, barite.

sericitic: illite, celadonite, sericite, adularia, quartz, pyrite, calcite, chlorite, fluorite.

propylitic: quartz, epidote, carbonate, adularia, albite, sericite, montmorillonite, zeolites, pyrite, magnetite.

2) METALISATION HORIZONS

silicified horizon: Sb, As, Au, Ag, Hg, Tl as native minerals, and in sulphide and sulphosalt minerals.

precious metal horizon: pyrargyrite, proustite, argentite, electrum, Ag sulphosalts.

base metal horizon: galena, sphalerite, chalcopyrite, argentite.

Figure 20. Hypothetical model of alteration and metalisation zones at an epithermal precious metal deposit. Modified after: Buchanan (1981); Giles and Nelson (1982); and, Berger and Eimon (1983).

of precious metals. The base of the sericitic alteration zone may host vein swarms, disseminations and multiphase breccias that contain precious metals. Below the level of boiling (Fig. 20), base metals may be deposited in propylitically altered rock. Anomalous concentrations of Au, As, Sb, Hg, and B are present in epithermal deposits. In the deeper and hotter parts of these systems base metals, Ag, Te, and Bi are deposited (White, 1981). The mechanism of metals concentration is thought to be a repeated cycle of sealing, boiling, and hydrofracturing. Sulphide minerals form during the boiling episode. The range in grades and tonnages of epithermal deposits is from about 0.05 to 100 million tons of ore that grades 0.03 to 2.0 oz/T Au and 2.0 to 25.0 oz/T Ag (Buchanan, 1981).

The Taylor-Windfall Model

The genesis of the Taylor-Windfall prospect is depicted by the generalized summary given in (cartoon form) Figure 21. A 1500 m thick succession of tuffaceous andesites (Kingsvale Group) of Late Cretaceous age was intruded by an 82 to 89 Ma (McMillan, 1976) complex of quartz diorite to quartz monzonite plutons (Coast Plutonic System). The presence of mafic to felsic dykes oriented parallel to large scale high angle faults implies that tectonic activity was concurrent with or predated intrusive activity. Hydrothermal fluids of probable magmatic origin permeated through large volumes of volcanic and plutonic rock to form widespread areas of pervasive propylitic alteration. All primary hornblendes and pyroxenes, and some plagioclase feldspars were destroyed, and a propylitic assemblage that contains biotite, epidote, chlorite, clinozoisite, calcite, laumontite, apatite, and magnetite was formed by replacement. This

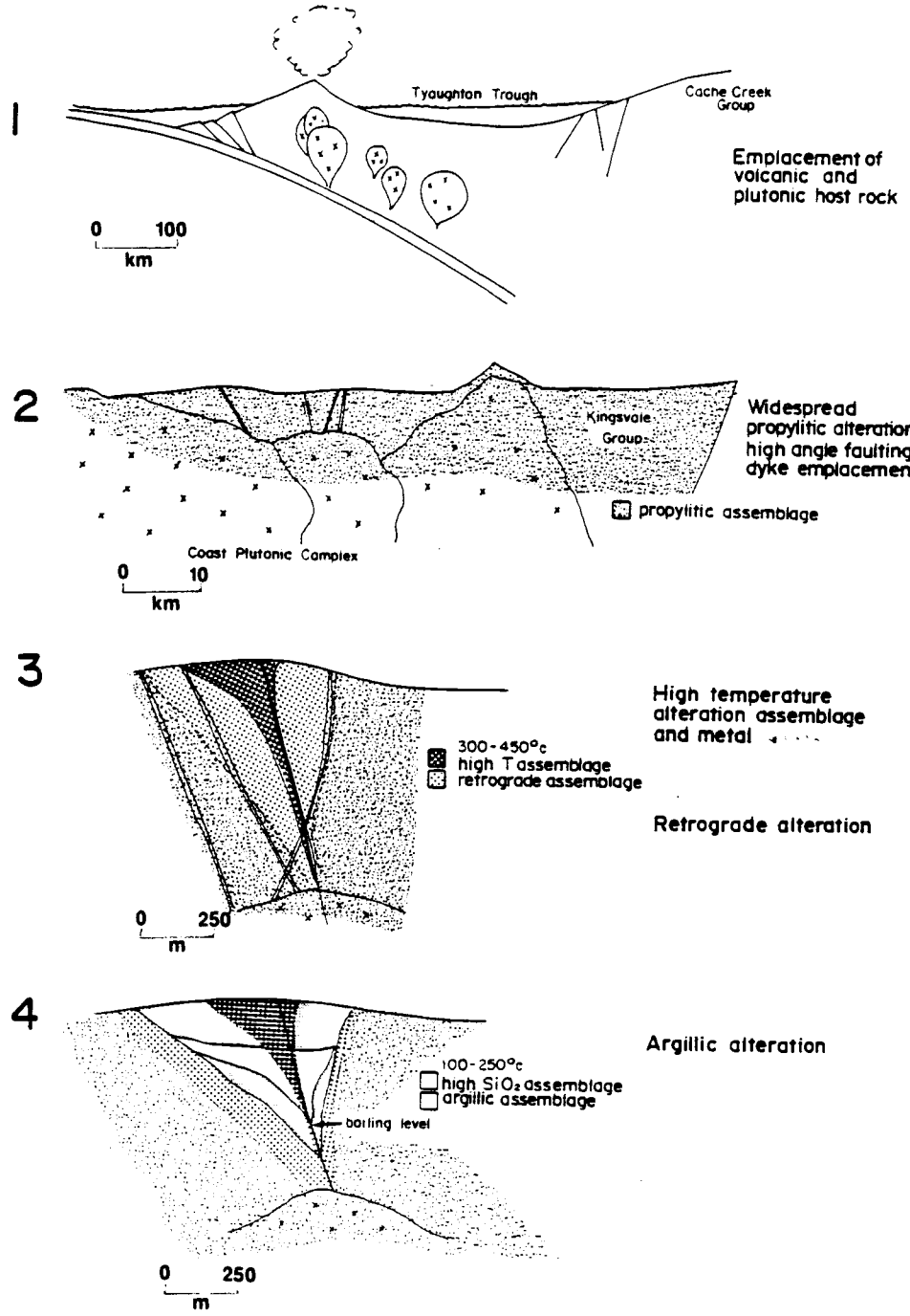

Figure 21. Genesis of the Taylor-Windfall prospect.

alteration resulted in depletions of the oxides CaO (100- 200 g/1000 cm^3), Na_2O (20-100 g/1000 cm^3) and MgO (10-100 g/1000 cm^3) from the host rocks.

The spatially restricted corundum-andalusite assemblage indicates the presence of a more evolved fluid (or a separate second fluid) that attained temperatures of 350°c and greater. This liquid was enriched in Au, Ag, As, Sb, Cu, Pb, Zn, Hg, B, SiO_2, and possibly Al_2O_3, as is implied by the high concentrations of these elements in veins spatially associated with the high-temperature minerals, and by additions of up to 753 g/1000 cm^3 of SiO_2 and 369 g/1000 cm^3 of Al_2O_3 to altered host rocks. The veins contain up to 0.9 oz/T Au and greater than 3.5 oz/T Ag (>100 ppm). Minerals of economic interest that localized in the veins are tennantite, enargite, tetradymite, galena, sphalerite, and native gold. As the vein and high-temperature minerals were formed, the hydrothermal fluid is believed to have become depleted with respect to metals, except Hg which is in high concentrations (500 ppb) in a sample of siliceous rock. This fluid attained SiO_2 saturation as a result of decreasing temperatures (Fig 12b) in both the root system (located between the quartz diorite exposures in the 1648 m level), and at the bedding plane contact between units 3 and 4, where host rocks contain up to 95 percent SiO_2.

This metal-deficient liquid may have mixed with oxygen-rich meteoric water and become extremely acid because of the oxidation of H_2S, and the concommitant release of H^+ ions. As a result of the influx of H^+ ions, sericite altered to an argillic assemblage of predominantly kaolinite and dickite. Fluid pressures may have become sufficiently high to cause hydrofracturing in the root zone, but the

hydrothermal liquids at this stage may have been too depleted in metals for this process to have any effect on the formation of ore. Fault movements during argillic alteration also may have prevented the cycle of sealing, boiling, hydrofracturing, and metal deposition that is expected in near-surface hydrothermal systems. Thus, the argillic alteration assemblage is barren of economic minerals.

Pleistocene alpine glaciation contributed to the erosion of 1200 m of overlying volcanic flows and tuffs, and exposed the resistant siliceous ridge. Local supergene oxidation of pyritic host rocks resulted in the formation of ferricrete along stream beds; the presence of which initially aroused the interests of prospectors to this area.

In summary, sulphide mineralisation at the Taylor-Windfall prospect formed at the same time, and in the same tectonic environment as some porphyry copper deposits in western British Columbia. Similar to the porphyry model, the prospect is hosted in rocks that are spatially associated with Cu-Mo bearing quartz diorites and quartz monzonites. The metaliferous corundum-andalusite bearing core at the property is rimmed by a funnel-shaped area of phyllic alteration that is in turn surrounded by propylitically altered rocks. Parts of all zones have been overprinted by an argillic alteration assemblage. This distribution of alteration assemblages is similar to that of the Frieda (Britten, 1980) and El Salvador porphyry copper deposits (Gustafson and Hunt, 1975). Metals at Taylor-Windfall are concentrated in two main veins; one of which is tourmaline-rich and the other is sulphide-rich. Breccias, disseminations and swarms of veins that host sulphide minerals were not observed at the prospect.

The metals and style of hydrothermal alteration present at the Taylor-Windfall prospect are similar to those found in some epithermal deposits. However, Taylor-Windfall has a corundum-andalusite assemblage that implies high fluid temperatures, and sinter and breccia that form in most epithermal systems are lacking. As stated by Sillitoe and Bonham (1984), epithermal deposits may be found in the upper level of some porphyry deposits, where precious metals concentrated near the surface. The grade and tonnage of the two veins at the property is about 1000 metric tons of 0.4 ounce of gold per ton. Therefore, as implied by styles of alteration and metalisation at Taylor-Windfall, the prospect may be located in the base of a small and apparently metal-deficient epithermal system that resides in the upper level of a larger buried porphyry system, connected to its intrusive heat and possible metals source by a deep-seated structure such as the Tchaikazan Fault.

The Taylor-Windfall prospect has many of the geologic "signatures" expected in the vicinity of an epithermal or porphyry ore body. These include an impressively large surface area of greater than 2 km^2 of siliceously and argillically altered volcanic rock, proximal plutonic rocks, large scale high angle faults, and gold-bearing veins.

Ore was not found in the area explored, possibly because; 1) ore, if formed, may have been removed by erosion and (or) leaching, 2) structures were not sufficiently deep to serve as conduits for for gold-bearing fluids and hosts for veins, 3) hydrothermal fluids had initially low concentrations of metals, 4) the system was short-lived and heat was not supplied for a sufficient length of time to

concentrate metals, and 5) fault activity during hydrothermal alteration prevented sealing, followed by cyclic repetitions boiling and hydrofracturing, which are the mechanisms by which precious metals are most effectively concentrated.

This thesis represents a detailed study of a potential ore body, and some expedient exploration techniques were used; rapid whole rock XRD analyses in conjunction with thin section examinations, and rapid SEM-EDS analyses of polished sections. Both techniques are not routinely used in the exploration industry, and the author believes that they are cost and time efficient and particularly useful at the early stages of property evaluations where host rocks are highly altered

Further general work in the study of hydrothermal deposits might include; 1) a comparison of the trace element, major oxide and mineralogic signatures of hydrothermally altered rock associated with uneconomic versus economic porphyry systems, and 2) a similar comparison for epithermal hot spring-related systems.

REFERENCES

Anderson, J. A.. 1982, Characteristics of leached capping and techniques of appraisal, in Titley, S. R., ed., Advances in geology of the porphyry copper deposits, Southwest North America: Tucson, University of Arizona Press, p. 275-296.

Bates, R. L. and Jackson, J. A., 1980, Glossary of geology: Falls Church, Virginia, Amer. Geol. Inst., 749 p.

Beane, E. R., 1982, Hydrothermal alteration in silicate rocks in Tiltey, S. R., ed., Advances in geology of the porphyry copper deposits, Southwest North America: Tucson, University of Arizon Press, p. 117-138.

Beane, E. R. and Titley, S. R., 1981, Hydrothermal alteration and mineralization: Econ. Geol. 75th Anniv. Vol., p. 214-269.

Berger, B. R. and Eimon, P. I., 1983, Conceptual models of epithermal precious metal deposits in Shanks, W. C., ed., Cameron volume of unconventional mineral deposits: New York, Soc. Min. Eng., AIME, p. 191-205.

Bradford, J., 1984, Four mineral deposits in the Taseko River area: Unpub. BSc. thesis, University of B. C.

British Columbia Department of Mines (now called Ministry of Mines, Energy, and Petroleum Resources) Annual Reports, 1921 (p. G194), 1922 (p. N138), 1923 (p. A168), 1924 (p. A168), 1931 (p. A110), 1934 (p. F24), 1935 (p. F17-F21), Taylor-Windfall, Chilcotin Mining District.

Britten, R., 1980, Geology of the Frieda Cu-porphyry prospect, Papau-New Guinea: Unpub. PhD thesis, Australia National University.

------ 1984, Alteration at the Taylor-Windfall Mine: Esso Minerals of Canada, Unpub. Rpt., 6 p.

Brimhall, G. H., 1977, Early fracture-controlled disseminated mineralization at Butte, Montana: Econ. Geol., v. 72, p. 37-59.

Buchanen, L., 1981, Precious metal deposits associated with volcanic environments in the southwest in Dickinson, W. R. and Payne, W. D., Relations of tectonics to ore deposits in the southern Cordillera: Arizona Geol. Soc. Digest, v. 14, p. 237-261.

Burnham, C. W., 1979, Magmas and hydrothermal fluids in Barnes, H. ed., Geochemistry of hydrothermal ore deposits: Toronto, John Wiley and Sons, p. 71-136.

Cairnes, C. E., 1943, Geology and mineral deposits of Tyaughton Lake map-area, British Columbia: Geol. Sur. Canada, Paper 43-15.

Cargill, P. G. Lamb, J., Young, M. J., and Rugg, E. S., 1976, Island Copper in Porphyry deposits of the Canadian Cordillera: Can. Inst. Min. Metal., Spec. v. 15, p. 206-226.

Carson, D. J., Jambor, J. L., Ogryzlo, P. L. and Richards, T., 1976, Bell copper: geology, geochemistry, and genesis of a supergene-enriched, biotitized porphyry copper deposit with a superimposed phyllic zone in Porphyry deposits of the Canadian Cordillera: Can. Inst. Min. Metal., Spec. v. 15, p. 245-263.

Creasey, S. C., 1959, Some phase relations in the hydrothermally altered rocks of porphyry copper deposits: Econ. Geol., v. 54, p. 351-373.

Davis, G. A., Monger, J. W. and Burchfiel, B. C., 1978, Mesozoic construction of the Cordilleran 'collage', central British Columbia to central California in Howell, D. G. and McDougall, K. A., eds., Mesozoic paleogeography of the Western United States: Soc. Econ. Paleon. Mineral., Pacific Coast Paleogeography Symposium 2, p. 1-32.

Dawson, G. M., 1887, Report on a geological examination of the northern part of Vancouver Island and adjacent coasts: Geol Sur. Canada, Ann. Rpt. 1886, pt. B.

Deer, W. A., Howie, R. A. and Zussman, J., 1962, Rock forming minerals: New York, John Wiley and Sons, v. 1-5.

Dolmage, V., 1924, Chilco Lake and vicinity, B. C.: Geol. Sur. Canada, Summary Rpt., p. 59A-75A.

------ 1929, Gunn Creek Map-area: Geol. Sur. Canada, Summary Rpt., p. 78A-93A.

------ 1932, Taylor-Windfall gold deposit: Cominco, Unpub. Rpt.

Dudas, F. O., Campbell, I. H. and Gorton, M. P., 1983, Geochemistry of igneous rocks of the Hokurko District, Northern Japan: Econ. Geol., Mono. 5, p. 115-133.

Eimon, P. I. and Anctil, T. J., 1981, Epithermal precious metal deposits: Northwest Mining Assoc. 87th Convention, Spokane, Washington, Unpub. Rpt., 17 p.

Eisbacher, G. H., 1974, Evolution of successor basins in the Canadian Cordillera in Dott, R. H. and Shaver, R. H., eds., Modern and ancient geosynclinal sedimentation: Soc. Econ. Paleon. Miner., Spec. Pub. 19, p. 274-291.

Field, C. W., Jones, M. B. and Bruce, W. R., 1974, Porphyry copper-molybdenum deposits of the Pacific Northwest: Soc. Min. Eng., AIME Trans., v. 255, p. 9-22.

Ford J. H., 1978, A chemical study of alteration at the Panguna porphyry copper deposit, Bougainville, Papau-New Guinea: Econ. Geol., v. 73, p. 703-720.

Frantz, J. D. and Wiesbrod, A., 1974, Infiltration metasomatism in the system K_2O-AiO_2-Al_2O_3-H_2O-HCl in Hofman, A. W. et al., eds., Geochemical transport and kinetics: Washington, Carnegie Inst., Pub. 634, p. 261-271.

Galloway, J. D., 1917, Bulkley Valley to Chilcotin District: B. C. Rpt. of Min. of Mines for 1916, p. 134-186.

Giles D. L. and Nelson, C. E., 1982, Principal features of epithermal lode gold deposits of the Circum-Pacific rim: Circum-Pacific Energy and minerals resource conference, Honalulu, Unpub. rpt., 16 p.

Gill, J., 1981, Orogenic andesites and plate tectonics: New York, Springer-Verlag, 390 p.

Gustafson, L. B. and Hunt, J. P., 1975, The porphyry copper deposits at El Salvador, Chile: Econ. Geol., v. 70, p. 857-912.

Harvey, R. D. and Vitaliano, C. J., 1963, Wall-rock alteration in the Goldfield District, Nevada: Jour. Geol., v. 72, p. 564-579.

Hemley, J. J. and Jones, W. R., 1964, Chemical aspects of hydrothermal alteration with emphasis on hydrogen metasomism: Econ. Geol. v. 59, p. 538-569.

Hemley, J. J., Montoya, J. W. and Luce, R. W., 1980, Equilibria in the system Al_2O_3-SiO_2-H_2O and some general implications for alteration/mineralization processes: Econ. Geol., v. 75, p. 210-228.

Henley, R. W. and McNabb, A., 1978, Magmatic vapour plumes and ground-water interaction in porphyry copper emplacement: Econ. Geol., v. 73, p. 1-20.

Hollister, V., 1978, Geology of the porphyry copper deposits of the western hemisphere: Hoboken, New Jersey, AIME Compu Comp Corp. 219 p.

Jeletzky, J. A. and Tipper, H. W., 1968, Upper Jurassic and Cretaceous rocks of the Taseko Lakes Map-area and their bearing on the geological history of south western B.C.: Geol. Sur. Canada, Paper 67-54, 218 p.

Kerr, P. F. and Jenney, P., 1935, The dumortierite-andalusite mineralization at Oreana, Nevada: Econ. Geol., v. 30, p. 287-300.

Kesler, S. E., Russell, N., Seaward, M., Rivera, J., McCurdy, K., Cumming, G. L. and Sutter, J. F., 1981, Geology and geochemistry of sulfide mineralization underlying the Pueblo Viejo gold-silver oxide deposit, Dominican Republic: Econ. Geol., v. 76, p. 1096-1117.

Krauskopf, K. B. 1967, Introduction to geochemistry: New York, McGraw Hill Book Co., 721 p.

Lane, R., 1983, Taseko year-end report: Westmin Resources, Unpub. Rpt., 31 p.

Lowder, G. G. and Dow, J. A., 1978, Geology and exploration of porphyry copper deposits in North Sulawesi, Indonesia: Econ. Geol., v., 73, p. 628-644.

Lowell, J. D. and Guilbert, J. M., 1970, Lateral and vertical alteration and mineralization zoning in porphyry copper ore deposits: Econ. Geol., v. 65, p. 373-408.

MacKenzie, J. D., 1921, A reconnaissance between Taseko Lake and Fraser River, B. C.: Geol. Sur. Canada, Summary Rpt. Pt. A., p. 70-80.

McMillan, W. J., 1976, Granite Creek property in Geology in B. C.: B. C. Min. Mines Pet. Res., p. 67-84.

Meyer, C., 1981, Ore forming processes: Econ. Geol. 75th Anniversary Vol., p. 6-41.

Meyer, C., and Hemley, J. J., 1967, Wall rock alteration in Barnes, H., ed., Geochemistry of hydrothermal ore deposits: New York, Holt, Rinehart, and Winston Inc., p. 166-235.

Monger, J. W. and Price, R. A., 1979, Geodynamic evolution of the Canadian Cordillera - progress and problems: Can. Jour. Earth Sci., v. 16, p. 770-791.

Payne, J. G., 1983, Petrography of Taylor-Windfall samples: Westmin Resources, Unpub. Rpt., 15 p.

Pettijohn, F. J., 1975, Sedimentary rocks: New York, Harper and Row, Publishers, 628 p.

Phillips, W. R. and Griffen, D. T., 1981, Optical mineralogy: San Francisco, W. H. Freeman and Co., 677 p.

Picot, P. and Johan, Z., 1982, Atlas of ore minerals: France, B. R. G. M. and Elsevier, 458 p.

Quintana Resources Inc., 1976, Empress property: B. C. Min. Mines Pet. Res., Assessment Rpt. 6085.

Ramdohr, P., 1980, The ore minerals and their intergrowths: Oxford, Pergamon Press, 1205 p.

Roddick, J. A., Muller, J. E. and Okulitch, A. V., 1979, Fraser River map-sheet: Geol. Sur. Canada, map 1386A.

Sillitoe, R. H., 1972, A plate tectonic model for the origin of porphyry copper deposits: Econ. Geol., v. 67, p. 184-197.

Sillitoe, R. H. and Bonham, F. H., 1984, Volcanic landform and ore deposits: Econ. Geol., v. 79, p. 1286-1298.

Sillitoe, R. H., Halls, C. and Grant, J. N., 1975, Porphyry tin deposits in Bolivia: Econ. Geol., v. 70, p. 913-927.

Souther, J. C., 1967, Acid volcanism and its relationship to the tectonic history of the Cordillera of B. C., Canada: Bull. Volcan., v. 30, p. 161-167.

Tipper, H. W., 1963, Taseko Lakes map-area: Geol. Sur. Canada, map 29-1963.

------ 1969, Mesozoic and Cenozoic geology of the northeast part of Mount Waddington map-area, B. C.: Geol. Sur. Canada, Paper 68-33, 103 p.

------ 1978, Taseko Lakes map-area (map sheet): Geol. Sur. Canada, Open File 534.

Titley, S. R., ed. 1982, Advances in geology of the porphyry copper deposits, southwest North America: Tucson, University of Arizona Press, 560 p.

Titley, S. R. and Hicks, C., eds., 1966, Geology of the porphyry copper deposits, southwest North America: Tucson, University of Arizona Press, 287 p.

Walthier, T. N., Araneda, R. and Crawford, 1983, The El Indio gold, silver, dopper deposit, Region of Coquimbo, Chile: Unpub. Rpt. 13 p.

Waskowiak, R., 1975, Contribution to the geochemistry of boron in the crystalline rocks of Ruhla-Brotterode, Thuringer Wald in Walker, C. T., ed., Geochemistry of boron: Stroudsburg, Penn., Dowden, Hutchinson and Ross Inc., p. 64-67.

Watanabe, T., 1975, Geochemical cycle and concentration of boron in the earth's crust in Walker, C. T., ed., Geochemistry of boron: Stroudsburg, Penn., Dowden, Hutchinson and Ross Inc., p. 388-399.

Webber, G. P. and Jellema, J. V., 1965, Comparisons of geochemical compositions of soil and bedrock of Mont St Hilaire, Quebec: Can. Jour. Earth Sci., v. 2, p. 44-58.

West, R. J. and Aiken, D., 1982, Geology of the Sierrita- Esperanza deposit in Titley, S. R., ed., Geology of the porphyry copper deposits, southwest North America: Tucson, University of Arizona Press, p. 433-446.

Wheeler, J. O., Aitken, J. D., Berry, M. J., Gabrielse, H., Hutchinson, W. W., Jacoby, W. R., Monger, J. W., Neblett, E. R., Norris, D. and Price, R. A., 1972, The Cordilleran structural province in Price, R. A. and Douglas, R. J. eds., Variations in tectonic styles in Canada: Geol. Assoc. Canada, Spec. Paper 11, p. 1-82.

White, D.E. 1981. Active geothermal systems and hydrothermal ore deposits: Econ. Geol. 75th Anniversary volume. p. 392-423.

Wojdak, P. J. and Sinclair, A. J., 1984, Equity Silver Ag-Cu-Au deposit: alteration and fluid inclusion studies: Econ. Geol., v. 79, p. 969-990.

APPENDICES

APPENDIX 1

X-ray diffraction

Qualitative XRD analysis

Billets that remained from 70 thin section slabs were hand pulverized, sieved, and the -80 mesh fraction was then pulverized with an alumina mortar and pestle.

Each sample was packed into a container and analysed using a Phillips 3100 X-ray diffractometer. The copper target x-ray tube was run at 40 kV and 35 mA; ratemeter set at 1; range set at 5; chart speed set at 60 inches per hour; goniometer scan speed set at $2^{o}20$ per minute. These parameters were found adequate for resolving kaolinite-dickite peaks with a separation of $0.09A^{o}$ in the 3.65 A^{o} region. Each sample was scanned from 5^{o} to $50^{o}20$ (17.66 to 1.82 A^{o}). The resulting $1^{o}20$ per 1/2 inch scale was also chosen because of time constraints (25 minutes per sample), and paper manageability (1.5 m of chart paper per sample).

Previous analyses of rocks collected on the property (Britten, 1984) and documented similar alteration suites enabled the author to compile a list of silicate and oxide minerals that were expected to occur at Taylor-Windfall; albite, K-alunite, K/Na-alunite, andalusite, anorthite, barite, biotite 1M, brucite, calcite, chlorite (undifferentiated), corundum, clinozosite, diaspore, dickite, dumortierite, epidote, fluorapatite, gibbesite, jarosite, kaolinite 1Md, magnesite, Ca-montmorillonite, Na-montmorillonite, muscovite 1M, orthoclase, pyrite, pyrophyllite 2M1, quartz, rutile, siderite, stilpnomelane, tourmaline (variations: schorl, dravite, elbaite), zoisite, and, zunyite. The locations of 5 to 10 diagnostic diffraction peaks were then plotted on a mylar overlay of the same scale as the XRD charts. Use of this overlay permitted rapid whole rock XRD data

interpretation. Figures A1 and A2 are examples of two XRD charts (at a reduced scale).

For results refer to Table A2. Problems in resolution were only encountered in samples that have high proportions of feldspars or tourmaline, or both. Alunite was difficult to identify and corundum may have been selectively removed during sample preparation, as it is hard, will not pulverize, and may have not passed through the -80 mesh sieve.

Quantitative XRD analysis

Quartz Samples GP 84 34C and GP 84 34B, which have low quartz contents and representative mineralogies, were prepared as described above. Known weights of each sample were mixed with a range of known weights of pure quartz (1 gm total mixture wieght), pulverized again, and splits analysed using XRD. The heights of the 112 quartz peaks were measured for each mixture. The percentage of original quartz in the two samples was calculated. The mean of the ratio of quartz added to peak height (q/h) is 0.85 +/- 0.14 (one standard deviation), as shown in Table A1. This mean ratio was used as an approximation of the relationship between total quartz concentration and peak height. Original quartz concentration of the two samples was taken as peak height multiplied by the mean ratio. On the basis of this, sample GP 84 34C contains 10 percent quartz, and 34B contains 18 percent quartz.

Total quartz in each of the ten mixtures was calculated, taking into account the original quartz in the two samples. The following example illustrates how this was done. A weight of 0.80 grams (g) of sample GP 84 34C was added to 0.20 g of pure quartz. As sample 34C is

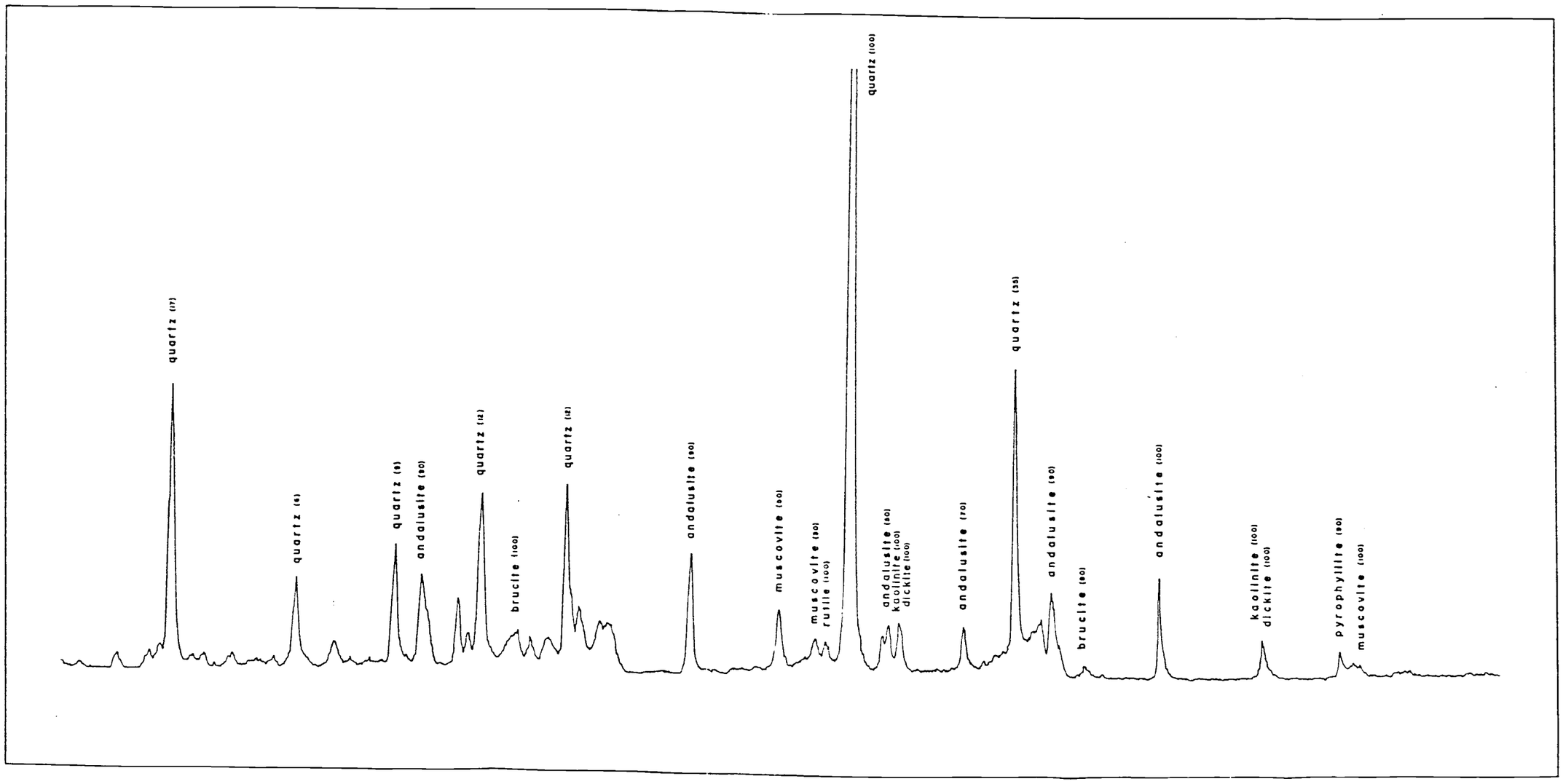

Figure A1. XRD chart of sample GP 84 45B.

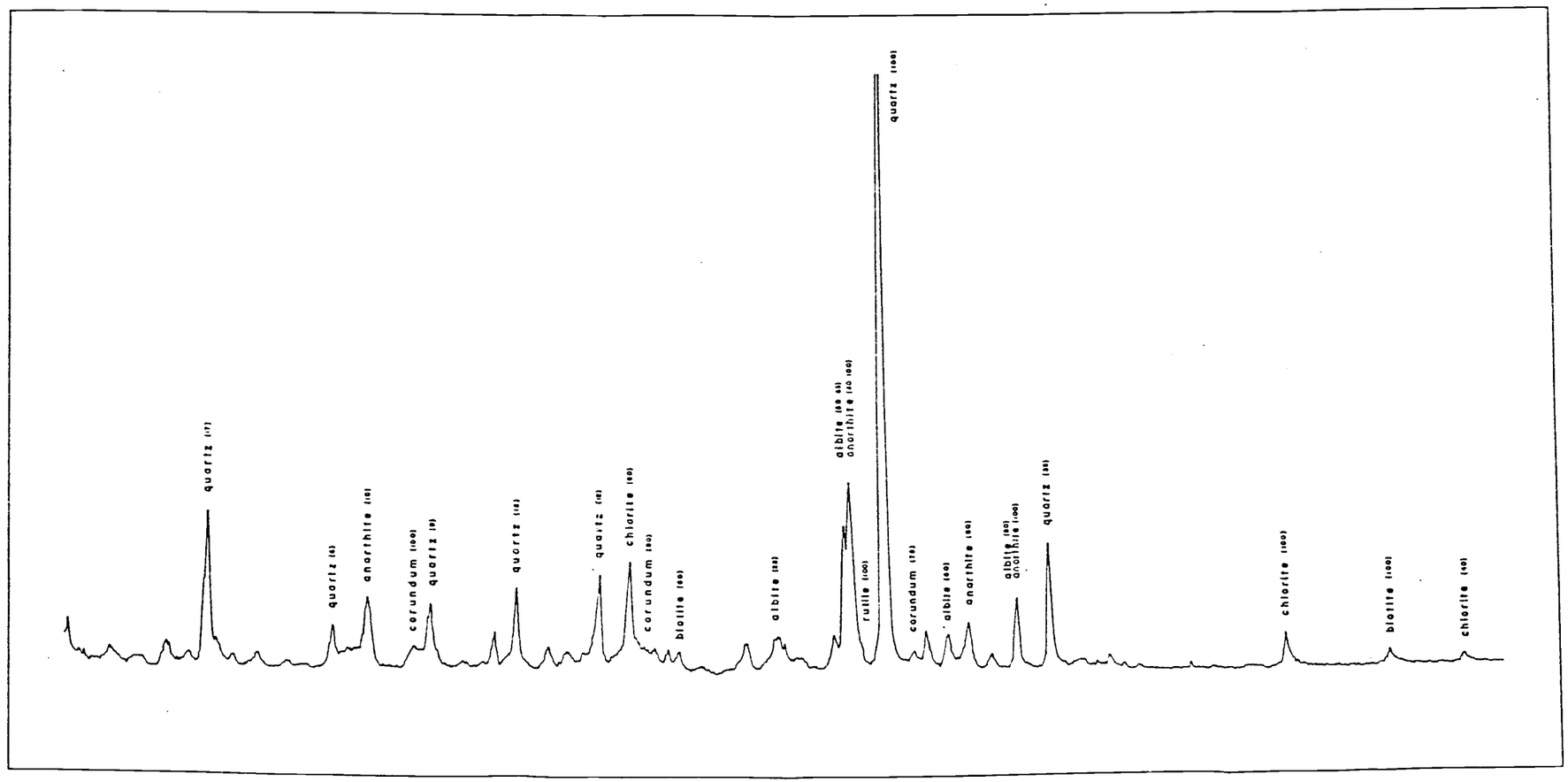

Figure A2. XRD chart of sample GP 84 34G.

TABLE A1

QUANTITATIVE XRD OF QUARTZ, DICKITE, MUSCOVITE

QUANTITATIVE XRD OF QUARTZ

sample number	peak height (h)	percent quartz added (q)	q/h	total percent quartz
Gp-84-34C	12	0	-	10 (=0.85x12)
	34	20	0.59	28
	70	55	0.71	59
	95	72	0.76	75
	104	87	0.84	88
	78	90	1.15	91
Gp-84-34B	18	0	-	15 (=0.85x18)
	59	33	0.55	43
	67	59	0.88	65
	67	78	1.16	81
	82	82	1.00	85
	104	87	0.84	90
			q/h mean = 0.85 +/- 0.14	
				q/h mean = 0.85 +/- 0

QUANTITATIVE XRD OF DICKITE 2m1

sample number	peak height (h)	percent dickite added (d)	d/h
GP-84-25F	128	42	0.33
	124	55	0.44
	140	61	0.44
GP-84-26A	26	10	0.38
	116	46	0.40
	164	70	0.43
GP-84-25F	23	8	0.35
GP-84-26A	10	3	0.30
			d/h mean = 0.38 +/- 0.04

QUANTITATIVE XRD OF MUSCOVITE

sample number	peak height (h)	percent muscovite added (m)	m/h
GP-84-21C	15	42	2.8
	43	42	1.0
	19	63	3.3
	37	63	1.7
	22	63	2.9
	70	81	1.2
	32	44	1.4
	47	50	1.1
	23	50	2.1
	36	69	1.2
			m/h mean = 1.93 +/- 0.83

known to contain 10 percent quartz, the 0.80 g contains approximately 0.08 g of quartz. Therefore, total quartz in the mixture is that added (0.20 g) plus the original quartz (0.08 g) which equals 0.28 g. As the mixture weighed 1 gram, the total quartz equals 28 percent. This technique assumes that all minerals are roughly of similar density.

Peak height versus total quartz was plotted, and a best fit line drawn by eye. The maximum error was determined visually (18 percent total quartz, Fig. A3), and is the difference between the calculated total percent quartz in a sample, and the value inferred from the line. The wide scatter of data points at the high abundances may be because peak heights were measured, rather than areas under the curves (which is known to correspond more closely with mineral concentration, but is extremely time consuming to measure). Total percent quartz was then estimated for all 70 samples by plotting peak heights on the graph (Fig. A3). Results are in the accompanying mineral tables.

Dickite 2m1 and muscovite Samples GP 84 25F and 26A were prepared as above and mixed with known weights of pure dickite from Taylor-Windfall. Both samples contain no original dickite or kaolinite and the problem of calculating original dickite in the sample was avoided. The 3.85 A^{o} (I/I=+100) peak height was measured, though there is also a kaolinite 1T peak at this location (I/I=80). Percent dickite (d) was plotted against peak height (h), and a best fit line was drawn as shown in figure A4. The error in slope is small (d/h mean = 0.38 +/- 0.04), thus there is a strong association between

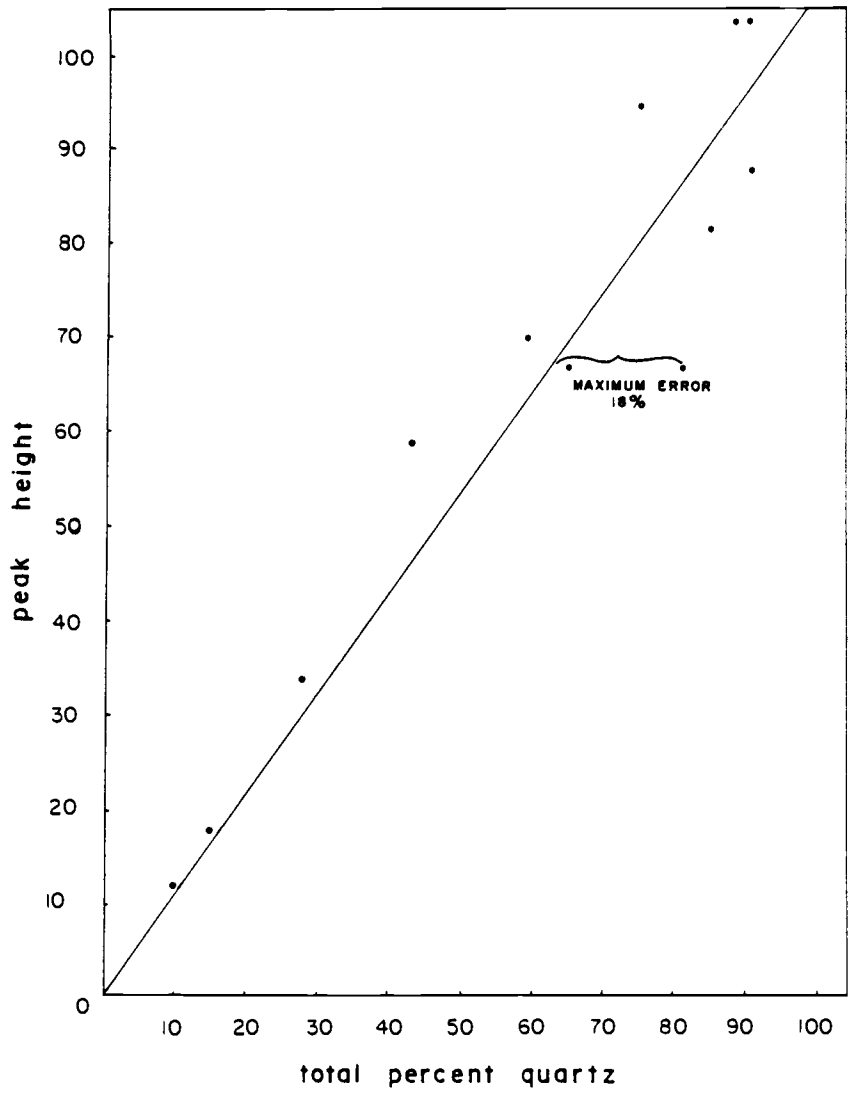

Figure A3. Quantitative XRD of quartz. Peak height versus total percent quartz.

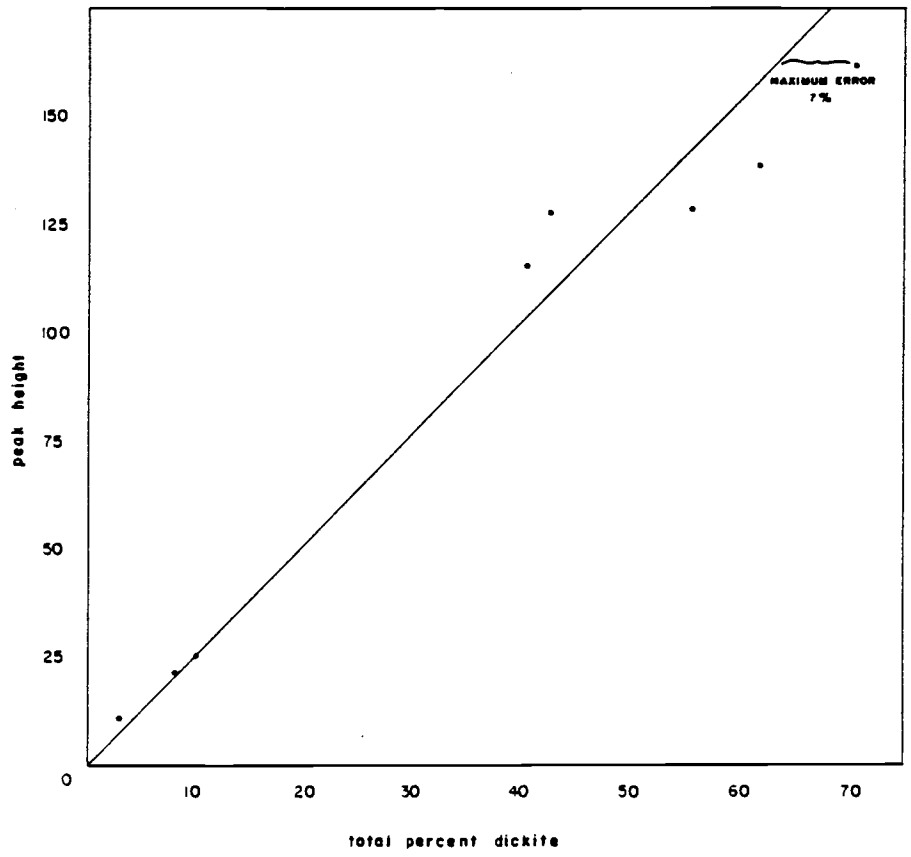

Figure A4. Quantitative XRD of dickite. Peak height versus total percent dickite.

peak height and percent dickite. The visually determined maximum error is also small (7 percent). Dickite and kaolinite concentrations in all 70 samples were estimated using the graph. Results are found in the mineralogy tables.

Similar determinations were carried out using muscovite. As table A1 illustrates, there is no relationship between peak height and muscovite percentage. The ratio of peak height to muscovite added is 1.93 +/- 0.83 (one standard deviation). Degree of preferred orientation of this sheet silicate is the principal factor that determines peak intensity. Slurrying and re-analysis of all 70 samples to remove the effects of preferred orientation was found too time consuming and quantitative XRD analyses for muscovite were not done.

TABLE A2

MINERALOGY TABLES

LEGEND

❖	mineral present, detected using thin section examination and/or XRD analyses
≈	mineral probably present, not observed in thin section, and XRD peaks overlap or are indistinct
16	percent mineral present, determined using quantitative XRD, except pyrite which was estimated visually in thin sections
▒	ghost of mineral present as was observed in thin sections

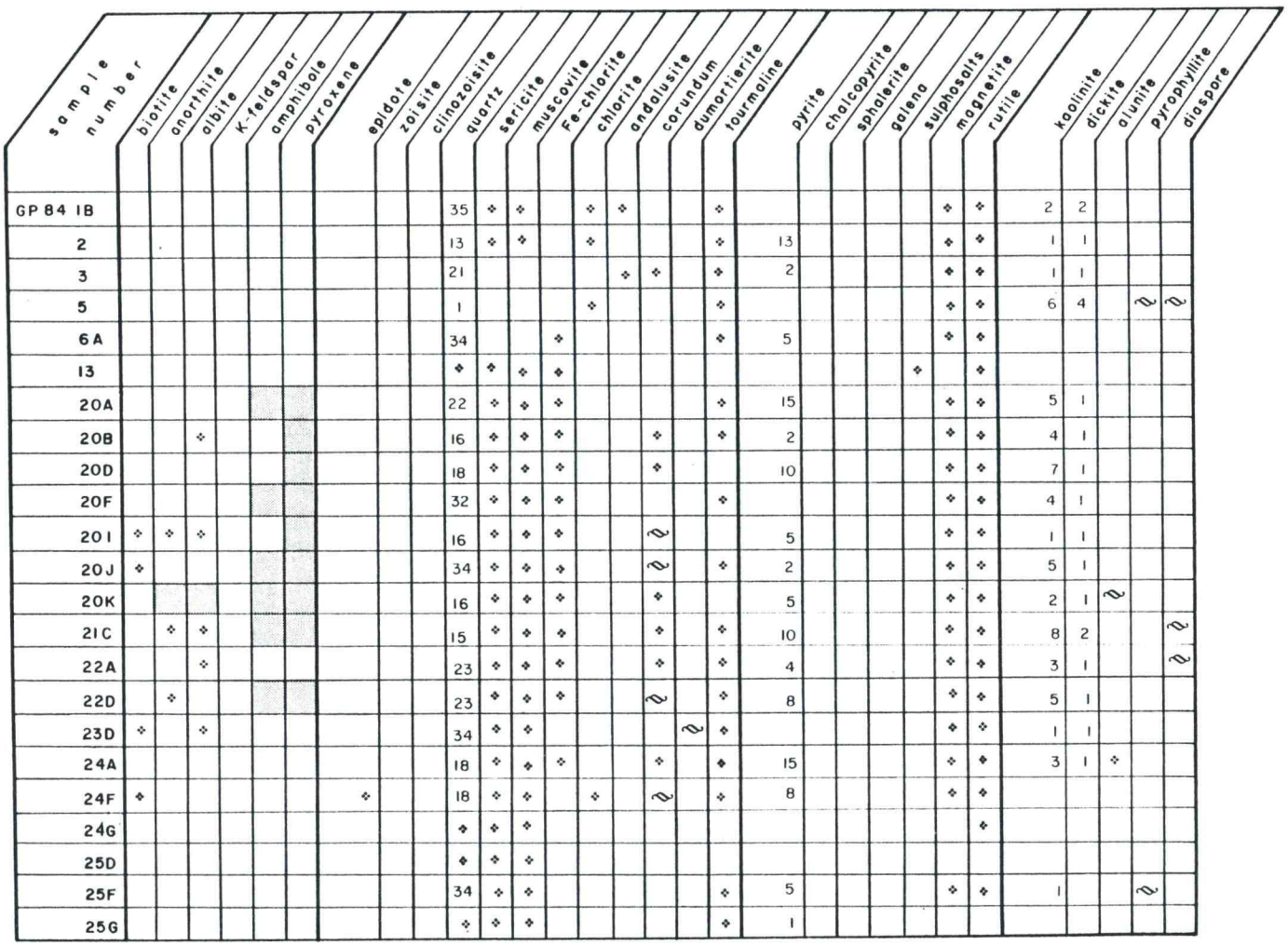

sample number	biotite	anorthite	albite	K-feldspar	amphibole	pyroxene	epidote	zoisite	clinozoisite	quartz	sericite	muscovite	Fe-chlorite	chlorite	andalusite	corundum	dumortierite	tourmaline	pyrite	chalcopyrite	sphalerite	galena	sulphosalts	magnetite	rutile	kaolinite	dickite	alunite	pyrophyllite	diaspore
GP 84 1B									35	❖	❖		❖	❖			❖						❖	❖	2	2				
2		.							13	❖	❖		❖				❖	13					❖	❖	1	1				
3									21					❖	❖		❖	2					❖	❖	1	1				
5									1				❖				❖						❖	❖	6	4		∂	∂	
6A									34			❖					❖	5					❖	❖						
13									❖	❖	❖	❖										❖		❖						
20A					▒	▒			22	❖	❖	❖					❖	15					❖	❖	5	1				
20B			❖		▒	▒			16	❖	❖	❖			❖		❖	2					❖	❖	4	1				
20D					▒	▒			18	❖	❖	❖			❖			10					❖	❖	7	1				
20F					▒	▒			32	❖	❖	❖					❖						❖	❖	4	1				
20I	❖	❖	❖		▒	▒			16	❖	❖	❖			∂			5					❖	❖	1	1				
20J	❖				▒	▒			34	❖	❖	❖			∂		❖	2					❖	❖	5	1				
20K		▒	▒		▒	▒			16	❖	❖	❖			❖			5					❖	❖	2	1	∂			
21C		❖	❖		▒	▒			15	❖	❖	❖			❖		❖	10					❖	❖	8	2			∂	∂
22A			❖		▒	▒			23	❖	❖	❖			❖		❖	4					❖	❖	3	1			∂	∂
22D		❖			▒	▒			23	❖	❖	❖			∂		❖	8					❖	❖	5	1				
23D	❖		❖						34	❖	❖					∂	❖						❖	❖	1	1				
24A									18	❖	❖	❖			❖		◆	15					❖	◆	3	1	❖			
24F	◆						❖		18	❖	❖		❖		∂		❖	8					❖	❖						
24G									◆	❖	❖													◆						
25D									◆	❖	❖																			
25F									34	❖	❖						❖	5					❖	❖	1			∂		
25G									❖	❖	❖						❖	1												

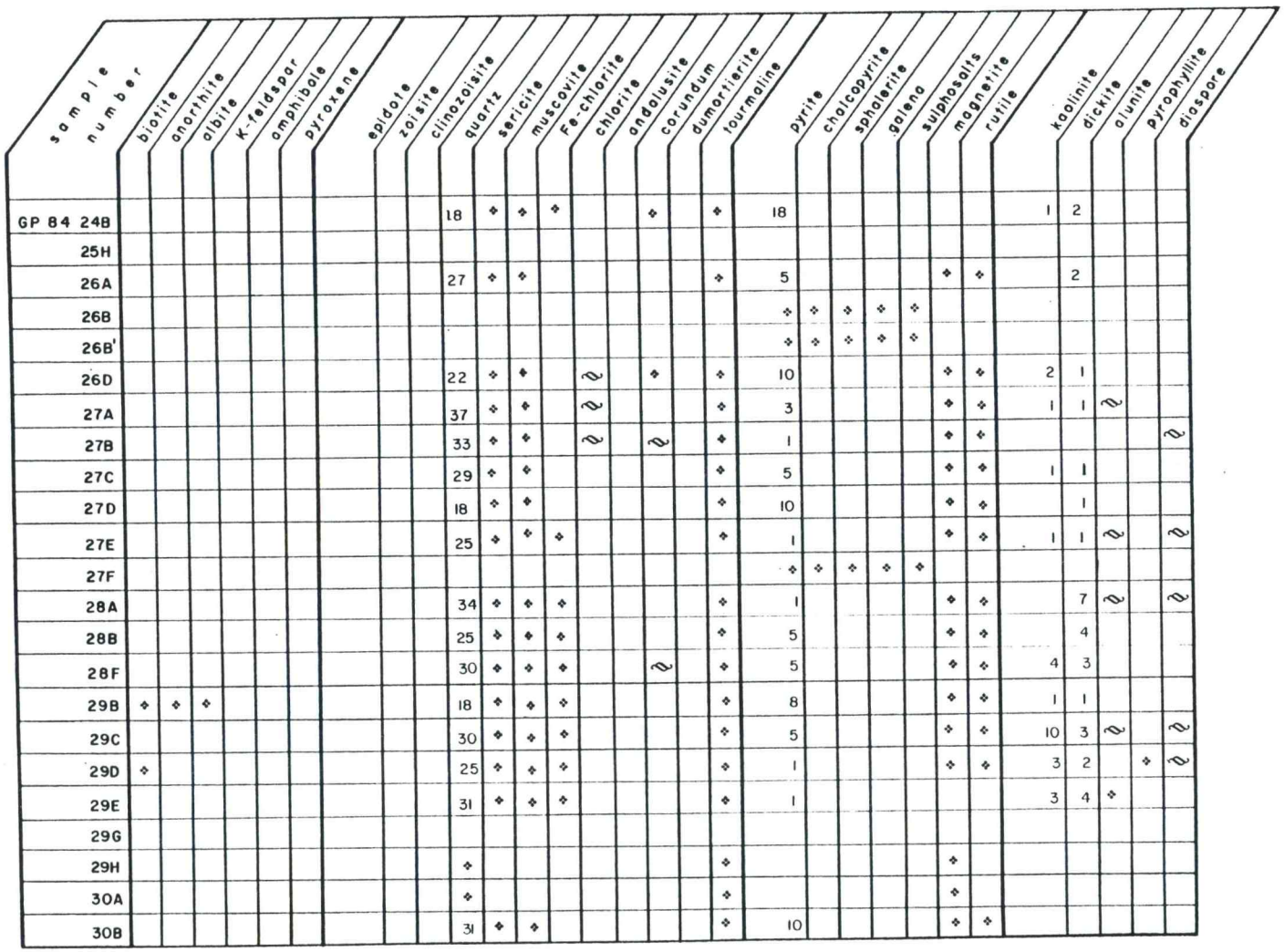
sample number
biotite
anorthite
albite
K-feldspar
amphibole
pyroxene
epidote
zoisite
clinozoisite
quartz
sericite
muscovite
Fe-chlorite
chlorite
andalusite
corundum
dumortierite
tourmaline
pyrite
chalcopyrite
sphalerite
galena
sulphosalts
magnetite
rutile
kaolinite
dickite
alunite
pyrophyllite
diaspore
GP 84 24B
25H
26A
26B
26B'
26D
27A
27B
27C
27D
27E
27F
28A
28B
28F
29B
29C
29D
29E
29G
29H
30A
30B

sample number	biotite	anorthite	albite	K-feldspar	amphibole	pyroxene	epidote	zoisite	clinozoisite	quartz	sericite	muscovite	Fe-chlorite	chlorite	andalusite	corundum	dumortierite	tourmaline	pyrite	chalcopyrite	sphalerite	galena	sulphosalts	magnetite	rutile	kaolinite	dickite	alunite	pyrophyllite	diaspore
GP 84 30C		◆	◆	◆					25	◆	◆	◆					◆	2					◆	◆	7	2				
30D	◆								27	◆	◆	◆					◆	3						◆	13	3				◆
31B		◆	◆	◆					30	◆	◆	◆					◆	1					◆	◆	4	1				
31C									24	◆	◆	◆					◆	1						◆	5	1	◆			
31D									27	◆	◆	◆					◆	8					◆	◆	7	2	◆			
32A									41	◆	◆	◆		◆			◆	1					◆	◆	2	2				
33A	◆		◆						22	◆	◆	◆		◆	◆		◆	8					◆	◆	1	1				
33B	◆		◆				◆	◆	16	◆	◆	◆			◆		◆						◆	◆	2	1		◆		
33D	◆						◆			◆	◆													◆	1	1				
34A	◆	◆	◆						18	◆	◆	◆						10					◆	◆	1	1				
34C	◆	◆	◆				◆		◆		◆	◆			◆		◆	8						◆	1	1				
34D	◆	◆	◆						10	◆	◆				◆		◆	8					◆	◆	6	2				
34G	◆	◆	◆				◆		◆	24	◆	◆	◆	◆	◆		◆	3					◆	◆	2	1				
35C									75			◆						1					◆	◆	1	1				
37A									1	◆	◆						◆						◆	◆				◆		
37B									50	◆	◆						◆	7					◆	◆	1	1				
38B									27	◆	◆	◆					◆						◆	◆						
40A	◆	◆	◆	◆					19	◆	◆	◆		◆	◆		◆	1					◆	◆	4	2				
40B									1	◆	◆						◆						◆	◆	1	1				
41A								◆	15	◆	◆						◆						◆	◆	1	1			◆	
41D							◆		35	◆	◆	◆		◆			◆	1					◆	◆				◆		
42A							◆		21	◆	◆	◆		◆			◆						◆	◆	1	4				
42C							◆	◆	25	◆	◆	◆		◆			◆						◆	◆	2	1				

sample number	biotite	anorthite	albite	K-feldspar	amphibole	pyroxene	epidote	zoisite	clinozoisite	quartz	sericite	muscovite	Fe-chlorite	chlorite	andalusite	corundum	dumortierite	tourmaline	pyrite	chalcopyrite	sphalerite	galena	sulphosalts	magnetite	rutile	kaolinite	dickite	alunite	pyrophyllite	diaspore
GP 84 43D									68	✦	✦	✦					✦						✦	✦						
43A												✦					✦						✦					≈		
43C		✦		✦						✦		✦		✦	✦		✦						✦					≈		
44B										✦				✦	✦								✦							
44C										✦							✦						✦							
44D										✦													✦							
44E									21	✦	✦	✦		✦									✦	✦	4	2				
45B									43	✦	✦	✦		✦									✦	✦	2	4	≈	✦	≈	≈
45C									29	✦				✦	≈		✦						✦	✦	2	1		≈		
46A			✦							✦	✦	✦		✦			✦		1											
46B		✦	✦	✦					24	✦	✦	✦				≈	✦		1				✦	✦		1	1		≈	
47A	✦		✦						✦	✦	✦	✦		≈	≈		✦		✦			≈	✦		✦	✦				
59																														
60																														
61																														
1648 dump																			✦	✦	✦	✦	✦							
DDH 84 01																														
10.0									✦								✦								✦			✦	≈	
57.5									✦	✦							✦								✦					
78.5									✦			✦					✦		✦											
80.0									✦	✦		✦											✦							
110.5																														

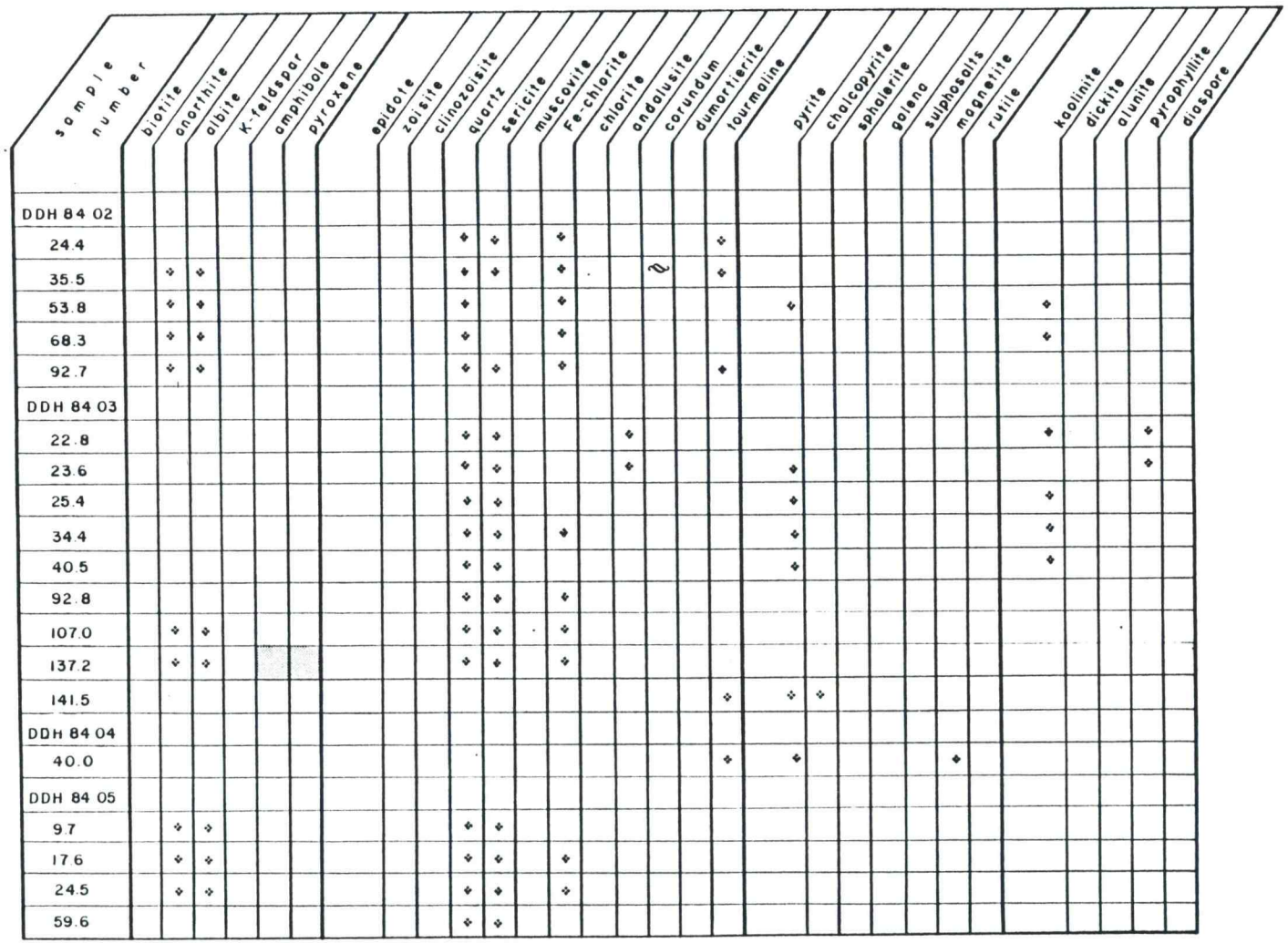
sample number
biotite
anorthite
albite
K-feldspar
amphibole
pyroxene
epidote
zoisite
clinozoisite
quartz
sericite
muscovite
Fe-chlorite
chlorite
andalusite
corundum
dumortierite
tourmaline
pyrite
chalcopyrite
sphalerite
galena
sulphosalts
magnetite
rutile
kaolinite
dickite
alunite
pyrophyllite
diaspore
DDH 84 02
24.4
35.5
53.8
68.3
92.7
DDH 84 03
22.8
23.6
25.4
34.4
40.5
92.8
107.0
137.2
141.5
DDH 84 04
40.0
DDH 84 05
9.7
17.6
24.5
59.6

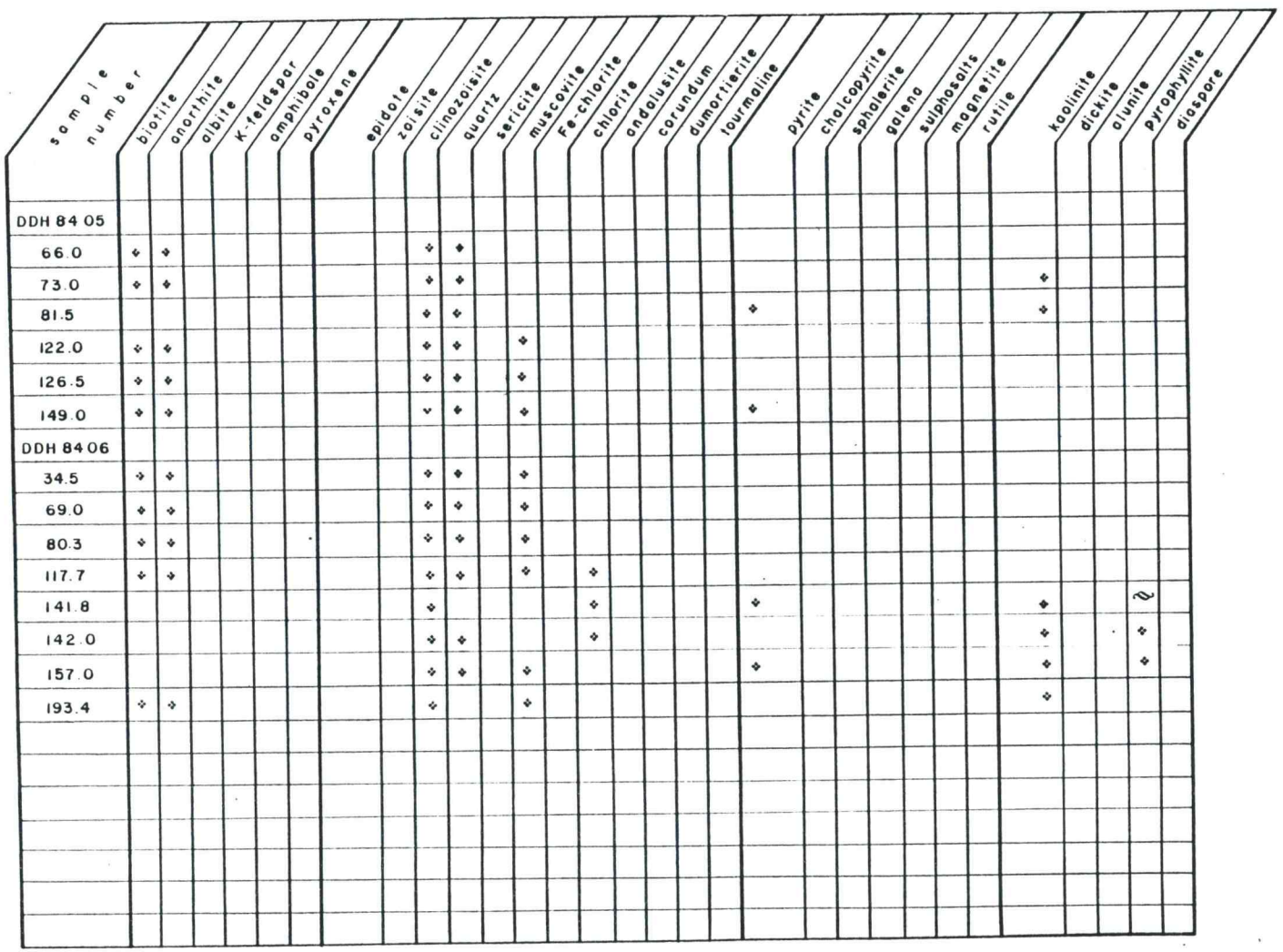
sample number
biotite
anorthite
albite
K-feldspar
amphibole
pyroxene
epidote
zoisite
clinozoisite
quartz
sericite
muscovite
Fe-chlorite
chlorite
andalusite
corundum
dumortierite
tourmaline
pyrite
chalcopyrite
sphalerite
galena
sulphosalts
magnetite
rutile
kaolinite
dickite
alunite
pyrophyllite
diaspore
DDH 84 05
66.0
73.0
81.5
122.0
126.5
149.0
DDH 84 06
34.5
69.0
80.3
117.7
141.8
142.0
157.0
193.4

APPENDIX 2

Major oxide geochemistry

Analytical method

Twenty rock samples were broken by hammer, and further reduced in an aluminium plated jaw crusher. Approximately 10 grams were ground in a shatter box. Samples were sent to Washington State University for analyses of the oxides SiO_2, Al_2O_3, TiO_2, Fe_2O_3, FeO, MnO, CaO, MgO, K_2O, Na_2O, and P_2O_5. Following is a synopsis of the analytical procedure (Hooper, 1984, per. com.).

Seven grams of lithium tetraborate ($Li_2B_4O_7$) and 3.5 grams of the rock powder were thoroughly mixed in a plastic jar on a spex ballmill, and then fused in graphite crucibles for five minutes at 1000°c. The lower surfaces of the cooled fluxed beads were ground smooth with fine silicon carbide powder and then rinsed with water.

The flat surfaces of the beads were irridatiated in a Philips P.W. 1410 manual spectrometer, using a chromium target tube. The recorded count rate for each element was related to the calibration curve derived from the count rate of eight analysed basalts supplied by the U.S. Geological Survey. The raw oxide values were corrected for absorbtion, and normalized to total 100 percent on a volatile free basis, and Fe^{2+}/Fe^{3+} was set arbitrarily at 2.547.

Instrument precision was routinely recorded by repeat measurement of a single bead, every tenth sample or so through the analytical run. Total precision has been calibrated and checked by preparing three separate beads from each of 13 basalt samples, as shown in Table A3.

TABLE A3

PRECISION OF XRF ANALYSES

Major elements	Instrument precision‡ 2σ	Number of measurements	Total analytical precision‡‡ 2σ
SiO_2	0.660	20	0.550
Al_2O_3	0.180	75	0.310
TiO_2	0.040	42	0.050
Fe_2O_3‡‡‡	0.090	36	0.350
MnO	0.003	43	0.010
CaO	0.100	50	0.220
MgO	0.180	92	0.150
K_2O	0.020	51	0.030
Na_2O	0.150	47	0.160
P_2O_5	0.006	37	0.014

‡Estimated machine variation for a selected bead, repeated the indicated number of times.
‡‡Total variation between 13 sets of triplicate beads.
‡‡‡Total Fe as Fe_2O_3.

TABLE A4

RAW MAJOR OXIDE AND DENSITY DATA

sample	density	SiO_2	Al_2O_3	TiO_2	Fe_2O_3	FeO	MnO	CaO	MgO	K_2O	Na_2O	P_2O_5
GP84-41B	2.87	71.74	20.24	0.96	1.03	1.18	0.13	0.00	0.08	4.26	0.34	0.04
GP85 46	2.64	66.67	24.93	1.29	3.00	3.44	0.04	0.00	0.00	0.20	0.36	0.07
GP85 20I	2.96	64.30	18.93	0.90	3.15	3.61	0.07	1.80	3.02	2.03	2.03	0.16
GP85 21C	2.67	61.86	18.20	0.98	4.19	4.79	0.08	3.00	3.77	0.47	2.50	0.17
GP84 22D	2.94	64.15	17.41	0.95	3.59	4.11	0.08	0.22	5.56	3.45	0.32	0.16
GP84 23D	2.54	80.76	13.19	0.06	0.34	0.39	0.09	0.06	0.00	2.28	2.80	0.02
GP84 24F	2.77	67.28	14.80	0.78	5.99	6.86	0.21	0.13	3.13	0.01	0.79	0.02
GP84 25F	2.75	64.71	20.15	1.07	2.31	2.65	0.07	1.33	1.29	5.59	0.66	0.15
GP84 26A	2.63	66.15	19.14	1.05	3.58	4.10	0.05	0.14	2.21	2.80	0.74	0.04
GP84 27B	2.57	70.74	20.10	1.07	0.55	0.63	0.02	0.18	0.51	5.40	0.74	0.06
GP84 29B	2.71	67.75	20.72	1.11	1.96	2.25	0.02	0.42	0.50	4.75	0.44	0.07
GP84 29E	2.46	73.19	20.52	1.00	0.37	0.42	0.01	0.72	0.08	2.27	1.40	0.04
GP84 32A	2.41	74.73	17.98	0.92	1.65	1.89	0.03	0.29	0.98	0.75	0.75	0.03
GP84 33A	2.70	64.61	19.19	1.07	3.16	3.62	0.05	2.15	1.44	2.12	2.49	0.10
GP84 33B	2.45	63.67	18.73	0.97	2.53	2.90	0.09	4.60	2.00	0.01	3.91	0.59
GP84 38B	2.70	64.69	19.86	0.95	3.36	3.85	0.04	0.03	4.10	2.50	0.55	0.08
GP84 44B	2.67	66.05	23.60	1.10	2.42	2.77	0.12	0.00	0.12	3.37	0.38	0.03
GP84 44C	2.26	94.76	2.19	0.76	0.59	0.68	0.20	0.00	0.00	0.56	0.23	0.03
Gp84 44D	2.51	94.84	0.66	0.87	1.47	1.69	0.17	0.00	0.00	0.20	0.08	0.03
GP84 44E	2.77	63.09	22.52	1.11	3.18	3.64	0.03	0.02	3.03	2.96	0.34	0.09
J241	-	58.38	15.53	0.797	7.64T	-	0.147	3.81	4.54	0.269	4.558	0.11
J242	-	57.41	16.92	0.824	6.78T	-	0.107	5.28	3.47	1.549	3.657	0.08
J262	-	63.76	14.71	0.665	4.74T	-	0.151	1.69	3.45	0.663	4.868	0.14
average andesite	2.65	61.4	10.9	0.64	1.2	3.8	0.13	8.2	5.7	1.0	3.3	0.1

‡ Results as percentages are normalized on a volatile free basis, and the Fe^{2+}/Fe^{3+} ratio is set at 1.147. GP series are from Taylor-Windfall, J series were collected by McMillan (1976) in the general area, and average andesite is from Gill (1981). Density was measured, and is given in units of grams per cubic centimeter.

TABLE A5

CONVERSIONS OF WEIGHT PERCENT OXIDE TO GRAMS PER 1000 CM^3

(samples listed in order of increasing absolute SiO_2 content)

sample	density	SiO_2	Al_2O_3	TiO_2	Fe_2O_3	FeO	MnO	CaO	MgO	K_2O	Na_2O	P_2O_5
GP84 33B	2.45	1560	448	24	62	71	2	112	49	0.2	96	14
" 25F	2.75	1583	554	29	63	73	2	37	35	154	18	4
" 21C	2.67	1651	486	26	112	128	2	80	101	12	67	4
" 26A	2.63	1740	503	28	94	108	1	4	58	74	19	1
" 33A	2.70	1744	518	29	85	98	1	58	39	57	67	3
" 33B	2.70	1746	536	26	91	104	1	1	111	67	15	2
" 44E	2.77	1747	624	31	88	101	1	0.5	84	82	9	2
" 6	2.64	1760	658	34	79	91	1	0	0	5	9	2
" 44B	2.67	1763	630	29	65	74	3	0	3	90	10	2
" 29E	2.46	1800	505	25	9	10	0.2	18	2	56	34	1
" 32A	2.41	1801	433	22	40	45	1	7	24	18	18	1
" 27B	2.57	1818	517	27	14	16	0.5	4.6	13	139	19	1
" 29B	2.71	1836	561	30	53	61	0.5	11	14	129	12	2
" 24F	2.77	1864	410	22	166	190	6	4	87	0.3	22	1
" 22D	2.94	1886	511	28	105	121	2	6	163	101	9	5
" 20I	2.96	1903	560	27	93	107	2	53	89	60	60	5
" 23D	2.54	2051	335	1.5	9	10	2	1	0	58	71	1
" 1B	2.87	2058	581	28	29	34	4	0	2	122	10	1
" 44C	2.26	2141	49	17	13	15	5	0	0	13	5	1
" 44D	2.51	2380	16	22	37	42	4	0	0	5	2	1
average andesite	2.65	1627	289	32	32	100	3	217	151	26	114	3

grams per 1000 cubic centimeters = [(density)(1000 cm^3)][weight percent]

EXAMPLE:	sample	density	weight % SiO_2	gms/1000 cm^3
	a	2.6	70	1820
	b	2.8	65	1820
	a-b	0.2	5	0

A five percent difference in SiO_2 concentration is implied by the differences in weight percent, but when the density contrast is accounted for, there is no difference in the real amount of SiO_2 between the two samples.

TABLE A6

GAINS AND LOSSES OF MAJOR OXIDES WITH RESPECT TO AVERAGE ANDESITE

(samples listed in order of increasing absolute SiO_2 content)

map unit	sample	SiO_2	Al_2O_3	TiO_2	Fe_2O_3	FeO	MnO	CaO	MgO	K_2O	Na_2O	P_2O_5
6	GP84 33B	-67	+158	-8	+30	-29	-1	-105	-102	-26	-18	+11
4A	" 25F	-44	+265	-3	+31	-27	-1	-180	-116	+128	-96	+1
5AA	" 21C	-24	+197	-6	+80	+28	-1	-137	-50	-14	-47	+1
1B	" 26A	+113	+214	-4	+62	+8	-2	-213	-93	+48	-96	-2
6	" 33A	+117	+229	-3	+53	-2	-2	-159	-112	+31	-47	0
3B	" 38B	+119	+247	-6	+59	+4	-2	-216	-40	+41	-99	-1
3A1	" 44E	+120	+335	-1	-56	+1	-2	-216	-67	+56	-105	-1
2A	" 6	+133	+369	+2	+47	-9	-2	-217	-151	-21	-105	-1
3A1	" 44B	+136	+341	-3	+33	-26	0	-217	-148	+64	-104	-1
1A	" 29E	+173	+216	-7	-23	-30	-2.8	-199	-149	+30	-80	-2
1A	" 32A	+174	+144	-10	+8	-55	-2	-210	-127	-8	-96	-2
1B	" 27B	+191	+228	-5	-18	-84	-2.5	-212	-138	+113	-95	-2
1	" 29B	+209	+272	-2	+21	-39	-2.5	-206	-137	+103	-102	-1
4A	" 24F	+237	+121	-10	+134	+90	+3	-213	-64	-26	-92	-2
5A	" 22D	+259	+222	-4	+73	+21	-1	-211	-12	+75	-105	-2
4A	" 20I	+276	+271	-5	+61	+7	-1	-164	-62	+34	-54	+2
7	" 23D	+388	+46	-30	-23	-90	-1	-216	-151	+32	-43	-2
2A1	" 1B	+431	+292	-4	-3	-66	+1	-217	-149	+96	-104	-2
3A1	" 44C	+514	-240	-15	-19	-85	+2	-217	-151	-13	-109	-2
2C	" 44D	+753	-273	-10	+5	-58	+1	-217	-151	-21	-112	-2
average andesite		0	0	0	0	0	0	0	0	0	0	0

Gains and losses are in units of grams per 1000 cm^3.

APPENDIX 3

Trace element geochemistry

Analytical method

Trace element analyses were done by Chemex Labs Limited (North Vancouver, B.C.). Samples weighing about 0.5 kg were crushed, split, and milled. Splits of 1 to 10 grams of milled rock were digested in hot acid, and analysed by atomic absorbtion spectrophotometry. Detection limits for the elements analysed by this method are 2 to 10000 ppm for Cu, 1 to >4500 ppm for Pb, 1 to 10000 ppm for Zn, 0.1 to 100 ppm for Ag, 1 to 10000 ppm for As, 0.005 to >27 ppm for Hg, and 0.2 to 1000 ppm for Sb. As gold is resistant to acids, samples were mixed with a flux, and fused by fire assay. Analyses were done by atomic absorbtion spectrophotometry. Lower detection limit is 0.001 ppm, and upper detection limit is 10 ppm. A number of samples that returned gold values of greater than 10 ppm were reanalysed by the conventional fire assay-gravimetric method. All results are in Table A7.

TABLE A7

ROCK GEOCHEMISTRY - TRACE ELEMENTS

Sample No.	Cu ppm	Pb ppm	Zn ppm	Ag ppm	As ppm	Hg ppm	Sb ppm	Au ppm
				Main drift 1648 m level				
17332	-	-	-	-	-	-	-	0.002
17333	17	6	18	0.4	7	0.05	1.0	0.002
17334	-	-	-	-	-	-	-	0.020
17335	56	2	48	0.2	12	0.03	0.3	0.005
17336	-	-	-	-	-	-	-	0.002
17337	106	9	61	0.3	7	0.02	0.4	0.002
17338	-	-	-	-	-	-	-	0.002
17339	166	5	63	0.3	10	0.02	0.4	0.010
17340	-	-	-	-	-	-	-	0.002
17439	90	13	31	0.3	27	0.04	13.0	0.040
17440	-	-	-	-	-	-	-	0.010
17441	32	2	10	0.1	6	0.03	0.8	0.010
17442	-	-	-	-	-	-	-	0.010
17443	156	17	46	0.1	19	0.03	0.8	0.005
17444	-	-	-	-	-	-	-	0.010
17445	270	21	47	0.1	15	0.04	0.4	0.045
17446	-	-	-	-	-	-	-	0.025
17324	-	-	-	-	-	-	-	0.005
17325	8	1	8	0.3	4	0.03	1.2	0.005
17326	-	-	-	-	-	-	-	0.002
17327	72	1	17	0.1	4	0.02	0.6	0.002
17328	-	-	-	-	-	-	-	0.002
17329	8	4	11	0.1	4	0.02	2.4	0.005
17330	-	-	-	-	-	-	-	0.005
17331	6	3	9	0.1	4	0.02	0.6	0.002
17332	-	-	-	-	-	-	-	0.002
17333	17	6	18	0.4	7	0.05	1.0	0.002
17198	-	-	-	-	-	-	-	0.055
17199	18	6	10	0.4	10	0.03	1.0	0.025
				Cross-cut 0				
17314	-	-	-	-	-	-	-	0.030
17315	180	9	107	0.1	39	0.13	10.0	0.055
17316	-	-	-	-	-	-	-	0.015
17317	32	5	26	0.1	11	0.04	1 9	0.010
17318	-	-	-	-	-	-	-	0.002
17319	20	4	14	0.1	6	0.03	1.1	0.005
17320	-	-	-	-	-	-	-	0.015
17321	100	3	20	0.1	7	0.02	1.2	0.002
17322	-	-	-	-	-	-	-	0.090
17323	100	3	23	0.2	6	0.02	1.2	0.010
17196	-	-	-	-	-	-	-	0.210
17197	200	53	82	2.5	51	0.17	59.0	3.100
17200	-	-	-	-	-	-	-	0.650
				Cross-cut 1				
17185	26	7	23	0.3	12	0.02	1.0	0.027

Sample No.	Cu ppm	Pb ppm	Zn ppm	Ag ppm	As ppm	Hg ppm	Sb ppm	Au ppm
17186	-	-	-	-	-	-	-	0.002
17187	46	1	23	0.03	5	0.02	0.6	0.002
17188	-	-	-	-	-	-	-	0.002
17289	15	1	7	0.1	4	0.01	0.5	0.002
17190	-	-	-	-	-	-	-	0.002
17191	47	2	10	0.3	4	0.01	0.4	0.002
17192	-	-	-	-	-	-	-	0.020
17193	84	4	18	0.1	5	0.03	1.0	0.015
17194	-	-	-	-	-	-	-	0.002
17195	16	37	150	0.3	9	0.16	2.6	0.200
17196	-	-	-	-	-	-	-	0.210
17429	112	2	15	0.1	33	0.02	1.0	0.030
17430	-	-	-	-	-	-	-	0.010
17431	104	3	16	0.1	11	0.02	1.2	0.010
17432	-	-	-	-	-	-	-	0.005
17433	34	2	18	0.1	19	0.02	1.0	0.015
17434	-	-	-	-	-	-	-	0.002
17435	65	2	23	0.2	14	0.02	1.6	0.190
17436	-	-	-	-	-	-	-	0.010
17437	40	6	22	0.1	12	0.02	4.6	0.035
17438	-	-	-	-	-	-	-	2.900
				Main drift				
17183	8	6	9	0.2	6	0.05	9.0	0.002
17184	-	-	-	-	-	-	-	2.590
17310	-	-	-	-	-	-	-	0.030
17311	500	91	300	1.7	180	0.16	37.0	4.050
17312	-	-	-	-	-	-	-	0.440
17313	10000	1330	10000	14.8	10000	12.00	1000.0	8.250
17427	50	10	14	0.1	25	0.03	1.6	0.190
17428	-	-	-	-	-	-	-	10.000
				Cross-cut 2				
17310	-	-	-	-	-	-	-	0.030
17351	5	1	12	0.1	5	0.02	0.1	0.010
17352	-	-	-	-	-	-	-	0.002
17353	4	1	9	0.1	7	0.02	0.1	0.002
17354	-	-	-	-	-	-	-	0.020
17355	16	7	17	0.4	12	0.02	4.2	0.002
17356	-	-	-	-	-	-	-	0.002
17357	182	57	36	0.1	72	0.11	18.6	0.002
17358	-	-	-	-	-	-	-	0.160
17359	61	21	22	0.1	36	0.04	6.8	0.010
17360	-	-	-	-	-	-	-	0.002
17361	6	4	9	0.1	6	0.02	0.2	0.002
17362	-	-	-	-	-	-	-	0.002
17363	5	5	10	0.1	5	0.02	0.1	0.002
17364	-	-	-	-	-	-	-	0.002
				Cross-cut 3				
17365	75	2	13	0.1	15	0.03	1.0	0.002
17366	-	-	-	-	-	-	-	0.002
17367	172	4	18	0.1	11	0.04	2.8	0.045

Sample No.	Cu ppm	Pb ppm	Zn ppm	Ag ppm	As ppm	Hg ppm	Sb ppm	Au ppm
17368	-	-	-	-	-	-	-	0.010
17369	164	6	18	0.1	11	0.06	8.2	0.010
17370	-	-	-	-	-	-	-	0.010
17371	168	3	12	0.1	6	0.02	0.5	0.020
17372	-	-	-	-	-	-	-	0.040
17373	283	3	16	0.1	6	0.02	0.5	0.002
17374	-	-	-	-	-	-	-	0.002
17375	6	2	19	0.2	5	0.05	0.2	0.002
17376	-	-	-	-	-	-	-	0.002
17307	10	21	54	0.4	6	0.07	0.4	0.002
17308	-	-	-	-	-	-	-	0.002
17309	2000	31	26	2.0	300	4.90	170.0	3.950
				Cross-cut 4				
17377	5	17	26	0.4	10	0.03	0.5	0.002
17378	-	-	-	-	-	-	-	0.015
17379	10	3	27	0.3	4	0.18	0.6	0.010
17380	-	-	-	-	-	-	-	0.035
17381	340	5	123	0.6	33	0.16	10.0	0.030
17382	-	-	-	-	-	-	-	0.020
17383	10	5	20	0.4	4	0.38	1.8	0.160
17384	-	-	-	-	-	-	-	0.025
17385	25	43	74	0.4	11	0.45	11.6	0.075
17386	-	-	-	-	-	-	-	0.050
17387	85	32	121	0.2	11	0.07	1.0	0.002
17388	-	-	-	-	-	-	-	0.002
17389	41	1	10	0.1	5	0.05	0.7	0.002
17390	-	-	-	-	-	-	-	0.002
17391	7	1	4	0.1	4	0.14	0.6	0.002
17392	-	-	-	-	-	-	-	0.002
17393	4	1	11	0.1	4	0.08	0.5	0.002
17394	-	-	-	-	-	-	-	0.002
17395	5	48	5	0.1	5	0.07	0.4	0.002
17396	-	-	-	-	-	-	-	0.840
17397	10	3	27	0.3	4	0.18	0.6	0.010
				Cross-cut 5				
38558	-	-	-	-	-	-	-	0.385
38559	4	20	21	0.1	9	0.52	0.2	0.110
38560	-	-	-	-	-	-	-	0.002
38561	9	5	31	0.2	9	0.26	2.2	0.002
38562	-	-	-	-	-	-	-	0.002
17416	-	-	-	-	-	-	-	0.002
17417	160	3	40	0.2	9	0.09	1.0	0.005
				Cross-cut 6				
17151	60	1	23	0.1	6	0.03	0.4	0.002
17152	-	-	-	-	-	-	-	0.002
17153	31	1	22	0.1	5	0.03	0.4	0.002
17154	-	-	-	-	-	-	-	0.002
17155	54	1	21	0.1	5	0.2	0.4	0.002
17156	-	-	-	-	-	-	-	0.002
17157	29	1	29	0.1	4	0.02	0.4	0.002

Sample No.	Cu ppm	Pb ppm	Zn ppm	Ag ppm	As ppm	Hg ppm	Sb ppm	Au ppm
17158	-	-	-	-	-	-	-	0.002
17159	10	5	23	0.2	6	0.10	0.3	0.002
17160	-	-	-	-	-	-	-	0.015
17161	7	7	22	0.3	11	0.10	0.1	0.002
17162	-	-	-	-	-	-	-	0.005
17163	8	6	13	0.2	5	0.08	1.2	0.010
17164	-	-	-	-	-	-	-	0.050
17165	27	15	34	0.3	9	0.06	1.0	0.005
17166	-	-	-	-	-	-	-	0.005
17167	8	6	12	0.4	5	0.07	0.4	0.002
17168	-	-	-	-	-	-	-	0.005
17169	8	2	26	0.1	7	0.07	0.4	0.015
17407	24	2	61	0.2	4	0.06	1.2	0.015
17408	-	-	-	-	-	-	-	0.010
17409	38	17	53	0.2	10	0.41	2.8	0.025
17410	-	-	-	-	-	-	-	0.015
17411	100	11	210	0.4	5	1.00	38.0	0.005
17412	-	-	-	-	-	-	-	0.002
17413	163	4	65	0.1	7	0.3	4.0	0.002
17414	-	-	-	-	-	-	-	0.002
17415	130	6	26	0.1	7	0.07	0.4	0.015
38563	270	2	61	0.3	1350	0.10	0.8	0.005
				Cross-cut 7				
17304	-	-	-	-	-	-	-	0.015
17305	8	2	21	0.4	7	0.15	0.1	0.002
17306	-	-	-	-	-	-	-	0.010
17170	-	-	-	-	-	-	-	0.002
17171	14	3	16	0.4	4	0.19	0.8	0.002
17172	-	-	-	-	-	-	-	0.002
17173	9	1	13	0.2	5	0.18	0.5	0.002
17174	-	-	-	-	-	-	-	0.002
17301	10	11	24	0.1	3	0.23	21.0	0.065
17302	-	-	-	-	-	-	-	0.010
17303	32	6	32	0.1	5	0.13	1.4	0.002
17398	-	-	-	-	-	-	-	0.002
17399	26	9	28	0.2	12	0.11	3.6	0.002
17400	-	-	-	-	-	-	-	0.005
				Cross-cut 8				
17418	-	-	-	-	-	-	-	0.002
17419	3	10	15	0.2	6	0.04	1.0	0.002
17420	-	-	-	-	-	-	-	0.030
17421	280	5	39	0.5	15	0.60	1.0	0.030
17422	-	-	-	-	-	-	-	0.002
17423	18	6	30	0.2	11	0.12	1.2	0.010
17424	-	-	-	-	-	-	-	0.045
17425	11	6	25	0.1	12	0.07	1.0	0.015
17426	-	-	-	-	-	-	-	0.010
17175	9	23	24	0.3	12	0.19	1.1	0.010
17176	-	-	-	-	-	-	-	0.035
17177	22	28	25	0.3	15	1.80	4.8	0.080
17178	-	-	-	-	-	-	-	0.065

Sample No.	Cu ppm	Pb ppm	Zn ppm	Ag ppm	As ppm	Hg ppm	Sb ppm	Au ppm
17179	9	10	22	0.3	17	0.33	1.9	0.065
17180	-	-	-	-	-	-	-	0.010
17181	12	9	28	0.3	11	0.23	1.0	0.015
17182	-	-	-	-	-	-	-	0.002
				1707 m level				
38574	-	-	-	-	-	-	-	0.002
38575	210	3	15	0.1	12	0.03	1.4	0.002
38576	-	-	-	-	-	-	-	0.010
38577	68	9	8	0.1	4	0.02	0.6	0.049
38578	-	-	-	-	-	-	-	0.015
38579	100	3	8	0.1	9	0.04	0.8	0.015
38580	-	-	-	-	-	-	-	0.020
38581	17	2	9	0.1	9	0.04	2.6	0.002
38582	-	-	-	-	-	-	-	0.025
38583	100	38	21	0.5	16	0.05	2.8	0.002
38584	-	-	-	-	-	-	-	0.002
38585	8	5	5	0.1	7	0.01	1.6	0.002
38586	-	-	-	-	-	-	-	0.002
38587	10	1	7	0.1	5	0.03	1.2	0.005
38588	-	-	-	-	-	-	-	0.105
38589	10	7	7	0.3	9	0.03	1.0	0.060
				Veins				
38590	-	-	-	-	-	-	-	10.000
38591	920	24	163	0.7	300	0.38	73.0	0.075
38592	-	-	-	-	-	-	-	2.200
38564	10	12	22	0.2	6	0.50	2.6	0.085
38565	10000	1450	10000	100.0	5700	24.00	1000.0	1.100
38566	10000	4300	9100	19.0	10000	26.00	1000.0	10.000
38567	500	63	124	1.0	150	0.30	105.0	0.200
38568	10000	2700	10000	6.7	8300	27.00	950.0	10.000
38569	240	37	452	0.7	81	0.25	26.0	0.175
38570	158	22	155	0.4	53	0.14	15.0	0.140
38571	4200	810	810	5.4	48	1.90	800.0	0.670
38572	-	-	-	-	-	-	-	10.000
38573	150	19	32	0.3	32	0.11	25.0	0.650
17251	-	-	-	-	-	-	-	0.030
17252	-	-	-	-	-	-	-	10.000
17253	-	-	-	-	-	-	-	0.175
17254	-	-	-	-	-	-	-	0.390
17255	-	-	-	-	-	-	-	0.180
17256	-	-	-	-	-	-	-	0.060
17257	-	-	-	-	-	-	-	0.015
17258	-	-	-	-	-	-	-	0.005
17259	-	-	-	-	-	-	-	0.050
17260	-	-	-	-	-	-	-	0.005
16261	-	-	-	-	-	-	-	0.025
17262	-	-	-	-	-	-	-	0.095
17263	-	-	-	-	-	-	-	0.110
17264	-	-	-	-	-	-	-	0.025
17265	-	-	-	-	-	-	-	0.002

Sample No.	Cu ppm	Pb ppm	Zn ppm	Ag ppm	As ppm	Hg ppm	Sb ppm	Au ppm
17341	-	-	-	-	-	-	-	0.030
17342	-	-	-	-	-	-	-	0.310
17343	-	-	-	-	-	-	-	0.430
17344	-	-	-	-	-	-	-	0.055
17345	-	-	-	-	-	-	-	0.845
17346	-	-	-	-	-	-	-	0.055
17347	-	-	-	-	-	-	-	0.005
17349	-	-	-	-	-	-	-	0.020
17350	-	-	-	-	-	-	-	0.010
17447	-	-	-	-	-	-	-	0.020
17448	-	-	-	-	-	-	-	0.025
17449	-	-	-	-	-	-	-	0.010
17450	-	-	-	-	-	-	-	0.660
38593	-	-	-	-	-	-	-	0.035
38594	-	-	-	-	-	-	-	0.040
38595	-	-	-	-	-	-	-	0.300
38596	-	-	-	-	-	-	-	0.010
38597	-	-	-	-	-	-		10.000
38598	-	-	-	-	-	-	-	0.355
38599	-	-	-	-	-	-	-	8.650
38600	-	-	-	-	-	-	-	0.025

Fire assay recalculations

Sample No.	Au Oz/T
17309	0.096
17428	0.190
38572	0.430
17197	0.100
17311	0.098
17313	0.198
38590	0.760
38592	0.028
38566	0.650
38568	0.312

APPENDIX 4

Scanning electron microscope-energy dispersive system (SEM-EDS) geochemistry

Scanning electron microscope-energy dispersive system geochemistry

A polished section from the main sulphide vein sample, GP84 27F, was repolished and coated with a layer of carbon, 250 A^{o} thick. The section was attached to a stub, a conducting strip was applied, and the sample was loaded into the vacuum chamber of a Semco-Nanolab 7 scanning electron microscope. The electron source for this SEM is a tungston filament, and the detector of the accompanying Kevex 7000 EDS is a Si-Li crystal. Voltage was maintained at 30 keV, and the lightest element that could be resolved is sodium (Z=11).

The secondary electron scan was observed and areas of high contrast were noted at low magnification. A number of backscatter photomicrographs were taken, as shown in the text. Areas of interest were analysed at high magnification using the EDS at a voltage range of 0.00 to 20.48 keV. Results were compared with observations from reflected microscope work, and are noted in the text. The SEM-EDS was successfully used both to identify unknown mineral phases and to confirm the presence of those identified under the reflecting microscope. Work was done by the author, under the supervision of John Knight (University of British Columbia).

APPENDIX 5

Plant fossil data

Plant fossil data

Stanley A.J. Pocock of Esso Resources Canada Limited (Calgary) examined a collection of plant fossils from Taylor-Windfall. He identified: Rhamnites sp, cf. R. eminens (Dawson) Berry; Protophyllocladus polymorpha (Lesq.) Berry; cf. Thuites corpuleatus Bell; Cladophlebis (Dennstaedtia) columbiana Dawson; Pseudoctenis latipennis (Heer) Seward; Nilssonia cf. mehli Berry; and, Pteridophyte fragments and other plant remains. Pockock stated that these are of Upper Cretaceous age, and are closely comparable with species recorded from the upper part of the Cretaceous of the Nanaimo and Comox Basins (Vancouver Island).

Fossil locations are: 1) an outcrop of shaley mudstone on the south bank of Battlement Creek, 2270 m upstream from the Taseko River - Battlement Creek junction; 2) a similar outcrop, approximately 500 m due east of a small lake, 2400 m at N055°E from the Taseko River - Battlement Creek confluence; and 3) a cliffy outcrop facing south, above treeline, approximately 3200 m N080°E from the Taseko River - Battlement Creek confluence.